

inaugural dissertation  
for  
obtaining the doctoral degree  
of the  
Combined Faculty of Mathematics, Engineering and natural Sciences  
of the  
Ruprecht – Karls – University  
Heidelberg

Presented by

Sumanjit Datta

BS-MS, Biological Sciences

Born in Kolkata, India

Oral examination: 31<sup>st</sup> August, 2022



# **Condensin-mediated chromosome compaction at single-molecule resolution**

Referees: Prof. Dr. Sylvia Erhardt

Dr. Justin Crocker



This work was carried out at the European Molecular Biology Laboratory (EMBL) and at the Biocenter of the University of Würzburg from July 2018 to May 2022 under the supervision of Prof. Dr. Christian H. Haering.

All major results in this thesis are published in the following articles:

1. Indra A. Shaltiel, **Sumanjit Datta\***, Léa Lecomte\*, Markus Hassler, Marc Kschonsak, Sol Bravo, Catherine Stober, Jenny Ormanns, Sebastian Eustermann, Christian H. Haering. A hold-and-feed mechanism drives directional DNA loop extrusion by condensin. *Science*, 2022 (in press).

\* Shared co-authors

2. **Sumanjit Datta\*\***, Léa Lecomte\*\*, Christian H. Haering. (2020). Structural insights into DNA loop extrusion by SMC protein complexes. *Current Opinion in Structural Biology*, 65, 102–109. (invited review).

\*\* Shared first authors



A PhD is 90% persistence and 10% intelligence

-Hugh Kearns



# Table of contents

## Summary

## Zusammenfassung

## Acknowledgement

<b>Introduction.....</b>	<b>1</b>
<b>1 The cell cycle.....</b>	<b>2</b>
<b>2 Chromosome dynamics during the cell cycle.....</b>	<b>3</b>
2.1 Interphase chromatin.....	3
2.2 Mitotic chromosomes.....	4
2.3 Mitotic chromosome organization by DNA loop extrusion.....	6
<b>3 Condensin.....</b>	<b>7</b>
3.1 Subunits of the condensin complex.....	7
3.2 Structural information on the condensin complex.....	11
3.3 Localization of the condensin complex.....	12
3.4 Condensin's interaction with DNA.....	13
3.5 In vitro activities of condensin.....	14
<b>4 DNA Loop extrusion.....</b>	<b>16</b>
4.1 Loop extrusion by SMC protein complexes.....	17
4.2 Symmetric vs asymmetric DNA loop extrusion.....	19
4.3 Models of DNA loop extrusion.....	20
<b>Aim of this study.....</b>	<b>23</b>
<b>Results.....</b>	<b>25</b>
<b>1 Characterization of the <i>Ct</i> condensin protein complex.....</b>	<b>26</b>
1.1 Purification of the <i>Ct</i> condensin protein complex.....	26
1.2 Mass spectrometry analysis of <i>Ct</i> condensin holocomplex .....	27
1.3 Structural characterization of purified <i>Ct</i> condensin holocomplexes.....	28
1.4 <i>Ct</i> condensin holocomplex displays DNA-stimulated ATPase activity.....	30
1.5 <i>Ct</i> condensin holocomplex has DNA binding activity.....	32
1.6 DNA compaction by the <i>Ct</i> condensin holocomplex.....	32

<b>2</b>	<b><i>Ct</i> condensin compacts DNA by loop extrusion.....</b>	<b>35</b>
2.1	Microfluidics set up.....	35
2.2	Imaging set up.....	36
2.3	Visualization of DNA loop extrusion by <i>Ct</i> condensin holocomplex.....	38
2.4	Resolving DNA loop extrusion by side flow.....	39
2.5	DNA loop extrusion by <i>Ct</i> condensin is strictly asymmetric.....	40
2.6	Anchor slippage of <i>Ct</i> condensin holocomplex during loop extrusion.....	42
2.7	Properties of loop extrusion by <i>Ct</i> condensin holocomplex.....	45
2.8	Effect of high salt on <i>Ct</i> condensin-mediated DNA loop extrusion.....	47
<b>3</b>	<b>Characterization of the <i>Ct</i> delta Ycg1 condensin complex.....</b>	<b>50</b>
3.1	Purification of the <i>Ct</i> delta Ycg1 condensin complex.....	50
3.2	The <i>Ct</i> delta Ycg1 complex can compact DNA.....	51
3.3	The <i>Ct</i> delta Ycg1 condensin displays DNA-stimulated ATPase activity.....	52
3.4	The <i>Ct</i> delta Ycg1 complex binds DNA.....	54
<b>4</b>	<b>The <i>Ct</i> delta Ycg1 complex changes direction while extruding loops.....</b>	<b>56</b>
4.1	Visualization of DNA loop extrusion by the <i>Ct</i> delta Ycg1 condensin complex.....	56
4.2	<i>Ct</i> delta Ycg1 condensin switches direction while extruding DNA loops .....	57
4.3	Properties of DNA loop extrusion by the <i>Ct</i> delta Ycg1 condensin complex .....	60
4.4	Fluorescence labeling of <i>Ct</i> condensin to track condensin during loop extrusion..	62
4.5	Difference between DNA loop extrusion properties of holocomplexes and delta Ycg1 complexes.....	64
4.6	The tendency to change direction of the delta Ycg1 complex is reversed by high salt.....	66
<b>5</b>	<b>‘Safety belt’ of <i>Ct</i> Brn1 plays crucial role for DNA loop extrusion.....</b>	<b>69</b>
5.1	Difference between <i>Sc</i> and <i>Ct</i> Brn1 ‘safety belt’.....	69
5.2	The ‘Safety belt’ of <i>Ct</i> Brn1 is essential for condensin activity.....	72
5.3	A Positively charged BC patch in Brn1 ‘safety belt’ is required for loop extrusion.....	73
5.4	Closure of the Brn1 ‘safety belt’ is necessary DNA loop extrusion.....	74

<b>Discussion.....</b>	<b>77</b>
<b>1 The <i>Ct</i> condensin holocomplex is functionally active.....</b>	<b>78</b>
1.1 The <i>Ct</i> condensin is structurally intact .....	78
1.2 Enzymatic activities of the <i>Ct</i> condensin holocomplex.....	80
<b>2 Loop extrusion by the <i>Ct</i> condensin holocomplex.....</b>	<b>82</b>
2.1 Strictly asymmetric loop extrusion by the <i>Ct</i> condensin holocomplex.....	82
2.2 Anchor slippage by the <i>Ct</i> condensin complex.....	83
<b>3 An active <i>Ct</i> delta Ycg1 condensin complex.....</b>	<b>84</b>
3.1 The <i>Ct</i> delta Ycg1 condensin complex is enzymatically active.....	84
3.2 Direction change by the <i>Ct</i> delta Ycg1 complex .....	85
3.3 Ycg1 acts as a negative regulator for condensin function.....	86
<b>4 The kleisin ‘safety belt’ is the anchor for condensin-mediated DNA loop extrusion.....</b>	<b>87</b>
<b>5 Physiological relevance of DNA loop direction changes.....</b>	<b>89</b>
<b>6 Outlook.....</b>	<b>91</b>
<b>Materials and Methods.....</b>	<b>93</b>
<b>1 Materials.....</b>	<b>94</b>
1.1 Laboratory Equipment.....	94
1.2 Protein purification columns.....	94
1.3 Software.....	94
1.4 Consumable and kits.....	95
1.5 Chemical reagents.....	95
1.6 Biological reagents.....	96
1.7 Bacterial strains.....	96
1.8 Plasmids.....	97
1.9 Primers.....	98
1.10 General buffers and media.....	100
<b>2 Methods.....</b>	<b>101</b>
2.1 General molecular biology techniques.....	101
2.2 General biochemical methods.....	103
2.3 <i>Ct</i> condensin protein expression.....	104

2.4	<i>Ct</i> condensin protein characterization.....	108
2.5	Loop extrusion assay.....	110
2.6	Computational analysis.....	113
<b>Supplementary.....</b>		<b>114</b>
<b>Contributions.....</b>		<b>118</b>
<b>References.....</b>		<b>119</b>
<b>Appendix.....</b>		<b>130</b>
1	Abbreviations.....	130
2	List of figures.....	131
3	List of tables.....	133



## Summary

During cell division, the genetic material of each cell, the DNA undergoes the most drastic rearrangements. The amorphous interphase chromatin condenses into short discernable mitotic chromosome during this process governed by a protein complex known as condensin. Condensin is a member of the structural maintenance of chromosome (SMC) family and comprised of five subunits. SMC2 and SMC4 along with a kleisin subunit, Brn1 form a tripartite ring and association of two additional HEAT (huntingtin, elongation factor 3, protein phosphatase 2A, Tor1 kinase) repeat proteins, Ycg1 and Ycs4 makes the functional pentameric complex. It has been postulated that condensin compacts genomes by a process called ‘loop extrusion’ where DNA is reeled in into a loop, but it wasn’t until recently that this was shown in real time. Purified condensin complex from budding yeast has been shown to extrude large DNA loops *in vitro*. On this account, the aim of my Ph.D. thesis was to generalize this process of ‘loop extrusion’ and get mechanistic insights for this process.

I first purified condensin complex of a thermophilic fungus called *Chaetomium thermophilum* (*Ct*), and characterized it biochemically and biophysically. I showed that the *Ct* condensin is intact and that it can compact DNA. Additionally, it has DNA stimulated ATPase activity and can readily bind DNA. Using advanced microfluidics and super-resolution microscopy, I then showed that the *Ct* condensin complex extrudes DNA loops in an asymmetric manner. To my surprise, a condensin complex lacking the Ycg1 subunit, previously attributed as the anchor module necessary for stable DNA binding, still showed DNA compaction, DNA-stimulated ATPase activity and even a DNA binding affinity similar to wildtype complex. My imaging experiments showed this sub-complex also loop extrudes, however unlike wildtype complex frequently changing direction. It is only when I in addition to Ycg1 also deleted the so-called Brn1 ‘safety belt’ (Brn1<sub>515-637</sub>), I no longer observed loop extrusion. Finally, I was able to show that patches of positive and of hydrophobic residues at the amino-terminal end of the ‘safety belt’ are essential for loop extrusion.

Purely asymmetric loop extrusion has been questioned on its ability to fully compact large eukaryotic genomes and loop extrusion with frequent direction changes has so far only been proposed in theoretical studies as a means to overcome this limitation. My discovery of direction

changes during loop extrusion provides the first real time experimental proof that such extrusion exists and that a mixture of asymmetric extrusion with direction change can accomplish full genome compaction. It is tempting to speculate that the mode of action shown for a thermophilic condensin protein complex could serve as example for the universal mode of chromosome compaction.

## Zusammenfassung

Während der Zellteilung erfährt das genetische Material jeder Zelle, die DNA die drastischsten Umlagerungen. Amorphes Interphasenchromatin kondensiert während eines Prozesses, der von einem Proteinkomplex namens Condensin bestimmt wird, zu einem kurzen, erkennbaren mitotischen Chromosom. Condensin ist ein Mitglied der SMC-Familie (Structural Maintenance of Chromosome) und besteht aus fünf Untereinheiten. SMC2 und SMC4 bilden zusammen mit einer Kleisin-Untereinheit namens Brn1 einen dreigliedrigen Ring und die Assoziation von zwei zusätzlichen HEAT-repeat (Huntingtin, Elongationsfaktor 3, Proteinphosphatase 2A, Tor1-Kinase) Proteinen namens Ycg1 und Ycs4 bildet den funktionellen pentamerischen Komplex. Es wurde postuliert, dass Condensin Genome durch einen Prozess namens "Schleifenextrusion" verdichtet, bei dem DNA in eine Schleife eingerollt wird. Erst vor kurzem wurde dies in Echtzeit gezeigt. Es wurde gezeigt, dass ein gereinigter Condensinkomplex aus Bäckerhefe *in vitro* große DNA-Schleifen extrudiert. Aus diesem Grund war es das Ziel meiner Doktorarbeit, diesen Prozess der "Schleifenextrusion" zu verallgemeinern und mechanistische Erkenntnisse für diesen Prozess zu gewinnen.

Ich habe zuerst den Condensinkomplex eines thermophilen Pilzes namens *Chaetomium thermophilum* (*Ct*) gereinigt und ihn biochemisch und biophysikalisch charakterisiert. Ich habe gezeigt, dass das *Ct* Condensin intakt ist und dass es DNA verdichten kann. Darüber hinaus hat es DNA-stimulierte ATPase-Aktivität und kann leicht an DNA binden. Mittels moderner Mikrofluidik und hochauflösender Mikroskopie zeigte ich dann, dass der *Ct* Condensinkomplex DNA-Schleifen asymmetrisch extrudiert. Zu meiner Überraschung zeigte ein Condensinkomplex dem die Ycg1-Untereinheit, die zuvor als das für stabile DNA-Bindung notwendige Ankermodul beschrieben wurde, fehlte, immer noch DNA-Verdichtung, DNA-stimulierte ATPase-Aktivität und sogar eine DNA-Bindungsaffinität ähnlich dem Wildtyp-Komplex. Meine bildgebenden Experimente zeigten weiter, dass dieser Subkomplex auch DNA-Schleifen extrudiert, jedoch im Gegensatz zum Wildtyp-Komplex häufig in wechselnder Richtung. Erst als ich neben Ycg1 auch den sogenannten Brn1-"Sicherheitsgurt" (Brn1<sub>515-637</sub>) löschte, konnte ich die Schleifenextrusion nicht mehr beobachten. Schließlich konnte ich zeigen, dass positive und hydrophobe Aminosäuren am amino-terminalen Ende des "Sicherheitsgurts" für die Schleifenextrusion unerlässlich sind.

Die rein asymmetrische Schleifenextrusion wurde hinsichtlich ihrer Fähigkeit in Frage gestellt, große eukaryotische Genome vollständig zu verdichten, und Schleifenextrusion mit häufigen Richtungsänderungen wurde bisher nur in theoretischen Studien als Mittel zur Überwindung dieser Einschränkung vorgeschlagen. Meine Entdeckung von Richtungsänderungen während der Schleifenextrusion liefert den ersten experimentellen Beweis in Echtzeit, dass eine solche Extrusion existiert und dass eine Mischung aus asymmetrischer Extrusion mit Richtungsänderung eine vollständige Genomverdichtung erreichen kann. Es ist verlockend zu spekulieren, dass die hier für einen thermophilen Condensinkomplex gezeigte Funktionsweise als universelles Modell für die Chromosomenverdichtung dienen könnte.

## **Acknowledgement**

I would like to thank Christian Haering for giving me the opportunity to join his group and let me follow my own ideas during my Ph.D. I express my gratitude to EMBL graduate office for selecting me into EMBL PhD program and letting me a part of this fantastic and multi-cultural place in the city of Heidelberg. I also thank EMBL stuff for their help. I sincerely thank Darwin Trust of Edinburgh for funding this Ph.D. work.

I would also like to thank my TAC members Jonas Ries, Justin Crocker, Edward Lemke and Sylvia Erhardt for their guidance and support as well as my defense committee members Sylvia Erhardt, Justin Crocker, Sebastian Eustermann and Elmar Schiebel.

I thank Shveta Bisht and Sol Bravo for helping me getting settled in the lab and getting me started with daily lab work. Sol has helped me with daily technical aspects while teaching me protein purifications and very fast pipetting in the hot lab. Her patience and support was most enjoyable. My sincere gratitude to Indra Shaltiel who has constantly guided and supervised me throughout my Ph.D. Without his mentoring, this project would not have been successful. I also thank Markus Hassler for sharing his vast expertise in structural biology and being patient with me always and his constant guidance helped me through my Ph.D. I will always miss our pre-covid morning coffee with Indra and Markus. I thank my former colleague Fabian for translating all the German letters to English and sharing his experience with me during our time together. I also thank my batch mate and colleague Léa for her support and ‘strategic thinking’. I also thank Catherine for her technical support and making us flammkuchen. I thank Toni for bringing some new flavors to the lab and I have enjoyed our chess matches together, although I can’t say it was much of a challenge. New lab members Julia and Guru have also been helpful during my thesis work.

I also thank Mandy Rettel from PCF for helping me with the mass spectrometry experiments and Marko Lampe from ALMF to show me and constantly helping me with the microscope.

I thank Jenny, Conny, Brigitta and Monica for welcoming us at the University of Würzburg and help us through the transition.

I am very thankful to Denny and Kenai for the time we spend together on our most enjoyable walks, long hikes, camping, late night star gazing. I will always cherish those great memories.

Finally, I want to thank Dr. Shravan Kumar Mishra from IISER Mohali who believed in me and gave an opportunity to a young bachelor student to join his lab for bachelor and master thesis work and teaching me the basics of scientific research and inspiring me to continue in this path and my school teacher Asit Baran Sen for his exceptional teaching that inspired me to opt biology for my future studies.



# **Part I**

## **Introduction**

# 1 The cell cycle

In eukaryotes, the cell cycle is highly organized with two distinct phases – interphase (I phase) and the mitotic phase (M phase). During I phase, the cell undergoes three preparatory steps – during the first gap phase (G1), the cell prepares for DNA replication; during synthesis (S) phase, DNA is replicated; during the second gap phase (G2), the cell prepares for division (**Figure 1A**).

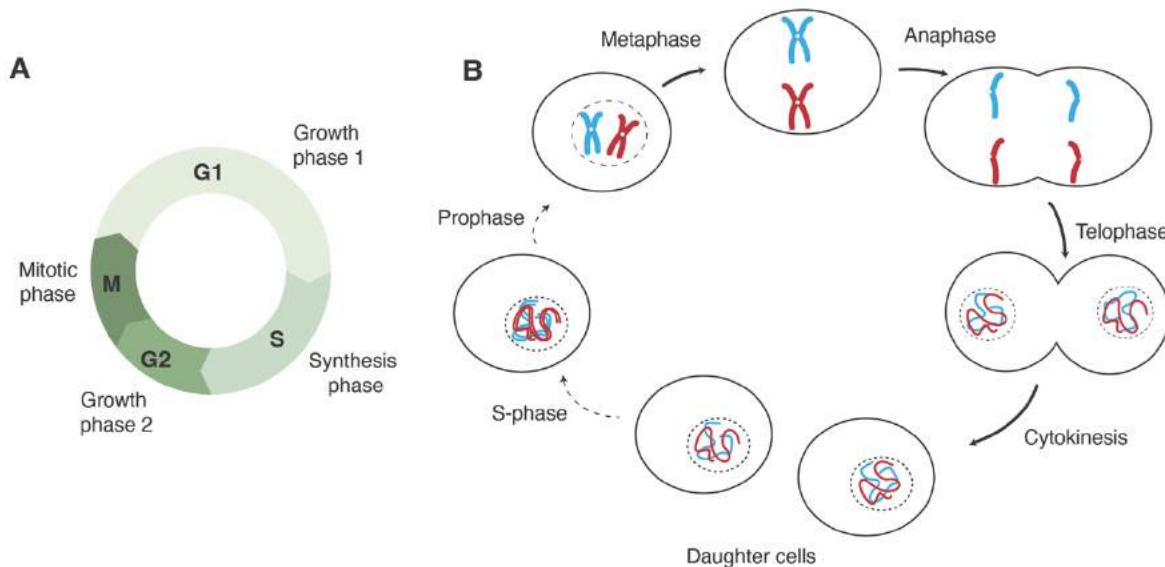


**Figure 1: The cell cycle.** **A.** Schematic representation of the eukaryotic cell cycle. A human somatic cell takes around 24 hours to divide. **B.** Chromosome dynamics during each step of cell cycle. Newly divided daughter cells progress through interphase with duplicated genome. During mitosis, the cell goes through drastic changes in chromosome morphology and cytokinesis produces two new cells with equal sets of chromosomes.

The M phase can be subdivided into the following phases: prophase, metaphase, anaphase, telophase, and cytokinesis. Chromatin compaction starts at prophase and fully compacted chromosomes are aligned on the ‘equatorial plate’ of the cell at metaphase (Fleming, 1882). The sister chromatids segregate equally during anaphase and move towards the cell poles. During telophase, chromosomes disassemble into amorphous chromatin and finally the cell divides during cytokinesis (**Figure 1B**).

## 2 Chromosome dynamics during the cell cycle

The genetic material inside the eukaryotic nucleus undergoes the most dramatic changes over the course of the cell cycle. Eukaryotic cells typically contain two copies of each chromosome, which are the least compacted during interphase and undergo massive compaction that forms characteristic chromosomes during mitosis.

### 2.1 Interphase chromatin

Interphase is when a cell grows, expresses genes, duplicates DNA and cellular organelles, and prepares for the subsequent cell division. During G1 phase, the cell primarily grows in size and expresses proteins needed for DNA replication. The DNA inside the nucleus at this stage is the least condensed, which is thought to facilitate gene transcription.

The first step of DNA organization is achieved by histone octamers. Each octamer wraps 146 base pairs (bp) of DNA to form nucleosomes (Olins & Olins, 1974; Luger et al., 1997; **Figure 2**). Nucleosomes are frequently equally spaced on DNA, resulting in a ‘beads-on-a-string’ appearance also known as the 11-nm chromatin fiber (Woodcock, 1973; Rattner & Hamkalo, 1978).

The 11-nm fiber was suggested to fold into a 30-nm chromatin fiber by nucleosome-nucleosome interactions (Schalch et al., 2005; Song et al., 2014; Robinson et al., 2006). These 30-nm chromatin fibers have been reconstituted *in vitro* in several structural and biochemical studies (Finch & Klug, 1976; Robinson et al., 2006; Huynh et al., 2005; Staynov, 2000; Kruithof et al., 2009). However, the existence of 30-nm fibers *in vivo* has been questioned, since cryo-EM and small angle X-ray scattering (SAXS) studies found no evidence for 30-nm fibers in a number of different cells (Cai et al., 2018; McDowall et al., 1986; Eltsov et al., 2008; Nishino et al., 2012). Instead, chromatin fibers have been suggested to resemble a flexible chain with diameters ranging between 5-25 nm (Ou et al., 2017).

*In vivo*, chromatin was initially thought to form an amorphous and entangled mass, without any major organization (Wischnitzer, 1973). Recent development in chromatin contact mapping

methodologies suggest, however, otherwise. Chromosome conformation capture (3C) methods combined with next-generation sequencing (Hi-C) revealed the presence of so-called topologically associating domains (TADs); chromosomal regions with higher interaction frequencies within a compartment than across compartments (Dekker et al., 2002, Chang et al., 2020; Dixon et al., 2012; Nora et al., 2012; **Figure 2**).

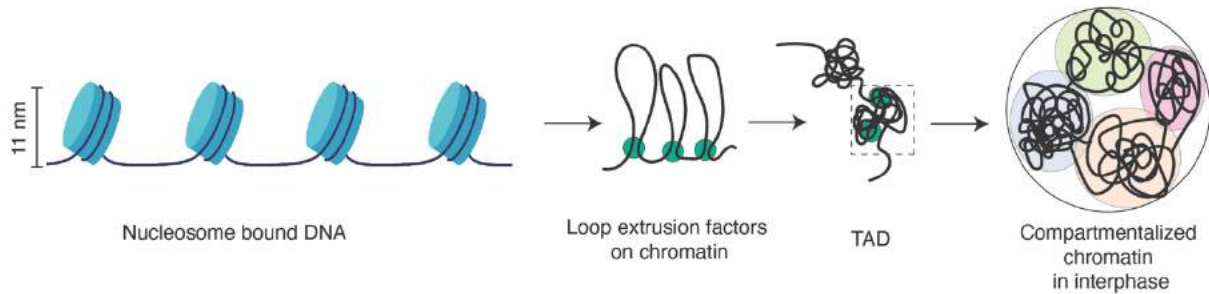


**Figure 2: Chromosome organization during interphase in 3D.** Histone octamers wrap DNA to form a 11 nm fiber. SMC complex such as cohesin (green circles) extrudes DNA loops resulting in TAD which has higher contact frequency within each TAD than across. Chromatin within each nucleus form compartments with high or low activity making euchromatin or heterochromatin.

In addition, direct visualization of chromatin regions using fluorescence *in situ* hybridization (FISH) showed a compartmentalized nucleus with distinct regions or territories (Bolzer et al., 2005). Hi-C methods showed that these territories are different in their overall genomic activity. Some of these distinct territories are more active than others; euchromatin has higher activity in terms of gene expression, whereas heterochromatin suppresses gene expression (Lieberman-Aiden et al., 2009). Even with such a level of organization, interphase chromatin undergoes further compaction to form mitotic chromosomes.

## 2.2 Mitotic chromosomes

Despite forming topologically associating domains and compartments that display differential gene expression profiles, interphase chromatin is still not fully compacted. To enable successful segregation of its genetic material during mitosis, the cell needs to package chromosomal DNA of

the size of mega-base to giga-base pairs. A human somatic cell contains almost 6.3 giga-base pairs of genetic material organized into 46 chromosomes (23x2 pairs) before DNA replication, or 92 chromatid pairs after replication. Individualization and condensation are essential to allow the proper segregation of these chromosomes.

As shown by Meselson and Stahl, DNA replication is semi-conservative in nature (Meselson & Stahl, 1958). Naturally, the parental DNA strands need to be unwound, which results in internal stress (Peter et al., 1998). Sister chromatids need to be individualized to prevent catenanes between sister chromatids during anaphase (Spell & Holm, 1994). Proteins of the topoisomerase family are involved in this individualization process: Type I topoisomerases cleave and re-seal single-stranded DNA (ssDNA) breaks, whereas type II topoisomerases cleave and re-seal double-stranded DNA (dsDNA) breaks (dsDNA; Champoux, 2001). It is topo II that resolves sister chromatid catenanes (Holm et al., 1985); Sundin & Varshavsky, 1981; Uemura et al., 1987). However, as topo II can also create catenanes as likely as it resolves them, it is the onset of mitotic condensation that is thought to provide directionality for the decatenation process (Holm, 1994; Uemura et al., 1987). In addition to catenations, sister chromatids are held together until anaphase onset by cohesin, a member of the Structural maintenance of chromosome (SMC) family of proteins (Nasmyth, 2001).

Chromosome condensation results in short x-shaped chromosomes. The wrapping of DNA around histones to form the 11-nm fiber is not sufficient for the entire condensation process. Even the debated 30-nm fiber falls short to achieve the level of condensation required (Marko, 2008). Therefore, an additional level of compaction was postulated. The hierarchical model for chromosome folding, for example, predicts the formation of a hollow solenoid of around 400 nm (Bak et al., 1977). An alternative model predicts the existence of a central proteinaceous scaffold (Earnshaw & Laemmli, 1983; Paulson & Laemmli, 1977) from which loops of DNA emerge. However, biophysical studies have argued against a continuous stiff protein scaffold and instead suggested that chromatin itself mediates the mechanical stability of mitotic chromosomes (Poirier & Marko, 2002).

Initially, mitotic chromosome folding was primarily attributed to nucleosome-nucleosome interactions (Schalch et al., 2005; Song et al., 2014, Robinson et al., 2006). Recent findings suggest, however, an important contribution by non-nucleosomal proteins. Topo II is one of the most abundant non-nucleosomal proteins found in mitotic chromosomes (Gasser et al., 1986; Lewis & Laemmli, 1982; Maeshima & Laemmli, 2003). Another abundant non-nucleosomal protein is the condensin complex, which is of great importance for mitotic chromosome compaction (Hirano et al., 1997; Hirano & Mitchison, 1994; Saitoh et al., 1994; Strunnikov et al., 1995). Recent in vitro reconstitution studies have shown that core histones, histone chaperones, topo II and condensin are sufficient to generate mitotic-like chromosomes (Shintomi et al., 2015). A later study by the same group showed that such chromosomes can be formed even after depletion of nucleosomes, providing further support to the conclusion that condensin is the driving force for chromosome compaction (Shintomi et al., 2017).

### **2.3 Mitotic chromosome organization by DNA loop extrusion**

Data from mapping of physical proximity of genomic loci using Hi-C methods in combination with polymer simulations are inconsistent with a hierarchical organization of mitotic chromosomes (Naumova et al., 2013). These data can best be explained by consecutive chromatin loops in the range of 80-120 kb. Formation of such DNA loops explains the changes in the Hi-C interaction maps of chromosome upon mitotic entry. Recent polymer simulations of chromosome dynamics showed that DNA loop extrusion can function as an active mode of DNA condensation and is sufficient to explain the formation of mitotic chromosomes (Goloborodko et al., 2016a) and to reproduce their experimentally determined physical properties. The DNA loop extrusion model states that two nearby chromatin sites are bound by specific loop-extruding factors (LEFs) that move along DNA to progressively increase the loop length (Nasmyth, 2001; Riggs, 1990; **Figure 2**). Extensive computer simulations have shown that DNA loop extrusion can indeed be the primary mode of DNA compaction, with average loop lengths observed experimentally matching the degree of compaction (Goloborodko et al., 2016a) and to segregate sister chromatids (Goloborodko et al., 2016b).

### 3 Condensin

Condensin is a member of the SMC protein family (Jeppsson et al., 2014) and has been discovered almost three decades ago (Hirano et al., 1997; Hirano & Mitchison, 1994; Strunnikov et al., 1995). Condensin complexes are essential for genome organization and can be found in all eukaryotic organisms (Hirano, 2016). Most eukaryotic organisms have two condensin complexes that differ in their subunit composition (Ono et al., 2003; Yeong et al., 2003).

Condensin is a pentameric protein complex with a molecular weight of ~650 kDa and consists of two SMC subunits (Smc2 and Smc4, common to all condensin complexes) and three non-SMC subunits (NCAPH, NCAPG, and NCAPD2 for condensin I; NCAPH2, NCAPG2 and NCAPD3 for condensin II; Ono et al., 2003). Most yeast species, such as the budding yeast *Saccharomyces cerevisiae* (*Sc*) and the fission yeast *Schizosaccharomyces pombe* (*Sp*) have only one condensin complex. Condensins from these species are closely related by sequence to condensin I of metazoans. The kleisin and the HEAT (**H**untingtin, **e**longation factor 3, **p**rotein **p**hosphatase 2**A**, **T**or1) repeat non-SMC subunits in budding yeast and fission yeast are named Brn1/Cnd2, Ycg1/Cnd3 and Ycs4/Cnd1, respectively (Hirano, 2012; **Figure 3B**).

#### 3.1 Subunits of the condensin complex

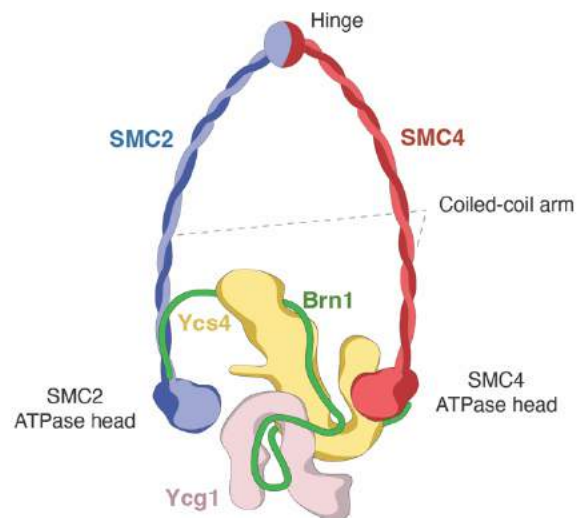
##### *SMC subunits: Smc2 and Smc4*

Smc2 and Smc4 are members of SMC protein family. These were the first subunits of the complex to be discovered in cultured chicken cells, *Xenopus* egg extracts, and both in budding and fission yeasts, and found to be required for mitotic chromosome assembly and chromosome segregation (Hirano & Mitchison, 1994; Saitoh et al., 1994; Saka et al., 1994; Strunnikov et al., 1995). Both subunits are similar in structure: The amino and carboxy termini interact with each other to form a globular ‘head’ domain; the central region folds into a globular ‘hinge’ half-domain; the ‘head’ and the hinge are connected via an anti-parallel coiled coil (Haering et al., 2002; **Figure 3A**). The head domains share close structural similarity with ATP binding cassette (ABC) transporters and

bind and hydrolyze ATP upon dimerization (Anderson et al., 2002; Stray & Lindsley, 2003; **Figure 4**). Two hinge half-domains of Smc2 and Smc4 heterodimerize (Schmiesing et al., 1998), giving rise to V-shaped molecules with two coiled-coils of a length of ~50 nm (Anderson et al., 2002; Diebold-Durand et al., 2017).

The Smc2 and Smc4 heads are active ATPase domains (Hopfner, 2016). Upon ATP binding, the heads engage and sandwich two ATP molecules. ATP binding is mediated by the Walker A motif of one head and the Walker B motif of the other (Haering et al., 2004; Muir et al., 2020). A recent structural study has suggested that first one ATP molecule binds to the Smc4 head, resulting in a partially head-engaged state with only the Smc4 binding site occupied with ATP. Only then a second ATP binds to Smc2 binding site and the heads are fully engaged (Hassler et al., 2019).

**A**



**B**

Species	SMC subunits		Condensin I			Condensin II		
	SMC2	SMC4	Kleisin	HEAT repeats		Kleisin	HEAT repeats	
<i>Saccharomyces cerevisiae</i>	Smc2	Smc4	Brn1	Ycg1	Ycs4	-	-	-
<i>Schizosaccharomyces pombe</i>	Cut14	Cut3	Cnd2	Cnd3	Cnd1	-	-	-
<i>Chaetomium thermophilum</i>	SMC2	SMC4	Brn1	Ycg1	Ycs4	-	-	-
<i>Homo sapiens</i>	SMC2	SMC4	NCAPH	NCAPG	NCAPD2	NCAPH2	NCAPG2	NCAPD3

**Figure 3: Condensin complex.** **A.** Schematic representation of condensin protein complex (image adopted and modified from Hassler et al., 2019). The SMC2 (in blue) dimerizes with SMC4 (in red) to form hinge domain and at one side and forms two ATPase head domains on the other which are connected via coiled-coil arms. The kleisin subunit, Brn1 (in green) connects SMC2 and SMC4. The HEAT repeat proteins, Ycg1 (in pink) and Ycs4 (in yellow) associate with Brn1 to form pentameric complex; **B.** Subunit composition of budding yeast, fission yeast, *Chaetomium thermophilum* (*Ct*) and human condensin complexes.

### ***The kleisin subunit: Brn1***

The kleisin subunit of condensin, Brn1 in budding yeast, was first discovered in *Drosophila* (Kania et al., 1995; Bhat et al., 1996) The kleisin connects the two SMC heads (Haering et al., 2002; Onn et al., 2007) and is member of a class of proteins found in both prokaryotes and eukaryotes (Schleiffer et al., 2003). The Brn1 kleisin of condensin is the central subunit that interacts with all other condensin subunits (Onn et al., 2007).

Brn1 is predicted to be mostly unstructured, without any major structural fold (Yoshimura & Hirano, 2016) except a helix-turn-helix (HTH) domain that interacts with the coiled coil of the ‘neck’ region of Smc2 and a winged-helix domain (WHD) that interacts with the Smc4 head (Haering et al., 2004; Onn et al., 2007; Hassler et al., 2019; **Figure 3A, 4**) This differential binding of Brn1 to different parts of the two SMC subunits creates a fundamental asymmetry in the complex. Binding of Brn1 to the SMC heads led to the postulation that SMC complexes are ring-shaped (Cuylen et al., 2011; Gruber et al., 2003; Haering et al., 2008; Onn et al., 2007). The interaction of Brn1 HTH and the Smc2 neck is thought to dissociate temporarily upon ATP binding, whereas the Brn1 WHD and the Smc4 binding interface seems to be constitutive (Hassler et al., 2019).

### ***The HEAT-repeats subunits: Ycg1 and Ycs4***

The other two non-SMC subunits of condensin complex are Ycg1 and Ycs4. These two proteins are member of HEAT-repeat protein family and are almost exclusively composed of tandem repeats of  $\alpha$ -helices that are connected via a short linker (Andrade & Bork, 199; Neuwald &

Hirano, 2000). HEAT-repeat proteins often assemble into a flexible solenoid form, despite only sharing low sequence homology (Hassler et al., 2019; Kschonsak et al., 2017; Manalastas-Cantos et al., 2019; **Figure 4**). Pulldown experiments followed by crosslinking mass spectrometry revealed the relative positions of these subunits within the pentameric condensin complex: Ycg1 binds to the central region of Brn1, whereas the Ycs4 binds to the closer to the N-terminal part. The interactions are independent of each other (Onn et al., 2007; Piazza et al., 2014).

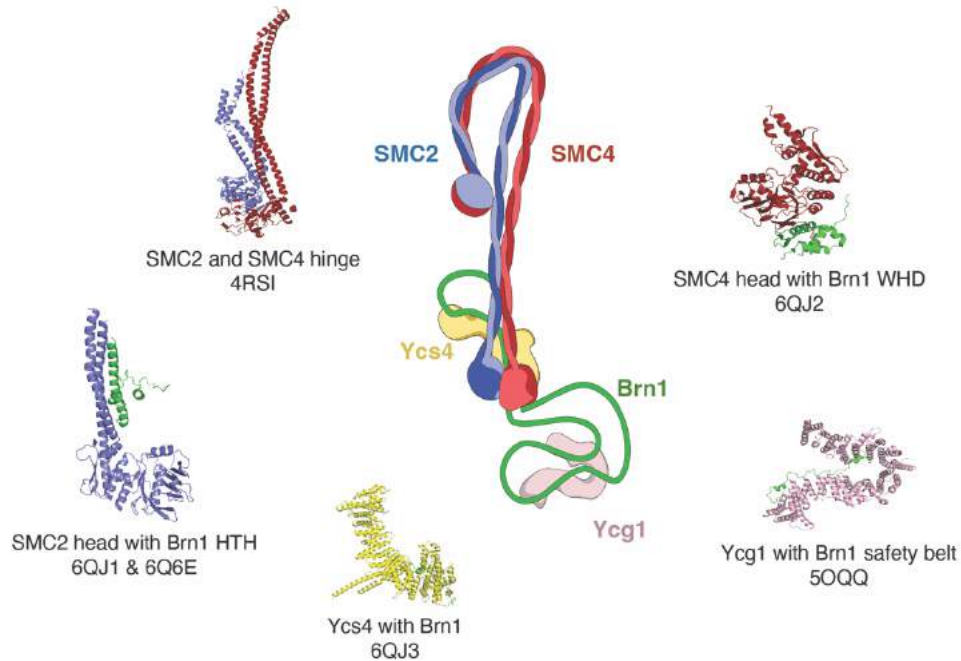


**Figure 4: Structure of condensin complex.** Cartoon of condensin holo complex as seen by cryo-EM (middle, Lee et al., 2020). Previous structural studies performed on different subunits of condensin – *Sc* SMC2 and SMC4 hinge domain with extended coiled coils (PDB ID – 4RSI; Soh et al., 2015), *Ct* SMC head with Brn1 helix-turn-helix (composite of two structures with PDB ID – 6QJ1 and 6Q6E; Hassler et al., 2019), *Ct* Ycs4 with Brn1<sub>225-512</sub> (PDB ID – 6QJ2; Hassler et al., 2019), *Sc* Ycg1 with Brn1<sub>384-531</sub> (PDB ID – 5OQQ, Kschonsak et al., 2017) and *Ct* SMC4 head with Brn1 winged helix domain (PDB ID – 6QJ3; Hassler et al., 2019).

In a previous study, Ycg1 in complex with Brn1 (Ycg1-Brn1<sub>515-637</sub>) was co-crystallized with DNA and provided the first direct evidence of DNA binding by an SMC complex subunit (Kschonsak et al., 2017; **Figure 4**). The structure of Ycs4 was also solved via X-ray crystallography and revealed how Brn1 binds to Ycs4 (*Chaetomium thermophilum* Brn1<sub>225-512</sub>, Hassler et al., 2019; **Figure 4**).

### 3.2 Structural information on the condensin complex

The members of the SMC family of proteins can be found in prokaryotes in the form of MukBEF, MksBEF, SMC-ScpAB complexes and in eukaryotes in the form of cohesin, condensin and SMC5/6 (Yatskevich et al., 2019). These proteins are involved in multitude of different functions. Cohesin is involved in many cellular processes involving sister chromatid cohesion, DNA repair (Losada et al., 1998; Nasmyth & Haering, 2009; Nishiyama, 2019), condensin is involved in mitotic chromosome compaction and segregation (Paul et al., 2019; Dekker & Mirny, 2016; Hirano, 201; Mirny et al., 2019) whereas SMC5/6 complex primarily plays role in DNA damage repair and genome stability (Aragón, 2018).

Despite the different functions of the various SMC protein complexes, they all share a similar 3D architecture. The SMC subunits dimerize to at the hinge domain on one side and, upon ATP binding, at the ATPase head domains on the other side. The kleisin subunit joins the heads even in the absence of nucleotide to form a tripartite ring. The HEAT-repeat subunits associate with the kleisin and complete the complex (reviewed in Datta et al., 2020; **Figure 3A, 4**).

One of the first structural studies was performed on bacterial SMC homodimers using rotary shadowing followed by electron microscopy (Melby et al., 1998). This revealed the flexible nature of the coiled-coil arms, with a variety of arrangements ranging from completely aligned coiled coils to fully open coiled-coils that result in a V-shaped architecture. Human and *Xenopus* condensin holocomplexes as well as yeast cohesin holocomplexes have also been imaged by this method and resulted in similar results (Anderson et al., 2002; Terakawa et al., 2017). Using Atomic Force Microscopy (AFM), the yeast condensin SMC dimers have been imaged, which suggested an even higher degree of flexibility than originally anticipated, with coiled-coil arms that can fold back onto the heads (Eeftens et al., 2017). Similar results were obtained with the *Sc* condensin holocomplex using the same method (Ryu et al., 2020). In contrast, x-ray crystallography combined with cross-linking mass spectrometry suggested that the bacterial SMC-ScpAB complex adopts a stiff rod-like shape (Diebold-Durand et al., 2017).

Many structural studies focused on a single or two subunits of the condensin complex have been performed, including the *Sc* Smc2-Smc4 hinge domain with extended coiled-coils, the *Ct* Smc2 head with Brn1<sub>HTH</sub>, the *Ct* Smc4 head with Brn1<sub>WHD</sub>, the *Ct* Ycs4 with Brn1<sub>225-512</sub>, and the *Sc* Ycg1 with Brn1<sub>384-531</sub> (Soh et al., 2015; Kschonsak et al., 2017; Hassler et al., 2019; **Figure 4**). Two recent studies have applied cryo-EM and negative staining to the budding yeast and human condensin holocomplexes, respectively (Kong et al., 2020; Lee et al., 2020; **Figure 4**). Lee et al. found that, in the absence of ATP, the coiled-coil arms are aligned, adopting a rod-like shape. The aligned coils bend at the so called ‘elbow’ region to fold back onto themselves (**Figure 4**). In the ATP-free state, the Ycs4 subunit is bound to the Smc4 head, while the other HEAT-repeat subunit, Ycg1, is loosely bound to the complex via the flexible Brn1 subunit. Upon ATP addition, the heads become fully engaged and Ycs4 is released. Only now Ycg1 binds to the Smc2 head. This drastic change in structure suggests that the complex is highly dynamic, which presumably has important roles for its functionality (**Figure 5**).

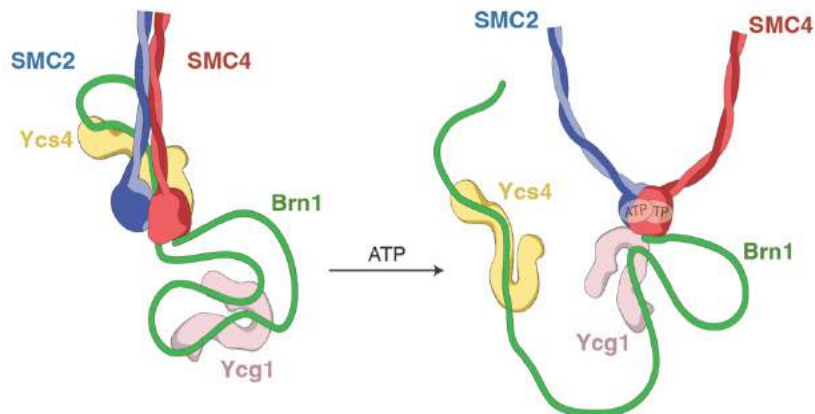


**Figure 5: ATP binding and structural rearrangement of condensin.** In the absence of ATP, the coiled-coils are aligned with each other, the heads are in close proximity. Ycs4 binds to SMC4 heads whereas Ycg1 is loosely bound to Brn1. Upon ATP addition the coiled-coil arms open, the heads are fully engaged. The Brn1 HTH releases from SMC2 neck region and therefore releasing Ycs4 from the complex and this allows Ycg1 to bind to SMC2 head (Image adopted and modified from Lee et al., 2020).

### 3.3 Localization of the condensin complex

Vertebrate condensin complexes associate with mitotic chromosomes along their central axis, with alternating condensin I and II foci seen by fluorescence microscopy (Hirano & Mitchison, 1994;

Maeshima & Laemmli, 2003; Ono et al., 2003; Saitoh et al., 1994). Chromatin immunoprecipitation followed by deep sequencing (ChIP-seq) revealed that certain chromosomal loci, like centromeres, telomeres, and the repetitive rDNA locus, are highly enriched for condensin (Ciosk et al., 2000; Wang et al., 2005). In human cells, condensin II is constitutively present in the nucleoplasm, whereas condensin I resides in the cytoplasm and only gains access to chromatin after nuclear envelop breakdown during prometaphase (Hirota et al., 2004). As a consequence, condensin II localizes to chromatin already during prophase, much earlier than condensin I. Condensin II was also observed to stably interact with chromosomes throughout mitosis, whereas binding of condensin I is mostly dynamic (Gerlich et al., 2006). Fluorescence correlated spectroscopy (FCS) on live cells led to the estimation that around 35,000 condensin II and 190,000 condensin I complexes bind to chromosomes during mitosis in human cells (Walther et al, 2018). This suggests that condensin II generates large loops of ~ 400 kb, which are then further divided into smaller ~80 kb-loops by condensin I, as modelled for chicken DT40 cells (Gibcus et al., 2018).

### **3.4 Condensin's interaction with DNA**

Till date, no specific DNA binding sequence has been identified for the condensin complex. ChIP experiments performed for condensin (I) in human cells, budding yeast or fission yeast showed an enrichment at pericentromeric regions, sub-telomeric regions, tRNA genes, and rDNA loci (D'Ambrosio et al., 2008; Piazza et al., 2014; Sutani et al., 2015; Wang et al., 2005), although condensin associates with chromosomes along their entire length. In budding yeast, condensin binding was also found to correlate with nucleosome-free regions (Piazza et al., 2014).

Several studies revealed that condensin complexes can directly bind to DNA. Full-length Smc2 and Smc4, as well as isolated Smc2-Smc4 hinge domains, bind DNA (Sakai, 2003; Stray & Lindsley, 2003; Griese et al., 2010; M. Hirano, 2002). In vitro and in vivo evidence supports the notion that the SMC head domains of prokaryotic complexes bind DNA (Vazquez Nunez et al., 2019). The HEAT-repeat subunits have also been shown to play a crucial role in DNA binding (Piazza et al., 2014). Structural work on the budding yeast and fission yeast condensin complexes has shown direct DNA binding by the Ycg1-Brn1 subcomplex (Kschonsak et al., 2017). DNA is

bound within a groove created by the Ycg1 subunit, while the Brn1 subunit wraps around DNA like a ‘safety belt’. The subcomplex formed by CAPG and CAPH of human condensin I creates a similar DNA binding site (Hara et al., 2019). Recently, MukBEF and the yeast condensin holocomplexes were shown to bind DNA in cryo-EM structures (Bürmann et al., 2021; Lee et al., 2022). These data suggest a direct mode of DNA binding for condensin.

### 3.5 In vitro activities of condensin

Different catalytic activities have been attributed to purified condensin complexes, all of which could play a role for DNA condensation. The condensin I complex immunopurified from *Xenopus* egg extracts introduces positive supercoiling into circular plasmid in the presence of ATP (Kimura & Hirano, 1997). This activity can most likely be attributed to monomeric condensin complexes (Bazett-Jones et al., 2002). In a recent in vitro study, *Sc* condensin was shown to travel along DNA that had been attached to a chemically modified glass slide, suggesting that condensin is a mechanochemical motor protein (Terakawa et al., 2017).

The purified *Sp* Smc2-Smc4 dimer has been shown to facilitate the re-annealing of ssDNA into dsDNA, whereas the holocomplex did not display such an activity. What was even more surprising was the finding that even after truncating the head domains of the dimer, DNA re-annealing was still observed (Sakai, 2003). It is still unclear how this activity would be related to mitotic chromosome condensation. It is tempting to speculate that condensin might mediate re-annealing of ssDNA during mitosis, which in turn relates to chromosome compaction.

The *Xenopus* condensin holocomplex was shown to hydrolyze ATP, and this activity was boosted by the presence of DNA (Kimura & Hirano, 1997). The human condensin I complex was later shown to possess ATP-dependent DNA supercoiling and knotting activities (Kimura et al., 2001). Recently, human condensin I and condensin II complexes showed DNA-stimulated ATPase activity (Kong et al., 2020). The *Sc* Smc2-Smc4 dimers also have DNA stimulated ATPase activity (Stray & Lindsley, 2003). The ATPase activity was also boosted by the presence of the non-SMC

subunits (Kimura & Hirano, 1997; Piazza et al., 2014). The ATPase activity of the *Sc* condensin holocomplex was also stimulated by DNA (Terakawa et al., 2017).

The immunopurified condensin complex from *Xenopus* egg extracts can compact linear DNA in the presence of ATP in magnetic tweezer experiments (Strick et al., 2004). While this process is strictly ATP dependent, binding to DNA itself is not. Similar magnetic tweezers experiments with the *Sc* condensin holocomplex also showed real-time DNA compaction (Eeftens et al., 2017). This study also showed that the electrostatic interaction between condensin and the DNA is ATP-independent, whereas DNA compaction requires ATP. Another study reported that oligomeric *Sc* condensin complexes compact DNA in a similar magnetic tweezers setup (Keenholtz et al., 2017). Bacterial MukB and the MukBEF complex were also shown to compact DNA in the presence of ATP (Chen et al., 2008).

## 4 DNA loop extrusion

Purified metaphase chromosomes imaged by electron microscopy revealed the emergence of loop-shaped DNA from the central ‘scaffold’ region (Earnshaw & Laemmli, 1983; Paulson & Laemmli, 1977; **Figure 6A**). These looped domains were thought to be essential for chromosome organization and had been suggested to constitute units of gene regulation or DNA replication (Goldman, 1988). DNA loops were originally hypothesized to attach to the base of scaffolding proteins (Cockerill & Garrard, 1986; Gasser & Laemmli, 1987).

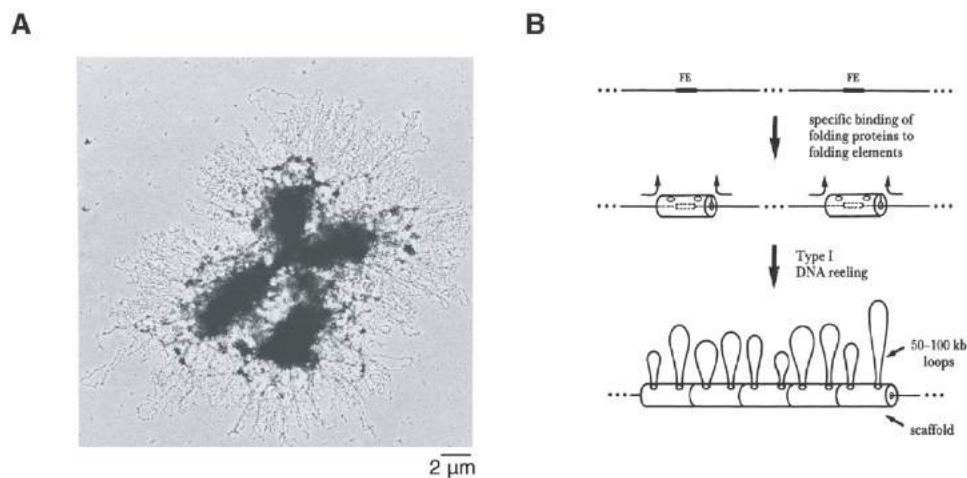


**Figure 6: DNA loops arrangement for chromosome organization.** **A.** Radial loops emanating from whole chromosome all along the chromatid arms as seen under electron microscope (Image taken and modified from Earnshaw & Laemmli, 1983). **B.** Specific DNA sites or folding elements (FE) are thought to be present every 50-100 kb along the DNA which harbors folding proteins to form a folding complex. These complexes reel in DNA from both sides to make 50-100 kb loops and these folding complexes are thought to form the central core of chromosome (Image taken and modified from A D Riggs, 1990).

It was proposed that proteins that are evolutionary related to bacterial type I restriction enzymes but do not possess DNase activity might bind to specific DNA sites and then reel in cis-DNA bi-directionally. This reeling process generates ‘DNA loops’ (50-100 kb), resulting in chromosome folding. These proteins would form a scaffold at the base of the loops (A D Riggs, 1990; **Figure 6B**). Nasmyth postulated that it might be possible that condensin associates with these ‘loops’ at their base and enlarge them in a progressive manner, thus creating a central axis (Nasmyth, 2001).

## 4.1 Loop extrusion by SMC protein complexes

SMC protein complexes have previously been hypothesized to extrude DNA loops to condense chromatin into chromosomes, and this activity has been attributed to be one of the most important factors for genome organization (Nasmyth, 2001; Goloborodko et al., 2016a; Goloborodko et al., 2016b). But it was not until recently that this process was visualized in real time. Ganji and colleagues used a single-molecule imaging approach, where biotinylated lambda phage DNA ( $\lambda$ -DNA, 48,502 bp) had been tethered to a passivated glass surface and was then imaged using Total Internal Reflection Fluorescence (TIRF) microscopy (Ganji et al., 2018). When purified *Sc* condensin holo complex was added to the imaging device using microfluidics, loop extrusion was observed for the first time. In these experiments, condensin reeled in DNA strictly from one side (Figure 7).

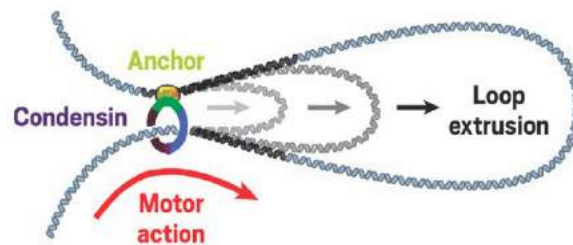


**Figure 7: DNA loop extrusion by *Sc* condensin complex.** Purified *Sc* condensin holo complex was added to tethered ( $\lambda$ -DNA in the imaging device and DNA loop extrusion was observed in real time. It was thought that condensin binds to DNA using its anchor site and reels DNA in from the motor site into the loop which grows with time. This extrusion is one-sided or asymmetric in nature (Image taken from Ganji et al., 2018).

Image analysis of these extrusion events confirmed an asymmetric (or one-sided) extrusion behavior. Consequently, condensin was thought to bind DNA via an ‘anchor site’, which might be created by the Ycg1 subunit, and to reel in DNA via a ‘motor site’ into the loop (Ganji et al., 2018). Furthermore, the condensin complex was fluorescently labeled and a dual-color imaging experiment showed a single condensin complex at the base of the loop. However, the detailed molecular mechanism of this asymmetric DNA loop extrusion process remained enigmatic.

Using a similar single-molecule imaging approach, the human cohesin complex was shown to extrude DNA loops (Davidson et al., 2019; Y. Kim et al., 2019). Both studies reported symmetric (or two-sided) loop extrusion, in contrast to the asymmetric loop extrusion observed for condensin. Cohesin required its ‘DNA loader’ complex NIPBL-MAU2 for loop extrusion. Subsequent studies using the fission yeast cohesin complex, human condensin I, and condensin II revealed a mixture of symmetric and asymmetric modes of loop extrusion (Kong et al., 2020; Higashi et al., 2021). The observed loop extrusion activities were cell-cycle dependent: *Xenopus* egg extracts from metaphase resulted in one-sided extrusion, egg extracts from interphase gave rise to symmetric loop extrusion (Golfier et al., 2020). Depletion experiments suggested that the cohesin complex is responsible for interphase loop extrusion, whereas the condensin complex is responsible for loop extrusion in mitotic extracts. Recently, the MukBEF complex was also reported to compact DNA by loop extrusion (Zhou, 2021).

Additional studies with the *Sc* condensin complex have shown that individual complexes can traverse each other when present in higher concentrations (2-10 nM) and form a compound loop structure called ‘Z-loop’. In this structure, three double strands of DNA are stretched in parallel with one condensin at each edge (Kim et al., 2020). These compound loop formations hence require at least two condensin complexes and the structure of the resultant loop resembles the letter ‘Z’. Kim and colleagues have shown that condensin complex can also extrude loops on supercoiled DNA (Kim et al., 2021).

All DNA loop extrusion studies mentioned so far have used naked DNA. However, DNA is bound to histones and other DNA-binding proteins in vivo, which could act as roadblocks for the condensin complex. *Sc* condensin was shown to bypass physical roadblocks like nucleosomes, RNA polymerases, or dCas9 while extruding DNA loops (Pradhan et al., 2021). Surprisingly, large DNA-bound nanoparticles (~200 nm) also did not block condensin-mediated loop extrusion and can be translocated into the loops. In the same study, the authors used a single-chain cohesin complex (all subunits of the tripartite ring are fused to each other) and have shown loop extrusion with all the roadblocks, suggesting a non-topological mode of loop extrusion.

## 4.2 Symmetric vs asymmetric DNA loop extrusion

DNA loop extrusion with symmetric and asymmetric behaviors raise the question how SMC complexes work at a molecular level to govern these differential modes of extrusion. For asymmetric loop extrusion to work, LEFs need one stable DNA binding site, one motor site that reels in DNA, and one putative transient DNA binding site (either embedded within the motor site or elsewhere) that would hold the pre-existing DNA loop during the extrusion process. For symmetric loop extrusion, LEFs either facilitate strand exchange between anchor and motor site during extrusion or require multiple transient DNA binding sites that can reel DNA into the loop. So far, the *Sc* condensin complex and *Xenopus* egg extracts from metaphase have resulted in strictly asymmetric (or one-sided) extrusion (Ganji et al., 2018; Golfier et al., 2020; **Figure 8**), whereas both human and fission yeast cohesin complexes and *Xenopus* egg extracts from interphase displayed symmetric (or two-sided) loop extrusion (Davidson et al., 2019; Kim et al., 2019; Golfier et al., 2020; Higashi et al., 2021; **Figure 8**). Davidson and colleagues showed the presence of one cohesin at the base of the loop, Kim and colleagues showed two cohesin complexes. How one cohesin complex performs symmetric loop extrusion might differ from the molecular mechanism used by the *Sc* condensin complex. However, it is tempting to speculate that two one-sided extruders can work together and reel DNA from both sides in a unidirectional manner to give rise to an overall bi-directional extrusion process (Kim et al., 2020).

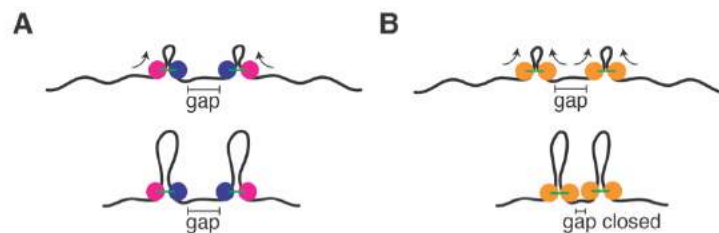


**Figure 8: Symmetric vs asymmetric loop extrusion.** **A.** Schematic representation of asymmetric or unidirectional loop extrusion with two LEFs are facing with their anchor sites to each other, leaving a gap in the chromatin. The pink circle represents the motor site that reels in DNA in the loop whereas the blue circle represents the anchor site that stably binds to DNA; **B.** Symmetric or bi-directional loop extrusion by one such LEF leaving no gap in chromatin. The yellow circles represent DNA interaction sites that reel in DNA.

Experiments with human condensin I and II complexes showed a combination of symmetric and asymmetric loop extrusion (Kong et al., 2020). About 80% of the extrusion events with the condensin I complex showed an asymmetric pattern, whereas, for the condensin II complex, loop extrusion was equally symmetric and asymmetric. It is, however, not fully clear how or why two human condensin complexes would implement different modes of extrusion.

Regardless of the mechanism, theoretical studies and computer simulations have preferred symmetric extrusion over asymmetric extrusion (Banigan et al., 2020; Banigan & Mirny, 2020a, 2020b). Two asymmetric LEFs that face each other with their anchor sites would leave a gap in between them and hence would not be able to compact the genome fully. Symmetric LEFs overcome this problem by reeling in DNA from both sides (**Figure 8**). It was also proposed that a combination of asymmetric and symmetric extrusion or an extruder that switches direction while extruding loops could also overcome this issue. Strictly one-sided extrusion would be sufficient to linearly compact a chromatin polymer only by 10-fold, which is far from enough to compact human genome which requires almost 1000-fold compaction (reviewed in Banigan & Mirny, 2020a).

### **4.3 Models of DNA loop extrusion**

SMC complexes display large conformational changes during their active cycles (reviewed in Hassler et al., 2018). Insights into these structural changes are crucial to understand how LEFs function. Changes in coiled-coil orientation, exchange of HEAT-repeat subunits, or linking ATP-independent with ATP-dependent DNA interactions are potentially important aspects to shed light onto the molecular mechanism of loop extrusion (Hassler et al., 2019; Lee et al., 2020; Bauer et al., 2021). The exact mechanism of loop extrusion remains, however, to be fully understood.

Three different models have been proposed to explain loop extrusion (Hassler et al., 2018). The ‘Sequential Walking Model’ assumes that two ATPase heads of condensin complex transiently bind DNA. The hinge acts as a stable anchor for DNA binding in this case. One of the head domains binds DNA locally whereas the other head domain binds to the same DNA at a distance. Binding of ATP to one of the heads triggers a conformational change that brings the heads together, ATP

gets sandwiched between the heads, and the heads disengage again upon ATP hydrolysis. The first head then binds DNA again at a distance and the cycle repeats (**Figure 9A**).

The ‘DNA Pumping Model’ sees condensin initially bound with ATP with the SMC heads engaged. The DNA is bound to the hinge and on top of the two heads. In this state, the coiled coils are open. Upon ATP hydrolysis, the coiled coils zip up, the heads disengage, and both DNA segment are pushed downwards into the chamber formed by the kleisin and the heads. Next, a pair of ATP molecule is bound to the heads, which opens the coiled-coil arms again and a new DNA segment is captured in the same orientation. The cycle repeats to increase the pre-existing DNA loop (**Figure 9B**).

In the ‘Extended Crunching Model’, the condensin coiled-coil arms are initially aligned with each other and the heads are disengaged. One DNA segment is anchored within the ‘safety belt’ and the other is bound to the neck region (coiled-coil region just above the ATPase head) of one of the heads. ATP binding opens the coiled-coil arms, engages the heads and provides access to a third DNA binding site within the hinge domain, with simultaneous release of the head-bound DNA segment. Due to their flexible nature, the coiled coils then fold into a butterfly-like conformation, where the heads are juxtaposed to the hinge domain. Upon ATP hydrolysis, the coiled coils fold back into their previous state (**Figure 9C**).

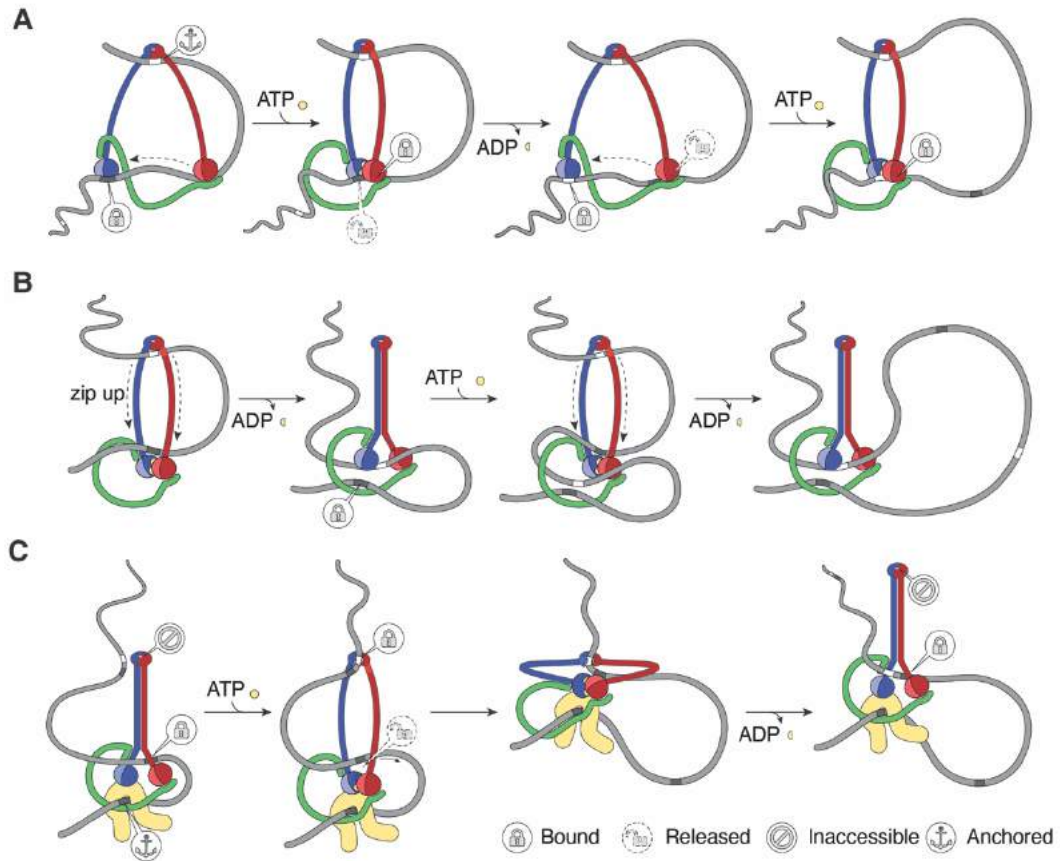


**Figure 9: Models of condensin mediated loop extrusion.** A – C. Schematic representation of ‘The Sequential Walking model’ in A, ‘The DNA Pumping Model’ in B and ‘The Extended Scrunching Model’ in C respectively (Image taken from Hassler et al., 2018).

## 5 Aim of this study

DNA loop extrusion has been widely accepted as the fundamental mode of DNA organization by SMC protein complexes, which govern a vast repertoire of functions inside the cell's nucleus. Understanding the detailed molecular mechanisms that drive loop extrusion is crucial. The condensin complex from budding yeast was the only complex that had been shown to extrude DNA loops at the beginning of this study (Ganji et al., 2018). Other SMC complexes, including human cohesin and condensin, were subsequently shown to extrude DNA loops (Davidson et al., 2019; Y. Kim et al., 2019; Kong et al., 2020).

I set out to generalize the concept of DNA loop extrusion for SMC protein complexes with a condensin complex from the thermophilic yeast *Chaetomium thermophilum* (*Ct*) purified from a heterologous expression system (insect cells). The aim of this work was to biochemically and biophysically characterize the *Ct* condensin complex.

I used single-molecule imaging to show that the *Ct* condensin complex also extrudes DNA loops. Surprisingly, a condensin complex that was lacking the Ycg1 subunit also extruded loops and this complex switched directions. This observation led to a project to dissect the identity and function of the 'anchor site' of the condensin complex. My work has shown that Ycg1 is dispensable for DNA loop extrusion and that the 'safety belt' region of the kleisin subunit Brn1 forms the true anchor for condensin. In Addition, I characterized the essential residues within the Brn1 safety belt necessary for DNA loop extrusion.



# **Part II**

## **Results**

# 1 Characterization of the *Ct* condensin protein complex

## 1.1 Purification of the *Ct* condensin protein complex

The five-subunit condensin protein complex was previously purified from the budding yeast *Saccharomyces cerevisiae* (*Sc*) and shown to extrude DNA loops in real time (Ganji et al., 2018). As this had been the only SMC protein complex to be shown to extrude DNA loops in vitro by the time of the beginning of this study, I decided to study condensin from another yeast species, *Chaetomium thermophilum* (*Ct*), in loop extrusion assays to challenge the idea of ‘loop extrusion’ as a general mode of DNA compaction by SMC protein complexes. *Chaetomium thermophilum* is a thermophilic fungus that has been characterized before (Kellner et al., 2016) and used as a source of proteins for in vitro and structural biology studies due to the increased thermostability of these proteins. Another advantage of using *Ct* condensin was that high-resolution structures of several subunits of the complex were already available, allowing precise engineering of the complex.

The *Ct* condensin holo complex was cloned into a baculovirus vector suitable for virus production and protein expression in Sf21 insect cells (ovarian cells isolated from *Spodoptera frugiperda*). I purified the condensin complex from 1-2 liters cultures through a series of purifications steps (**Figure 10A**).

I first used Ni-NTA (Ni-Nitriloacetic acid) affinity purification against the 8x histidine affinity tag located on the Brn1 C-terminus to isolate the complex from the cell lysate. Next, I purified the complex further by anion exchange chromatography and finally by size exclusion chromatography (SEC). The holocomplex eluted in a single peak from SEC, indicating that the purification scheme resulted in a single species (**Figure 10B**). I was able to distinguish 4 bands on SDS-PAGE (**Figure 10C**).

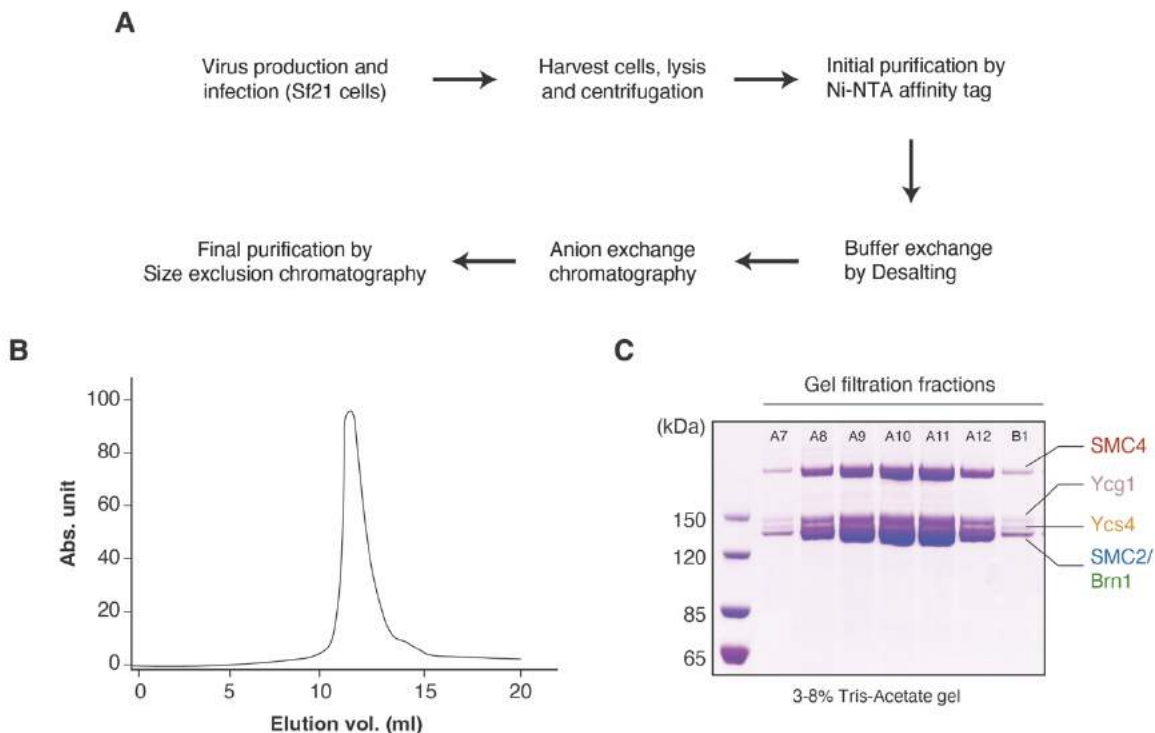


**Figure 10: Purification of the *Ct* condensin protein complex.** **A.** Flowchart of purification steps of *Ct* condensin protein complex from insect cells; **B.** Gel filtration profile of *Ct* condensin complex from size exclusion chromatography; **C.** SDS-PAGE analysis of fractions of purified condensin complex eluted from size exclusion chromatography. Samples were analyzed on 3-8% NuPAGE gel in Tris-Acetate buffer.

## 1.2 Mass spectrometry analysis of *Ct* condensin holocomplex

I pooled the eluent fractions from SEC, concentrated them and ran them on SDS-PAGE (**Figure 11A**). Based on the intensity of the fastest migrating band, I suspected that two subunits of condensin complex were running very close to each other on SDS-PAGE. To test this hypothesis and since the migration pattern of the condensin subunits were not in complete correspondence to their theoretical molecular weight, I used mass spectrometry analysis to identify each band. Both in-gel and in-solution samples were digested with trypsin and subjected to mass spectrometry analysis by EMBL Proteomics Core Facility. In-gel samples revealed the identity of each band from top to bottom: Smc4, Ycg1, Ycs4, Smc2, Brn1. There were no major contaminants from Sf21 insect cells found in the purified samples.

A stoichiometric analysis of the different subunits was performed from in-solution samples based on intensity based absolute quantification (iBAQ, Schwanhäusser et al., 2011) from two different protein preps. The stoichiometry of the Brn1:Smc2:Smc4:Ycg1:Ycs4 subunits was found to be 1.3:1.0:1.0:0.7:0.7 (**Figure 11B** and **supplementary table 1**). This result indicates that the Ycg1 and Ycs4 HEAT-repeat subunits are underrepresented in relation to the SMC and the kleisin subunits. The SMC subunits from the Sf21 insect cells were detected in very low quantities (1:1,000 when compared to the *Ct* proteins; **supplementary table 1**), which suggests that the *Ct* condensin proteins did not interact with the insect cell condensin proteins.

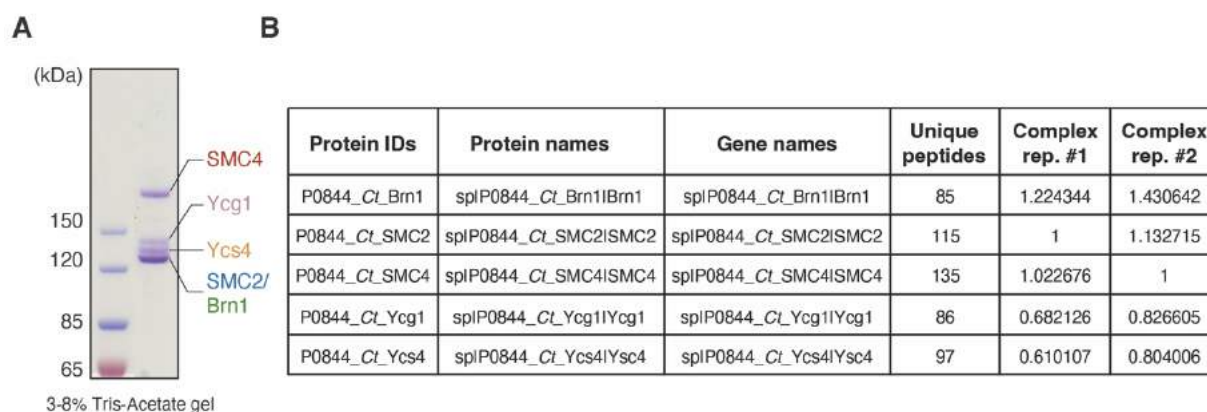


**Figure 11: Mass spectrometry analysis of *Ct* condensin holocomplex.** **A.** Pooled fractions from size exclusion chromatography were analyzed on 3-8% NuPAGE gel in Tris-Acetate buffer; **B.** Simplified mass spectrometric analysis of purified condensin complex and the corresponding stoichiometric values are indicated.

### 1.3 Structural characterization of purified *Ct* condensin holocomplexes

The gel filtration profile suggested that the purified condensin complex was monomeric and did not aggregate into multimers under the purification conditions (**Figure 10B**). In order to visualize the condensin holocomplex, I performed rotary shadowing followed by electron microscopy. I sprayed the purified protein complex onto mica sheet, dried the samples and coated them with a layer of Platinum (Pt) and Carbon (C) at a low angle, followed by imaging in a transmission electron microscope. I observed separate complexes on the imaging surface and was able to distinguish several distinct features, like the globular SMC hinge domain, coiled-coils and head domains (**Figure 12A**). In some instances, I observed isolated SMC subunits, whereas in others, I

was able to identify the HEAT-repeat subunits in the vicinity of the head domains (magnified image **Figure 12A**). This is consistent with the results of the mass spec analysis.

In addition, I also observed complexes with different conformations of the coiled-coil arms (**Figure 12B**). Similar to what has been observed for *Sc* condensin holocomplexes (Terakawa et al., 2017), I could distinguish at least four different shapes resembling the letters V, O, Y and I. V-type complexes have two open coiled-coil arms which are connected only at the globular hinge domain at one end and separated ATPase head domains. O-type complexes are connected at the hinge and head domains to form a ring-shaped structure. Y-type complexes have partially aligned coiled-coil arms starting from the hinge, which separate towards the head domains. In I-type complexes, the arms are fully aligned with each other along the entire length. These results indicate that the coiled-coil arms of *Ct* condensin complexes have the same structural flexibility as *Sc* condensin complexes.

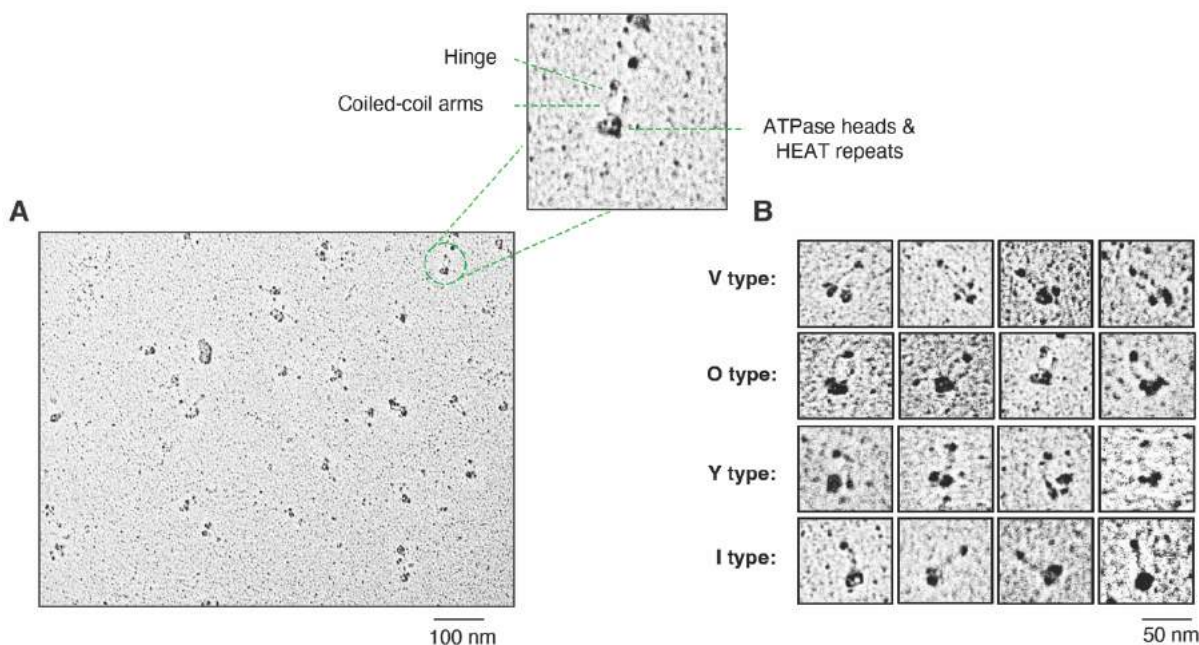


**Figure 12: Structural characterization of purified *Ct* condensin holocomplexes.** **A.** Purified *Ct* condensin complex (0.06  $\mu\text{M}$ ) were treated for rotary shadowing. Individual condensin complexes were imaged with electron microscope. All the features of SMC complex like hinge, coiled-coil and heads with HEAT repeats can be seen in the magnified image; **B.** Examples of protein complexes with different orientation of coiled-coil arms.

However, this method has one major caveat: the sample preparation includes harsh treatment where samples are dried under high vacuum and coated with Pt/C on the mica surface. Difference in the coiled-coil conformations observed in these micrographs could partially be a result of experimental artefacts.

#### 1.4 *Ct* condensin holocomplex displays DNA-stimulated ATPase activity

One of the common features of SMC proteins is their ability to hydrolyze ATP sandwiched between their ATPase head domains, although all SMC complexes studied so far display rather low ATPase rates in vitro. This is also the case for the Smc2 and Smc4 subunits of the condensin complex, which have been structurally and biochemically characterized before (Hassler et al., 2019). Since condensin's ATPase activity is required to compact DNA, I quantified the ATP hydrolysis rates (number of ATP molecules hydrolyzed per second by one condensin complex) of *Ct* condensin in the presence and absence of DNA.

I performed radioactive ATP hydrolysis assays by incubating purified *Ct* condensin (0.5  $\mu$ M) at temperatures ranging from 25 to 50°C with 5 mM ATP with or without a relaxed DNA substrate for 10 min. I spotted the samples onto a thin layer chromatography (TLC) membrane at regular time intervals and then separated ATP and ADP using a polar buffer (**Figure 13A**).

The results of the ATPase assay show that the condensin protein complex hydrolyzes ATP at basal rates (0.5-3.3 molecules/sec from 25°C to 50°C) that can be stimulated by DNA approximately 2.5-fold (2.0-7.2 molecules/sec from 25°C to 50°C) (**Figure 13B**). The *Ct* condensin complex displayed the highest ATPase activity at 50°C among all tested conditions, consistent with the report that *Chaetomium* is a thermophilic fungus. Note that spontaneous ATP hydrolysis at 50°C could affect the basal activity at this temperature.

When I tested an ATP-binding deficient 'Q-loop' mutant (Smc2 Q147L, Smc4 Q421L), I observed no ATPase activity. As expected, the mutant complex is enzymatically inactive (**Figure 13C, D**).

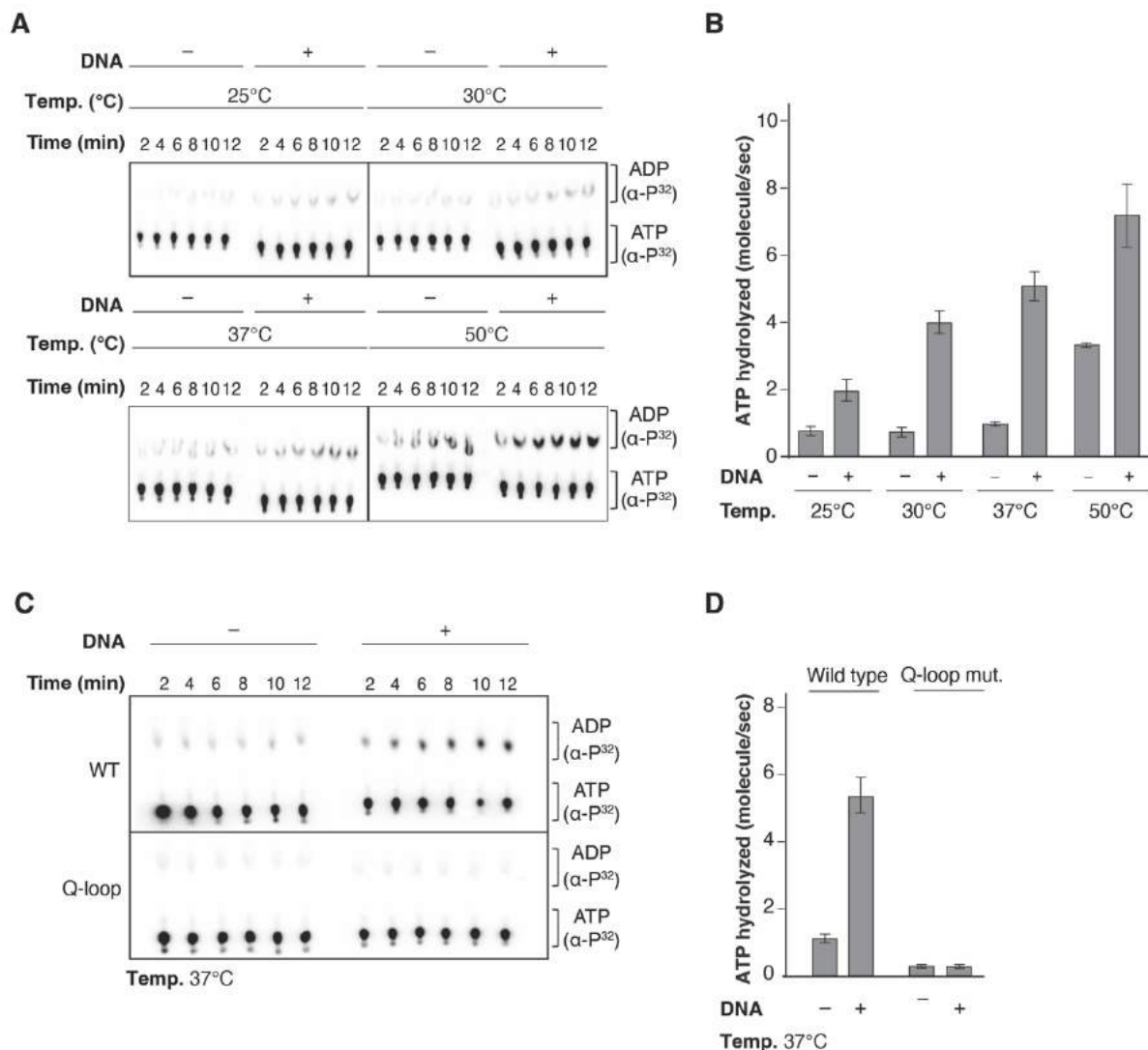


**Figure 13: *Ct* condensin holocomplex displays DNA-stimulated ATPase activity.** **A.** Representative images of TLC plates with two distinct fractions of ATP and ADP after ATP hydrolysis by *Ct* condensin protein complex under various conditions as indicated; **B.** ATPase rates of *Ct* condensin holocomplex (0.5 μM) with or without DNA (25 nM 6.4 kbp) at different temperatures as indicated. The error bars indicate standard deviation (SD) and are calculated from at least 3 independent experiments; **C.** Representative images of TLC plates with wild type condensin complex and ATP binding deficient mutant ‘Q-loop mutant’ same as in A, note the zero to almost no intensity for ADP; **D.** ATPase rates for wild type condensin complex and ‘Q-loop mutant’ at 37°C, error bars indicate standard deviation (SD) and are calculated from at least 3 independent experiments.

### 1.5 *Ct* condensin holocomplex has DNA binding activity

*Sc* condensin complex has been previously shown to bind DNA in gel shift assay (Kschonsak et al., 2017). To directly visualize the DNA binding property of *Ct* condensin, I performed Electrophoretic Mobility Shift Assay (EMSA). I used 6-carboxyfluorescein (6-FAM) labelled dsDNA of 35 bp and 51 bp (5 nM) as substrates and incubated them with increasing amounts of *Ct* condensin holocomplex (as indicated) with or without ATP (1 mM). After a brief incubation of 10-15 min, I separated unbound (U) and protein-bound (B) DNA complexes by electrophoresis.

The *Ct* condensin holocomplex shifts DNA starting at a protein concentration of 10 nM for 51 bp dsDNA whereas ~ 40 nM protein is needed to upshift the 35 bp dsDNA (**Figure 14**). I observed no notable differences in DNA binding in the presence of ATP.

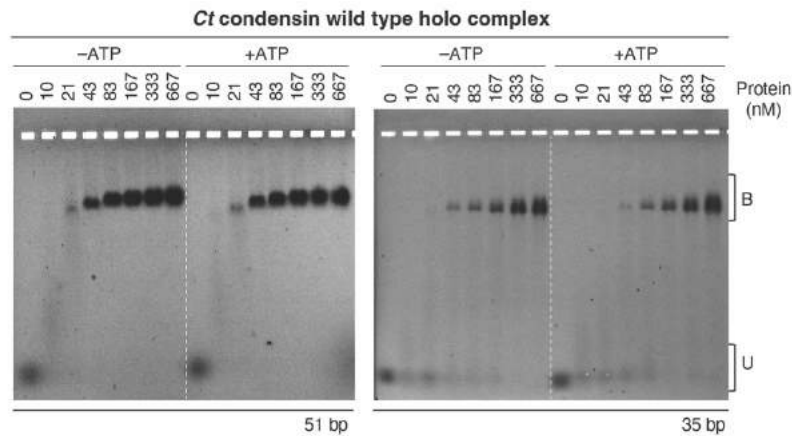


**Figure 14: *Ct* condensin holocomplex has DNA binding activity.** Gel shift assay of fluorescently labeled 35 bp and 51 bp dsDNA in presence of increasing amount of condensin complex with or without 1 mM ATP. The unbound and the protein-bound fraction of DNA is indicated as ‘U’ and ‘B’ respectively.

### 1.6 DNA compaction by the *Ct* condensin holocomplex

So far, I have observed ATPase activity and DNA binding by *Ct* condensin complex. To test whether this complex can also compact DNA, I imaged plasmid DNA by rotary shadowing in the

presence and absence of condensin complex. I sprayed a 6.4-kb relaxed plasmid onto mica, dried the samples, coated them with Pt/C and imaged them in the electron microscope.

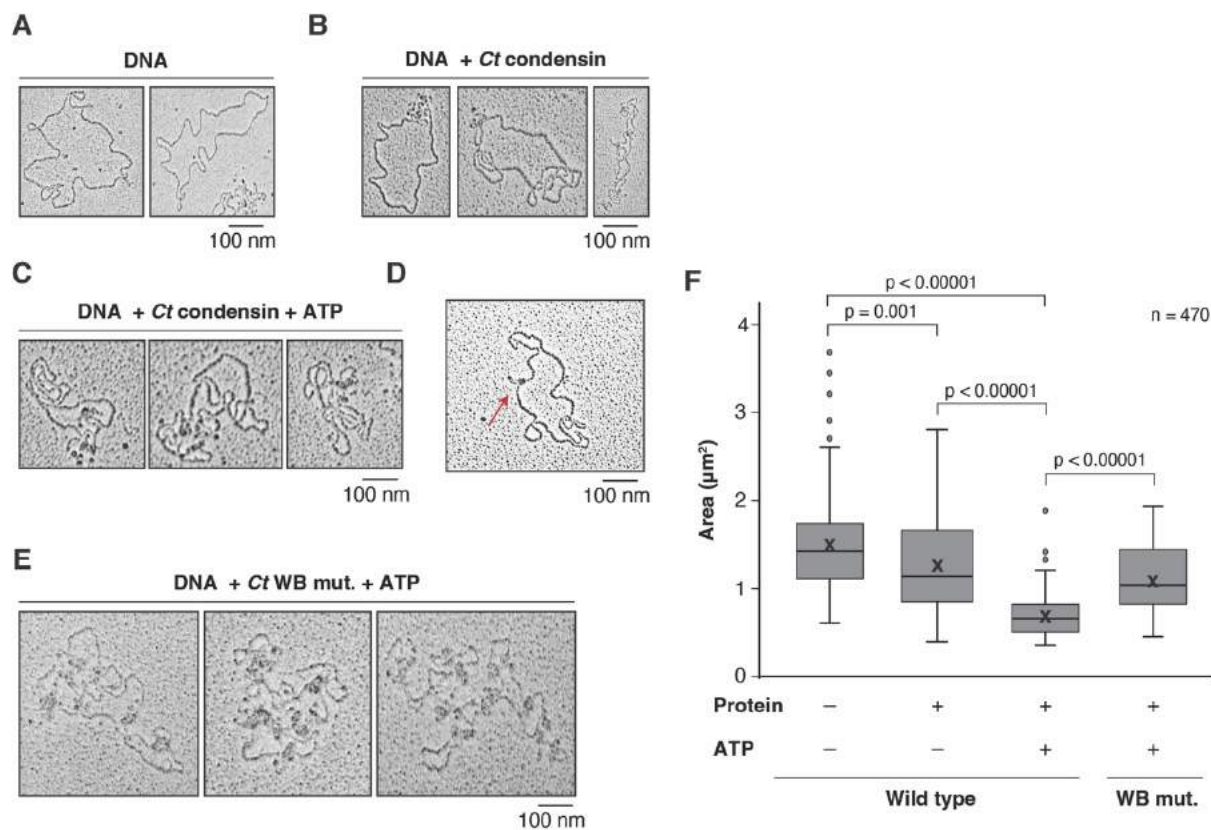


**Figure 15: DNA compaction by the *Ct* condensin holocomplex.** A-E. Example micrographs obtained by rotary shadowing followed by electron microscopy of plasmid DNA under different conditions. A - only DNA, B - DNA only with  $0.06 \mu\text{M}$  protein, C - DNA with both protein and  $1 \text{ mM}$  ATP, D - a single condensin complex on DNA as indicated by red arrow, E - DNA with condensin  $0.06 \mu\text{M}$  walker B mut. complex with ATP; F. DNA compaction quantification plot where the area of DNA is plotted against different protein conditions. The lines indicate median, crosses indicate mean, box represents first and third quartile of the data and the whiskers mark the median  $\pm 1.5$  (third quartile – first quartile). A total of 470 DNA from each date set were randomly selected and the area within was calculated. Mann-Whitney P-test was performed (significance  $< 0.05$ ), p value indicates the degree of difference between the data sets.

In the absence of protein, I observed circular DNA plasmids (**Figure 15A**). In most cases, the DNA was laid out without overlapping strands, forming a complete circle. When I incubated the DNA with protein ( $0.06 \mu\text{M}$  condensin holocomplex) but without ATP, the plasmid DNA images resembled those of the DNA-only samples, with some cases of DNA overlap (**Figure 15B**).

The degree of overlapping DNA strands dramatically increased when I added 1 mM ATP to the DNA-protein samples. Most plasmids appeared as compacted DNA species with many overlapping DNA strands (**Figure 15C**). In addition, I could now observe many protein complexes that frequently clustered on the DNA. To observe single condensin complexes on DNA, I diluted the protein concentration to 0.001  $\mu\text{M}$ . This allowed imaging of single condensin complexes on one plasmid DNA molecule (**Figure 15D**). In these cases, the protein bound to the DNA molecule in the vicinity of its SMC heads domains and the HEAT-repeat subunits.

To quantify the compaction of DNA by *Ct* condensin, I measured the surface area covered by each plasmid DNA molecule under the different conditions. To calculate the area of a DNA molecule, I encircled them using the ‘Free-hand line tool’ in FIJI (Schindelin et al., 2012) and calculated the area within. The area covered by DNA of the DNA-only sample and the DNA-with-protein sample in the absence of ATP were similar (median  $\pm$  SD,  $1.34 \pm 0.54 \mu\text{m}^2$  and  $1.13 \pm 0.53 \mu\text{m}^2$ ; **Figure 15F**).

The compactness of the DNA-covered area is greatly increased in the presence of condensin and ATP (median  $\pm$  SD,  $0.67 \pm 0.22 \mu\text{m}^2$ ; **Figure 15F**). This indicates that the condensin complex actively compacts DNA in presence of ATP. To test this conclusion, I used an ATPase-deficient ‘Walker B’ mutant (Smc2 E1116Q, Smc4 E1475Q). The mutant complex bound to the plasmid DNA but failed to compact DNA to the same extent as the wild-type complex in the presence of ATP (median  $\pm$  SD,  $1.10 \pm 0.35 \mu\text{m}^2$ ; **Figure 15E, F**). The electron micrographs showed more protein clusters than in the case of the wild-type complex (**Figure 15E**). This analysis suggests that the purified *Ct* condensin compacts DNA in a manner that depends on its ATPase activity.

In summary, I succeeded in the expression and purification of *Ct* condensin holocomplexes from insect cells to homogeneity. Rotary shadowing experiments showed that the complexes are intact and also suggested that *Ct* condensin can compact DNA in an ATP-dependent manner. The *Ct* condensin complex binds DNA and displays ATPase activity, which is increased in the presence of DNA.

## 2 *Ct* condensin compacts DNA by loop extrusion

### 2.1 Microfluidics set up

Real time DNA loop extrusion was first visualized with the *Sc* condensin complex using a custom-made microfluidics device (Ganji et al., 2018). For my study of *Ct* condensin, I have used a similar device with minor modifications. Briefly, I chemically modified glass slides with holes arranged in a manner showed below (**Figure 16**) and passivated slide and cover slip with PEG and PEG-biotin. By using two-sided sticky tapes, I attached the cover slip onto the glass slide, thereby creating microfluidics chambers. After assembly of the device, I coated the imaging surface with streptavidin.

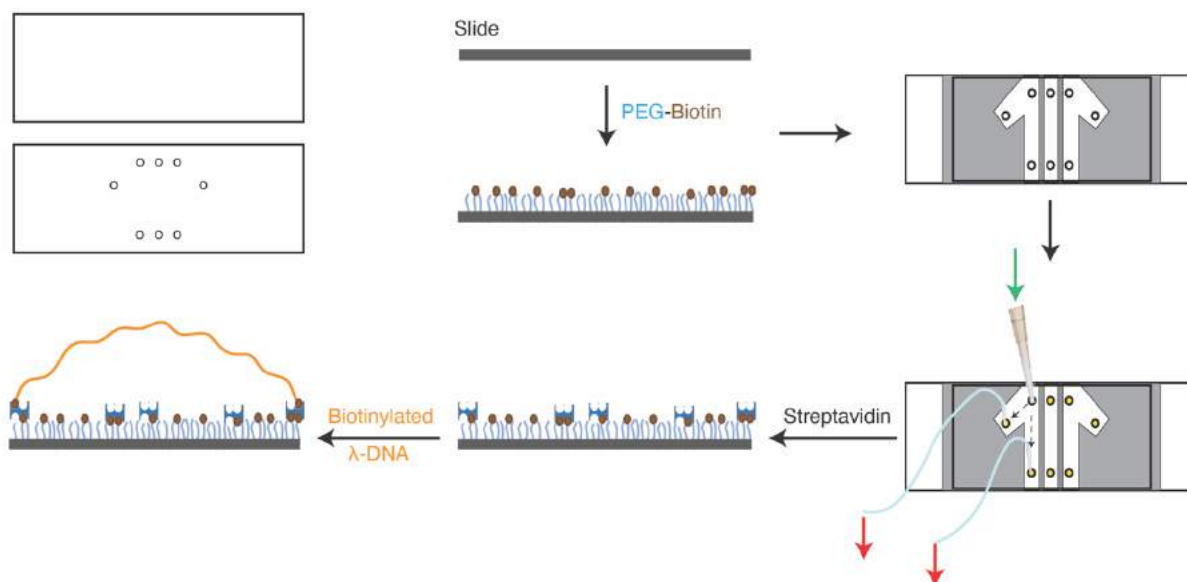


**Figure 16: Microfluidics set up.** Visual representation of different steps used in making each microfluidics device for imaging. The green arrow indicates the inlet for introducing DNA, imaging buffer, protein etc. and the red arrow indicates the direction of the outlet using a mechanical pump. The DNA is stained orange to illustrate that it is intercalated with Sytox Orange (SxO).

## 2.2 Imaging set up

All imaging for this study was performed at the EMBL Advanced Light Microscopy Facility. I placed the assembled imaging device under the microscope and subsequently flowed in biotinylated lambda DNA ( $\lambda$ -DNA, 48,502 bp), which was fluorescently labeled with the intercalating dye Sytox Orange (500 nM, SxO) using a mechanical pump with a flow rate of 2-8  $\mu$ l/min. I used a 532 nm LASER at Highly Inclined and Laminated Optical sheet (HILO) mode to visualize the DNA on a Leica GSDIM TIRF microscope (**Figure 17A, B**). Whereas a conventional confocal microscope illuminates the entire sample-field, a TIRF microscope ensures sample illumination of only first 100-200 nm of the sample plane, thus I could image individual DNA molecules (**Figure 17C**). I manually controlled the flow rate for DNA binding in the imaging device. The bound DNAs were either tethered on one or both sides, for my studies I only focused on double-tethered DNA molecules (**Figure 17D**).

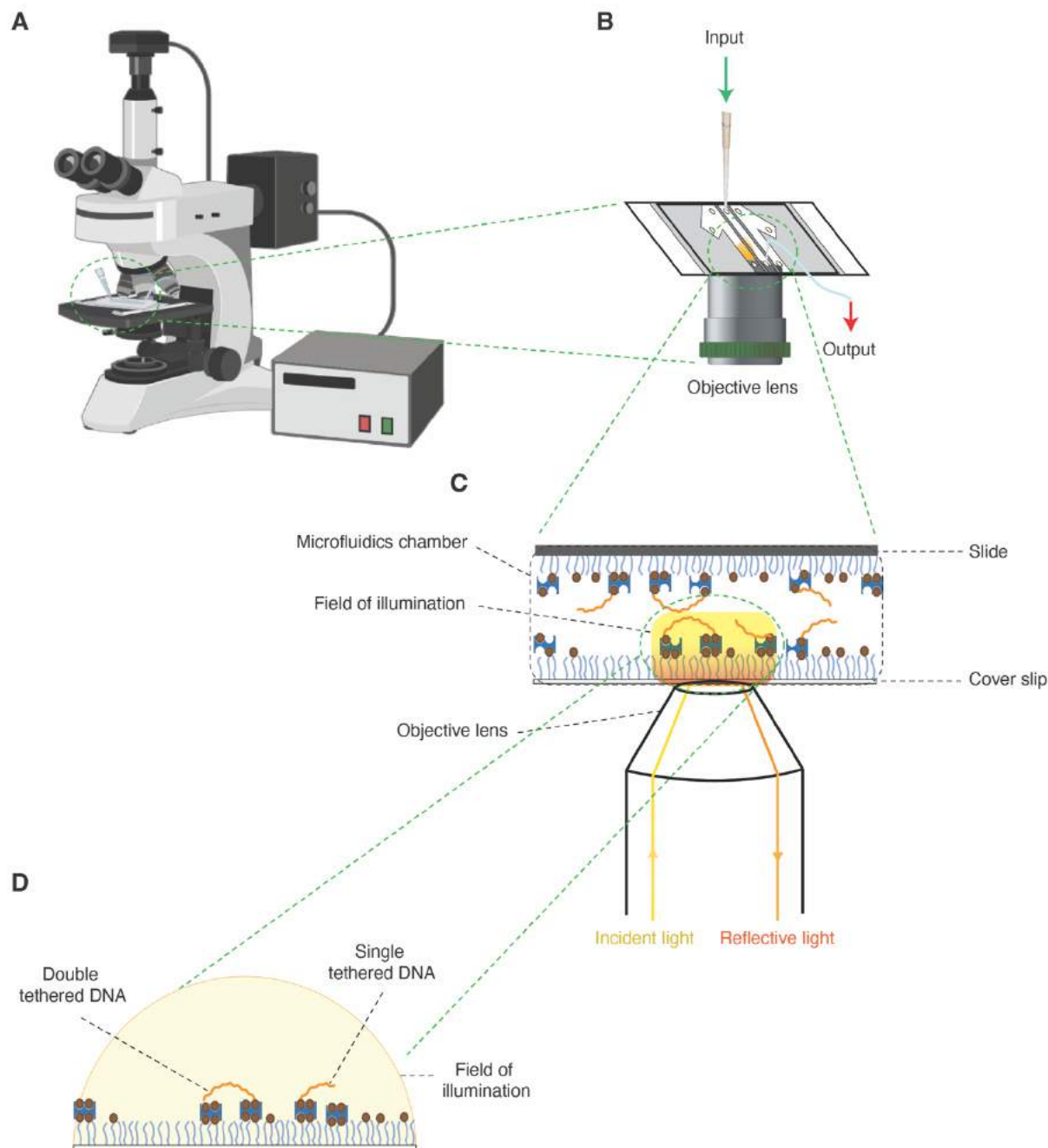


**Figure 17: Imaging set up.** **A.** A schematic of an assembled microfluidics imaging device staged under a fluorescence microscope. (Adopted from ‘Fluorescence microscope’ by BioRender.com, 2022. Retrieved from <https://app.biorender.com/biorender-templates>); **B.** Magnified image of the imaging device placed on top of an objective lens for sample illumination, the green arrow indicates sample inlet whereas the red arrow indicates the direction of flow as achieved by using a mechanical pump. (Adopted from ‘Objective’ by BioRender.com (2022). Retrieved from <https://app.biorender.com/biorender-templates>); **C.** Schematic illustration of a single microfluidics chamber within the imaging device and the illuminated area by TIRF microscopy is shown; **D.** Both double-tethered and single-tethered DNA was imaged within the field of sample illumination, only double-tethered DNA were analyzed.

### 2.3 Visualization of DNA loop extrusion by *Ct* condensin holocomplex

After assembling the imaging device and loading DNA, I flowed in 1 nM purified *Ct* condensin holocomplex with 1 mM ATP using the same flow direction (**Figure 18A**). In this exemplary image, the DNA is shown with pseudo color magenta. Whereas the SxO fluorescence signal was equally distributed over the length of the  $\lambda$ -DNA before addition of the protein (0 sec, **Figure 18B**), the fluorescence signal intensified at one spot (bright orange/yellow dot) after adding protein (35 sec, **Figure 18A, B**). These fluorescent dots or speckles became more intense over time (70 and 130 sec, **Figure 18B**).

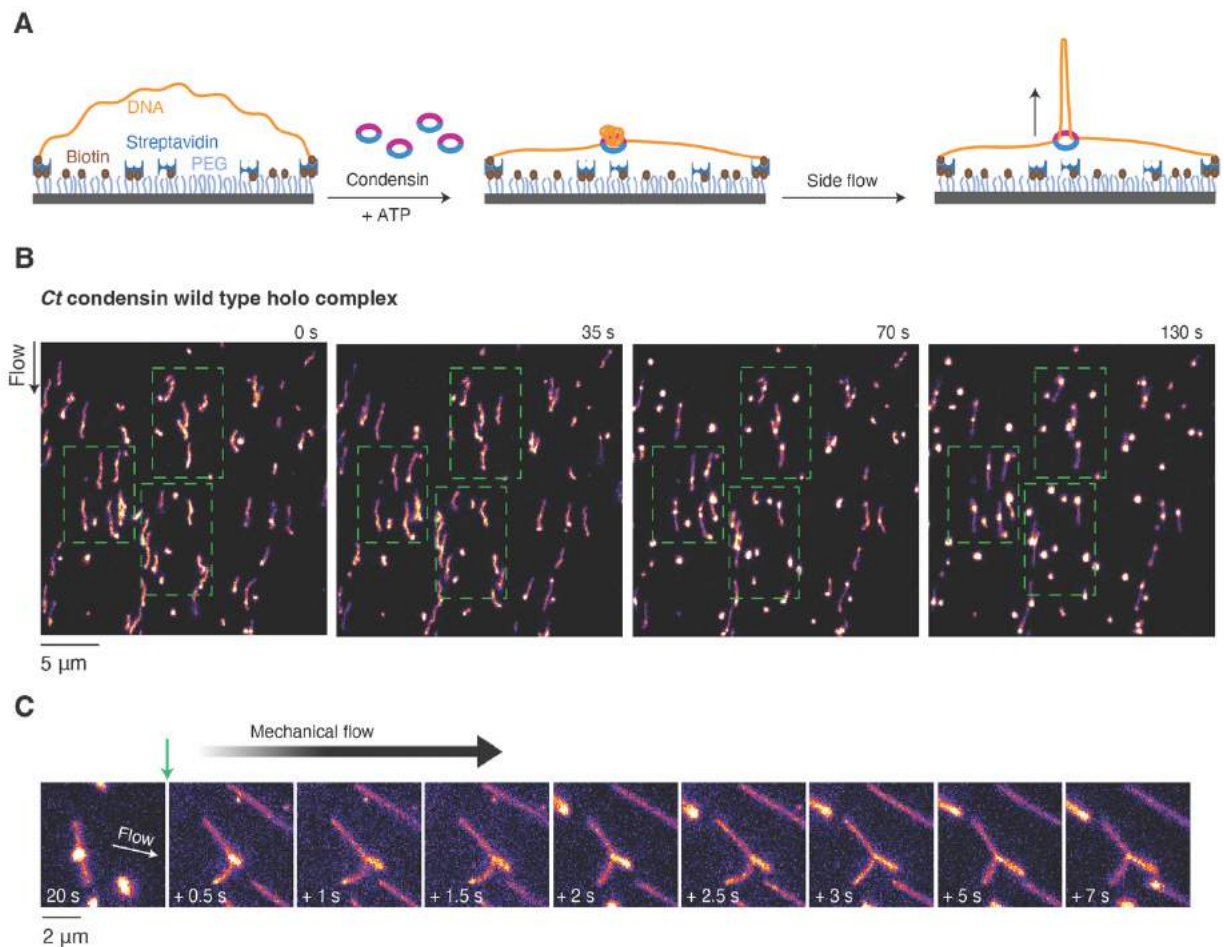


**Figure 18: Visualization of DNA loop extrusion by *Ct* condensin holocomplex.** **A.** Schematic representation of double-tethered DNA bound to a modified glass surface and loop formation on DNA, which could be extended using a flow at an acute angle to the DNA axis; **B.** Image sequence of an event where intense dots were observed

after flushing in *Ct* condensin protein complex in an imaging field of view. The green rectangles indicate the DNAs with such dots and how they grew in size over time; C. Image sequence of a single double-tethered DNA with an existing intense dot after passing condensin protein complex using the same flow direction, the image was taken 20 sec after the protein was flowed in. Once a mechanical flow was applied at an acute angle to the DNA, the compacted DNA region was extended and a loop was visible in the direction of the flow. The green arrow indicates the time when the mechanical flow was applied.

This observation suggested that the condensin protein complex catalyzes the formation of these intense dots of DNA that correspond to DNA loops, or that condensin forms non-active protein aggregates on DNA, thus accumulating fluorescence signal.

To distinguish between the two possibilities, I first applied condensin holocomplex same as mentioned above and observed similar dot, I then switched to other flow to manually apply a side flow at an acute angle to DNA axis (side flow, **Figure 18A**). This extended the compacted DNA region into a loop (**Figure 18C**) suggesting that *Ct* condensin holocomplex can extrude DNA loops.

## 2.4 Resolving DNA loop extrusion by side flow

To directly observe the process of DNA loop extrusion, I flowed in biotinylated  $\lambda$ -DNA as described above. I then introduced the condensin complex into the imaging chamber while using side flow (15  $\mu$ l/min), which resulted in the formation of arcs for DNA molecules that were tethered to the surface at both ends (0 sec, **Figure 19A**). Within a few seconds, recognizable intense dots of fluorescence became visible on some DNA arcs (3 sec, **Figure 19A**). The dots then increased in size and, due to the side flow, they were stretched into loop structures (16 sec, **Figure 19A**). However, due to the high flow rate, these loops frequently snapped (44 sec, **Figure 19A**).

One additional example of loop extrusion by the *Ct* condensin complex using side flow also has been shown (**Figure 19B**). These examples demonstrated that the DNA compaction observed by *Ct* condensin corresponds to the extrusion of DNA loops.

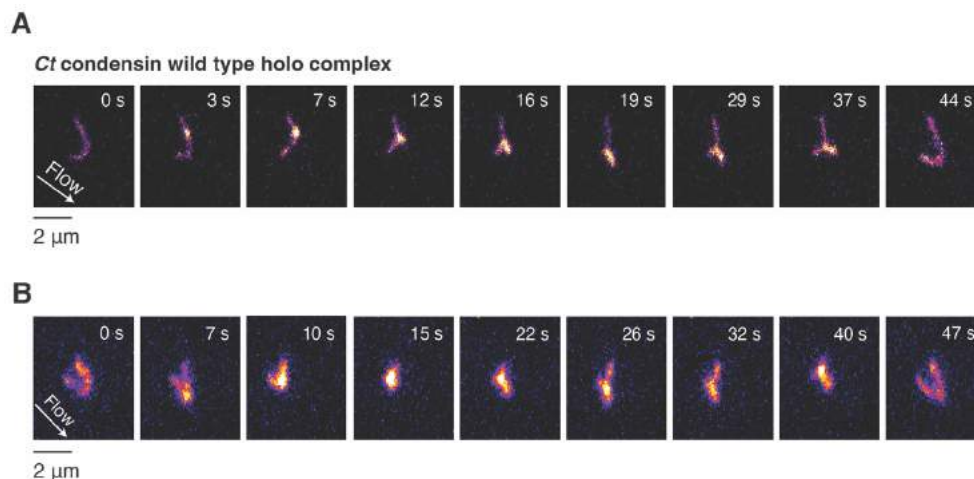


**Figure 19: Resolving DNA loop extrusion by side flow. A-B.** Image sequence of two separate events of loop extrusion by the *Ct* condensin holocomplex on double-tethered DNA. The arrows indicate the direction of the flow which was used to introduce protein into the imaging chamber.

## 2.5 DNA loop extrusion by *Ct* condensin is strictly asymmetric

After I had successfully demonstrated DNA loop extrusion by *Ct* wild type condensin complex, I characterized the biophysical properties of this process. I first flowed DNA into the imaging chamber (at 2-8  $\mu\text{l}/\text{min}$ ), followed by condensin (1 nM) in the presence of 1 mM ATP using the same flow direction. This created single and double-tethered DNAs which were now oriented parallel to the direction of flow. Within a few seconds of flowing in protein, intense fluorescent dots started to appear on DNA molecules, similar to the ones shown in **Figure 18B**.

I then selected one of these DNAs (**Figure 20A**) and generated a kymograph by stacking all frames for the length of imaging (usually 2-8 min, **Figure 20B**). The kymographs uses same pseudo color scheme for DNA and loop as mentioned before. At the beginning the experiment, an extended DNA molecule is visible before the extrusion starts by condensin (0 sec, **Figure 20A**). After addition of protein, an intense dot of fluorescence emerges on the DNA molecule (10 sec, **Figure 20A**) and then increases in intensity over time (16-73 sec, **Figure 20A**).

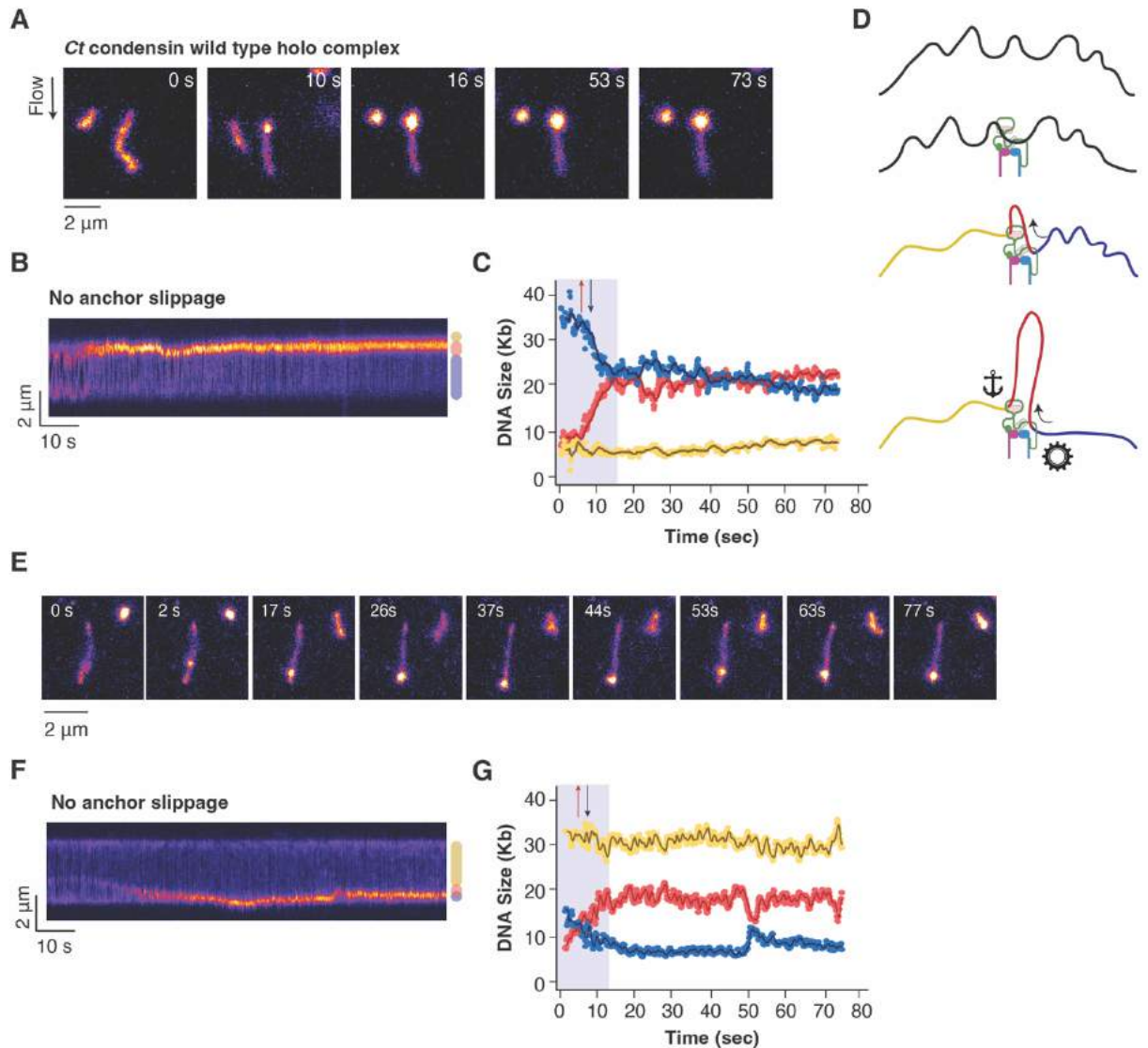


**Figure 20: DNA loop extrusion by *Ct* condensin is strictly asymmetric.** **A.** Image sequence of a DNA loop extrusion event by *Ct* condensin complex, DNA is stained with SxO and is visualized using pseudo color in FIJI. The arrow indicates the direction of flow used to add protein; **B.** The kymograph here represents the extrusion events when projected in 2D, the DNA within the loop is indicated as red, DNA above the loop as yellow and below the loop as blue; **C.** The quantification plot shows change in the DNA size during the loop extrusion event, the color code is same as described in B. The red and blue arrows indicate the increase and the decrease in red and blue line respectively within the blue shaded region; **D.** Schematic representation of the sequence of events happening in A; **E.** Image sequence of a second loop extrusion event as in A; **F.** A representative kymograph of event depicted in E same as in B; **G.** Quantification of the loop extrusion event shown in E as in C.

To quantitate this DNA loop extrusion process, I used a custom-made image analysis algorithm (courtesy of Dr. Indra A. Shaltiel) in FIJI (Schindelin et al., 2012). The algorithm measures the

fluorescence signals within the loop and on either side of the loop, converts them to DNA lengths (in bp) and plots these values over time (**Figure 20C**). The quantification plot represents the asymmetric nature of the loop extrusion event: the DNA within the loop (shown as a red line) increases in length as the DNA below the loop (shown as a blue line) is being reeled into the loop, whereas the DNA above the loop remains stable (shown as a yellow line). Within the blue shaded region, the loop grows only at the expense of DNA below the loop (**Figure 20C**) and hence represents an example for ‘asymmetric’ or ‘one-sided’ DNA loop extrusion. Once the loop reached an equilibrium state, the size of the loop plateaus (blue and red line at ~ 30 sec, **Figure 20C**), whereas the DNA above the loop (yellow line, **Figure 20C**) stays the same over the entire duration of extrusion event. This asymmetric loop extrusion process is illustrated in **Figure 20D** and suggests the presence of a ‘motor’ side and an ‘anchor side, respectively, in the complex. This is consistent with previously described DNA loop extrusion by the *Sc* condensin complex (Ganji et al., 2018).

An additional example for an asymmetric DNA loop extrusion event by the *Ct* condensin holocomplex is presented in **Figure 20E-G**. An intense fluorescence dot first appears near the center of the double-tethered DNA molecule and then increases in size gradually over time. The blue shaded region in the plot again marks the initial extrusion period where the loop (red line) grows as the DNA from the below the loop (blue line) is being reeled into the loop, whereas the DNA above the loop (yellow line) stays the same (**Figure 20G**). This example also shows the dynamic nature of the DNA loop, since the loop sometimes decreases in size, presumably due to DNA slippage through the protein binding sites.

## 2.6 Anchor slippage of *Ct* condensin holocomplex during loop extrusion

So far, I have established that the *Ct* condensin complex loop extrudes DNA in an asymmetric (one-sided) manner (**Figure 20**). Further analysis of DNA loop extrusion events revealed that the condensin complex occasionally seemed to slip during a loop extrusion event on the double-tethered DNA (**Figure 21**). For example, the DNA molecule marked with green circle showed an intense fluorescent dot that appeared near the bottom anchor point, representing a DNA loop (7 sec, **Figure 21A**). The dot increased in size and simultaneously migrated towards the central region

of the DNA (note that this movement is in the opposite direction of the buffer flow, 22-36 sec; **Figure 21A**). The kymograph also shows that the beginning of loop extrusion started at the bottom of the double-tethered DNA and then the loop moved up (**Figure 21B**). The quantification plot indicates a typical asymmetric loop extrusion event within the blue shaded region, where DNA within the loop (red line) increased with a corresponding decrease in DNA from the region above the loop (blue line), whereas the DNA below the loop (yellow line) stayed the same (**Figure 21C**). In contrast to the events described before (**Figure 20**), the DNA below the loop (yellow line) then gradually increased, while the DNA above the loop (blue line) decreased (yellow shaded region, **Figure 21C**). This can only be explained if the anchor side was slipping as the distance between the anchor point of the tethered DNA and the initial position of the anchor side of the condensin complex changed over time (**Figure 21C**). Since the migration of the loop was opposite to that of the direction of the buffer flow in the imaging chamber, anchor slippage caused by the buffer flow can be ruled out. The schematic depiction of the event mentioned above shows the slipping of the anchor of the condensin complex on the DNA during the extrusion event (**Figure 21D**).

Among many DNA loop extrusion events by the *Ct* condensin holocomplex, I noticed one event where the loop migrated along the entire length of the tethered DNA (**Figure 21E-G**). The loop can be first seen at around 4 sec near the top tethered point, then increases in size and moves downwards, and finally remains at the bottom anchor point before it snaps. Due to the angle created between the DNA axis and the direction of the flow, the loop can also be seen extended in the image sequence (21.7 sec, **Figure 21E**). The corresponding kymograph similarly displays the path of the loop (**Figure 21F**). The disappearance of the loop towards the end of the kymograph reflects the snapping of the loop, possibly due to the dissociation of the protein. The quantification plot of this event (**Figure 21G**) also follows the similar asymmetric nature as previously described, with the red line increasing, the blue line decreasing, and the yellow line remaining unchanged in the blue shaded region. Within the yellow shaded region, the yellow line increases at the expense of the blue line, similar to the slipping event described in **Figure 21C**. The sudden decrease in the red line at the end of the yellow shaded region indicates the loop snapping event.

These examples of anchor slipping by the *Ct* condensin complex during DNA loop extrusion suggest that, although the extrusion itself is one-sided, the grip of the anchor side can be loose and cause the protein complex to slip while it extrudes DNA loops.

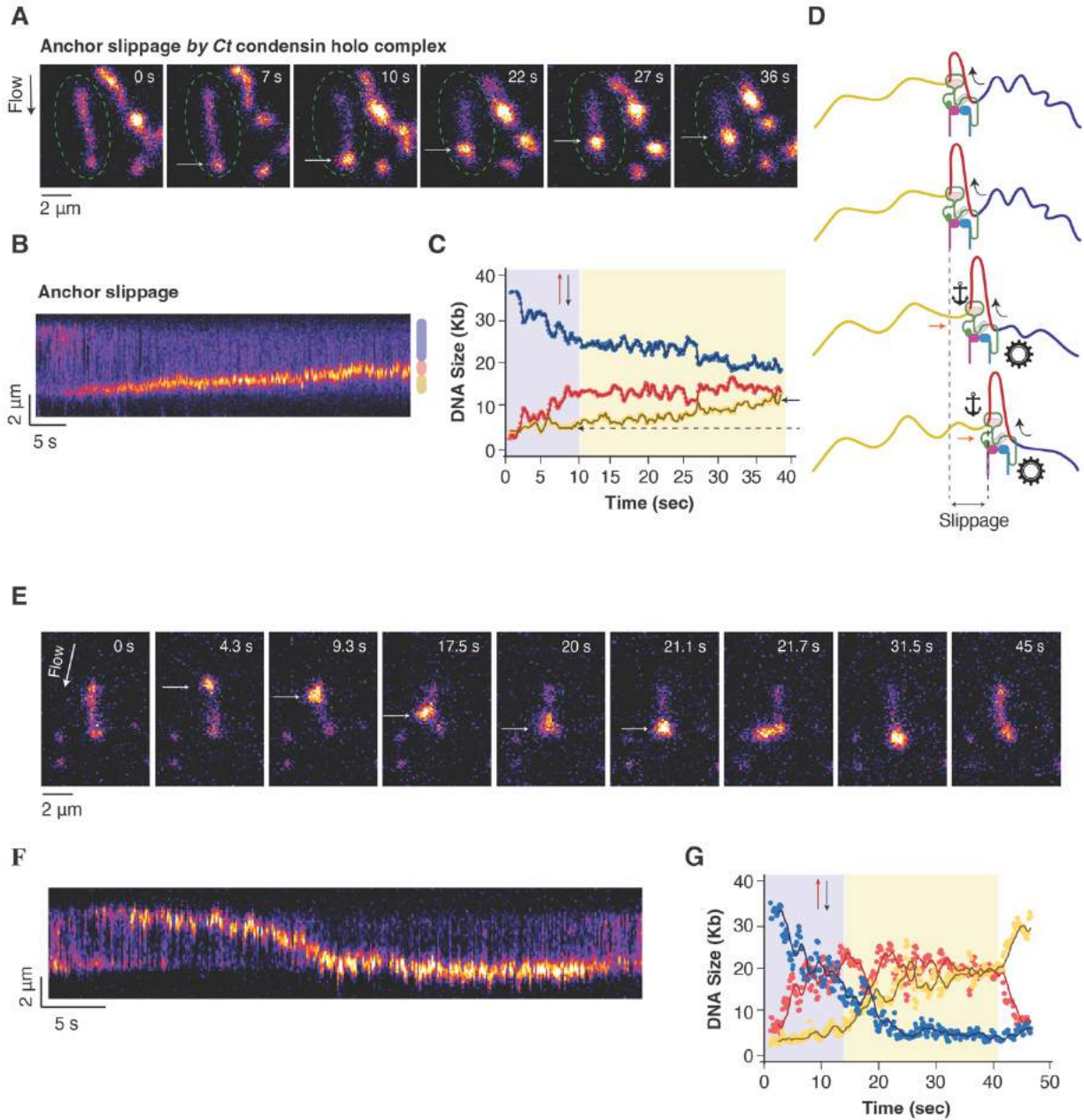


**Figure 21: Anchor slippage by *Ct* condensin holocomplex during loop extrusion.** **A.** Image sequence of a DNA loop extrusion event by *Ct* condensin complex with anchor slippage, DNA is stained with SxO and is visualized using pseudo color in FIJI. The black and the white arrows indicates the direction of flow used to add protein and the position of the loop within the DNA molecule respectively; **B.** The kymograph here represents the extrusion event, the DNA within the loop is indicated as red, DNA below the loop as yellow and above the loop as blue; **C.** The quantification plot shows change in the DNA size during the loop extrusion event, the color code is same as described in B. The red and blue arrows indicate the increase and the decrease in red and blue line respectively within the blue shaded region whereas the yellow line gradually increase within the yellow shaded region. Note that the position of the yellow line beginning of the shaded region is marked with a dotted arrow whereas the end of the line is marked with a solid arrow and the increase in the length of the yellow

line is anchor slippage; **D**. Schematic representation of the sequence of events happening in A, the red arrows indicate the direction of the slippage by condensin complex; **E**. Image sequence of a second loop extrusion event where the loop traverses the entire length of the DNA. The arrow indicates the direction of the flow used to add the protein; **F**. A representative kymograph of event depicted in E same as in B; **G**. Quantification of the loop extrusion event shown in E as in C. The blue shaded region shows the main extrusion event, the yellow shaded region shows the slipping event.

## 2.7 Properties of loop extrusion by *Ct* condensin holocomplex

One of the first values that I calculated from these DNA loop extrusion events was the rate of loop extrusion by the *Ct* condensin holocomplex. As described before, the extrusion event is strictly asymmetric, since DNA within the loop is reeled in only from one side (**Figure 20C, G**). The intensity plots describe the dynamics of such extrusion events, and the rate of extrusion can be calculated from at least 50 consecutive data points (usually 75-100 data points) of the red line in the region where the increase is most linear. The positive slope calculated from the increase of the red line during the initial extrusion period is the rate at which DNA is reeled into the loop. I calculated the rate of loop extrusion for the complex holocomplex from 55 extrusion events and obtained a value of  $780 \pm 530$  bp/s (median  $\pm$  SD, **Figure 22A**).

My previous experiments proved that *Ct* condensin displays an ATPase activity that can be stimulated by DNA (**Figure 13**) and that DNA compaction is increased in presence of both holocomplex and ATP (**Figure 15**). It is hence likely that the process of DNA loop extrusion also depends on ATP. To test this hypothesis, I performed the imaging experiments as described above but this time did not add 1 mM ATP to the imaging buffer. In this case, I observed no loops on double-tethered DNAs (0/62 DNAs, **Figure 22A**). Similarly, when I depleted  $Mg^{2+}$  ions (in the form of  $MgCl_2$ ), which is required for the coordination of ATP at the active site and nucleophilic attack of water, from the imaging conditions, I observed no loops (0/56 DNAs, **Figure 22A**). Finally, when I tested the ATP-binding deficient Q-loop mutant of *Ct* condensin, I again observed no loops (0/60 DNAs, **Figure 22A**). Collectively, these experiments prove that DNA loop extrusion by *Ct* condensin is an ATP-dependent process.

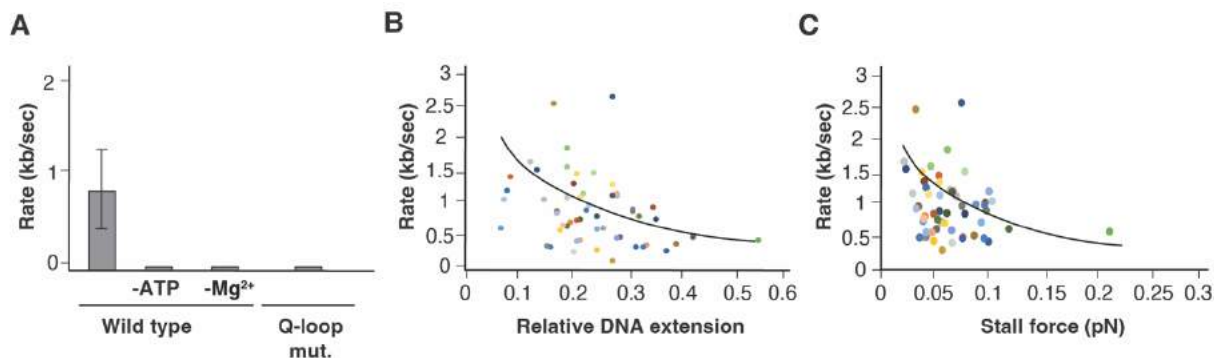


**Figure 22: Properties of loop extrusion by *Ct* condensin holocomplex.** **A.** Rate of loop extrusion of condensin holocomplex under different imaging conditions; **B.** Rate of loop extrusion is plotted against the relative DNA extension in relation to its 16.5  $\mu\text{m}$  contour length. The solid line serves as a visual guide; **C.** Rate of loop extrusion is plotted against the force exerted within the DNA due to increased DNA stretching upon loop increase. The solid line serves as a visual guide.

I next tested whether the end-to-end tether length of the double-tethered DNA affects the loop extrusion rates. With a shorter end-to-end tethered DNA, the DNA double helix is more relaxed before the start of the extrusion process and hence condensin should be able to reel in DNA faster, with less resistance to work against. This is in contrast to a longer end-to-end tethered DNA, where the DNA is already stretched before the start of loop extrusion. I calculated the relative DNA length by dividing the length of the double-tethered DNA (measured in  $\mu\text{m}$ ) in the imaging device by the contour length of  $\lambda$ -DNA ( $\sim 16.5 \mu\text{m}$ ; Salomo et al., 2006).

When I plotted the extrusion rate against the relative DNA extension, the effect of the end-to-end tether length of the  $\lambda$ -DNA became evident, as the loop extrusion rates on shorter DNA tethers showed higher rates, while longer DNA tethers showed lower extrusion rates ( $n=55$ , **Figure 22B**).

This inverse correlation between the extrusion rates and the relative extension length of DNA is also force dependent. As condensin reels in DNA within a DNA loop, the amount of free DNA between the two tethered points (excluding the loop itself) decreases and subsequently further extrusion becomes harder as condensin has to reel in DNA against more internal tension. The stalled force on the DNA molecules with loop was calculated as described in Salomo et al., 2006. When I plotted the extrusion rates against the force, I observed a similar inverse correlation

(**Figure 22C**). More than 99% of the extrusion events by holocomplex, the extrusion rates dropped significantly when the tension within the DNA reaches  $\sim 0.1$  pN. These findings suggest that *Ct* condensin is a fast DNA-loop extruding motor, which stalls at moderate forces.

## 2.8 Effect of high salt on *Ct* condensin-mediated DNA loop extrusion

For the experiments described above, I have used a relatively low amount of salt in my imaging experiments, as reported for previous experiments with *Sc* condensin (50 mM; Ganji et al., 2018). As for many DNA-binding proteins, salt concentrations play a huge role for the affinity of the interaction. To test the effect of high salt on *Ct* condensin loop extrusion, I first flowed in DNA in imaging buffer containing 50 mM salt, as usual, and then introduced the *Ct* condensin complex in buffer with 125 mM salt. Unlike the high frequency of DNA loop extrusion events observed in low salt buffer (loops on  $\sim 60\%$  of the double-tethered DNAs, **Figure 32A**), the presence of high salt conditions greatly reduced the loop extrusion efficiency (10/37 DNAs). However, the extrusion events observed under these conditions were still asymmetric (for an example, see **Figure 23A-C**). The loop starts at  $\sim 2.5$  sec and lasts only till 22 sec, whereafter it snaps (**Figure 23A**). The kymograph and the quantification plot show a typical loop extrusion pattern with one-sided extrusion in the blue shaded region and rapid decrease in the DNA loop size after loop snapping (red line, **Figure 23B, C**).

Upon analyzing the extrusion events with high salt, I observed an example where the DNA loop size gradually decreased and then completely disappeared (**Figure 23D**). At the beginning of the image acquisition period, a loop near the top anchor point could already be seen (marked with a green circle, 0 sec), which maintained the same fluorescence intensity for 20 sec. The fluorophore intensity then decreased till a distinguishable intense dot could no longer be seen (39-54 sec, **Figure 23D**). This gradual decrease in the fluorophore intensity is most likely due to a reduced DNA binding affinity of condensin in the presence of the increased salt concentration. The representative kymograph shows the bright yellow/orange line (loop in DNA) continue to reduce in intensity and towards the end no clear intensity was seen (**Figure 23E**). The quantification plot

validates this observation with a 20-kb DNA size within the loop at the beginning, which then gradually goes down as the blue line (DNA below the loop) increases in size (**Figure 23F**).

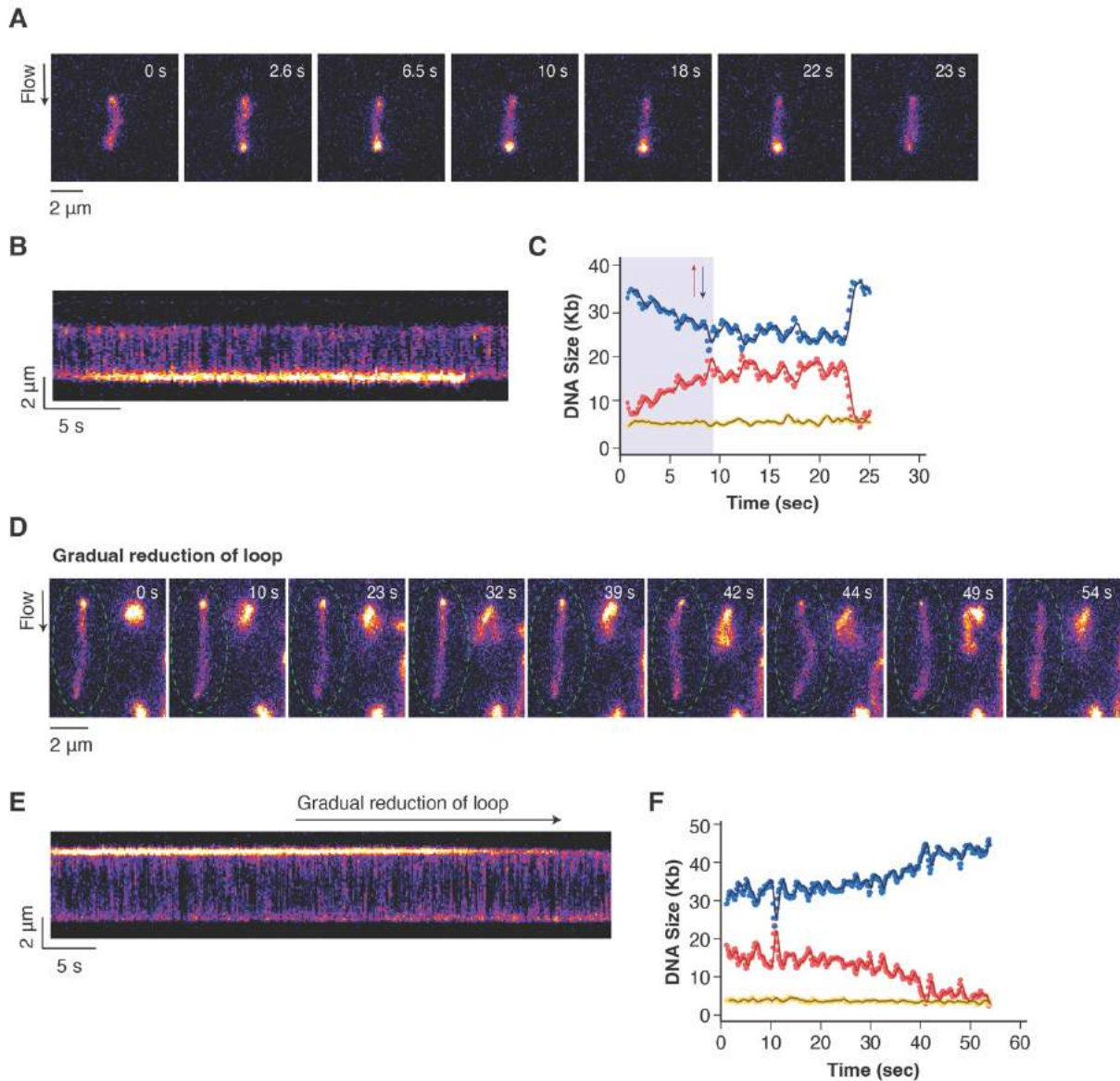


**Figure 23: Effect of high salt on *Ct* condensin-mediated DNA loop extrusion.** **A.** Image sequence of a DNA loop extrusion event by *Ct* condensin complex at 125 mM salt concentration, DNA is stained with SxO and is visualized using pseudo color in FIJI. The arrow indicates the direction of flow used to add protein; **B.** The kymograph here represents the extrusion events when projected in 2D, the DNA within the loop is indicated as red, DNA above the loop as blue and below the loop as yellow; **C.** The quantification plot shows change in the DNA size during the loop extrusion event, the color code is same as described in B. The red and blue arrows indicate the increase and the decrease in red and blue line respectively within the blue shaded region; **E.** Image sequence of an event with gradual loop release as the intense fluorophore dots continues to fade away with time; **F.** A representative kymograph of event depicted in E same as in B; **G.** Quantification of the loop release event

shown in D. The red line indicating DNA within the loop which continues to decrease as the DNA below the loop (blue line) keeps increasing revealing an asymmetric nature.

Taken together, I conclude that, *Ct* condensin extrude DNA loops in a strictly asymmetric manner with occasional anchor slippage. However, in the presence of high salt (125 mM), the extrusion efficiency is rather low and formed loops can be gradually released. These findings indicate that DNA loop extrusion is a reversible process.

### 3 Characterization of the *Ct* delta Ycg1 condensin complex

#### 3.1 Purification of the *Ct* delta Ycg1 condensin complex

As mentioned before, a condensin subcomplex formed by *Sc* Ycg1-Brn1 was shown to bind DNA in co-crystal structures and a *Sc* condensin complex that was missing the Ycg1 subunit displayed reduced DNA binding (Kschonsak et al., 2017). Since mutations in this binding site caused *Sc* condensin complexes to slip during DNA loop extrusion experiments (Ganji et al., 2018), it has been suggested that the Ycg1 subunit with the attached Brn1 ‘safety belt’ forms a DNA ‘anchor site’.

To test the role of the Ycg1-Brn1 DNA binding site in the *Ct* condensin complex, I purified a *Ct* delta Ycg1 condensin complex using the same protocol as for the *Ct* condensin holocomplex. SDS-PAGE analysis of the fractions from a gel filtration step confirmed that the band corresponding to Ycg1 subunit is missing in this complex (**Figure 24A, B**).

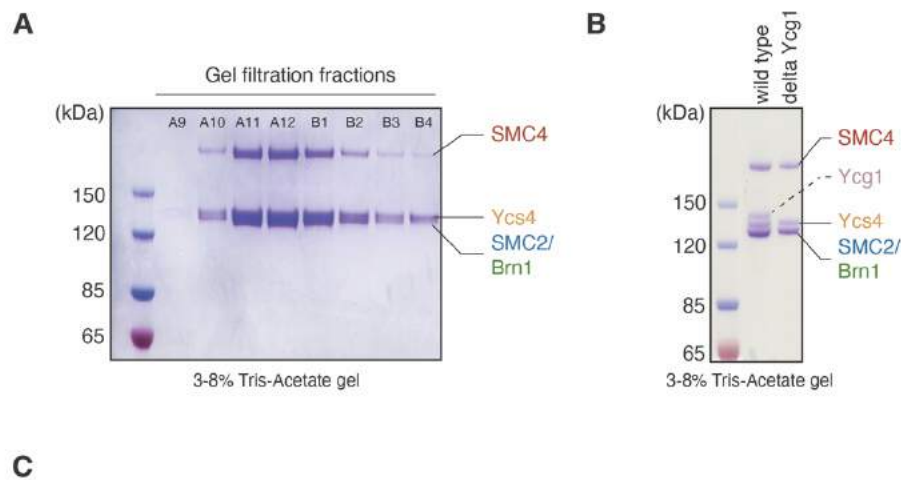


**Figure 24: Purification of the *Ct* delta Ycg1 condensin complex.** **A.** *Ct* delta Ycg1 complex was purified same as the condensin holocomplex. SDS-PAGE analysis of the protein fractions of *Ct* delta Ycg1 complex collected from gel filtration; **B.** Samples from gel filtration fractions were pooled together, concentrated and analyzed by SDS-PAGE. Both samples on A and B were ran on 3-8% Nu-PAGE gel in Tris-Acetate buffer; **C.** Mass spectrometric analysis of purified condensin complex and corresponding stoichiometric values are indicated. The value in red represents absence of Ycg1 from the complex with 1000-fold lower intensity.

I also performed mass spectrometry analysis of the delta Ycg1 condensin complex to determine the stoichiometry of the individual subunits. The mass spectrometry analysis revealed no significant contaminations, like, for example, the presence of endogenous Sf Ycg1 from the host cells. The stoichiometry analysis showed that similar intensity pattern for the SMC subunits, Brn1 and Ycs4 like in the case of the holocomplex, whereas no intensity corresponding to the Ycg1 subunit was detected (**Figure 24C**). Together with the SDS-PAGE, mass spectrometry reveals that the *Ct* delta Ycg1 complex is truly lacking the Ycg1 subunit.

### 3.2 The *Ct* delta Ycg1 complex can compact DNA

To test whether the four-subunit *Ct* delta Ycg1 complex is intact, I performed rotary shadowing as described for the holocomplex and imaged the stained complexes in the electron microscope. With the resolution limits of this method, I was able to identify tetrameric complexes (**Figure 25A**). Electron density corresponding to the globular hinge domain, coiled-coil arms and ATPase heads was visible just like for the holocomplex preparations (**Figure 25A**). Various coiled-coil conformation can also be seen in the electron micrographs.

To test whether the *Ct* delta Ycg1 complex also compacts DNA, I incubated the tetrameric complex with circular DNA and then performed rotary shadowing followed by electron microscopy. I then compared the areas enclosed by DNA after incubation with delta Ycg1 or holocomplexes. To my surprise, incubation with the *Ct* delta Ycg1 condensin complex induced a significant DNA compaction in the presence of 1 mM ATP (median  $\pm$  SD,  $0.69 \pm 0.24 \mu\text{m}^2$ ; **Figure 25C**). This data indicates that the *Ct* delta Ycg1 complex can compact DNA even without the Ycg1 subunit. However, I cannot rule out artefacts arising in this assay due to the harsh treatment during sample preparation discussed before.

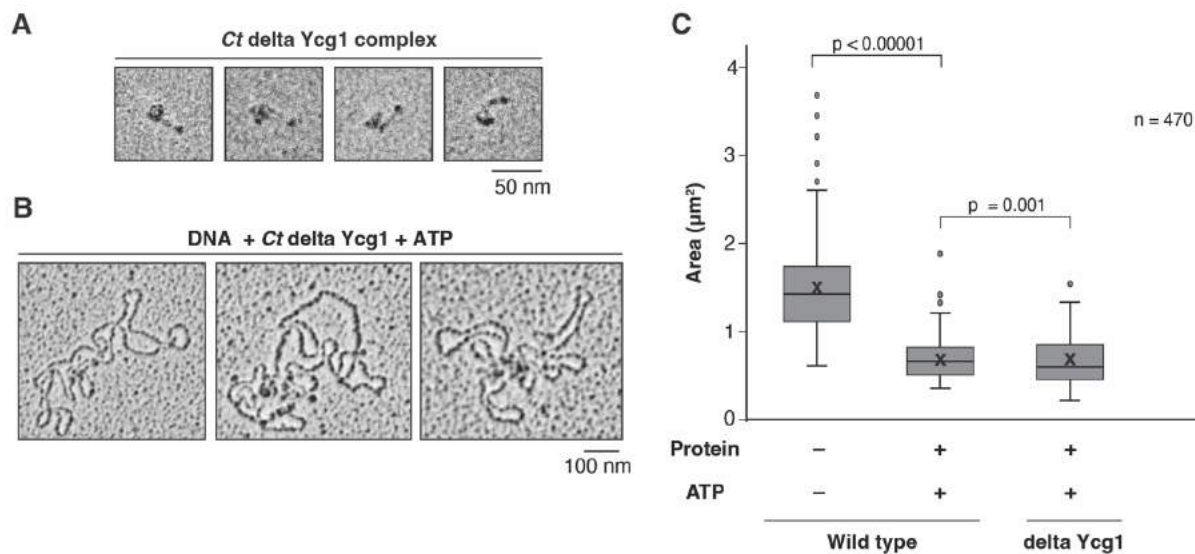


**Figure 25: The *Ct delta Ycg1* complex can compact DNA.** **A, B.** Example micrographs obtained by rotary shadowing followed by electron microscopy of *Ct delta Ycg1* condensin complex and plasmid DNA with both  $0.06 \mu\text{M}$  protein and  $1 \text{ mM}$  ATP; **C.** DNA compaction quantification plot where the area of DNA is plotted against different protein conditions. The lines indicate median, crosses indicate mean, box represents first and third quartile of the data and the whiskers mark the median  $\pm 1.5$  (third quartile – first quartile). A total of 470 DNA from each data set were randomly selected and the area within was calculated. The plot of wildtype is same in figure 15F. Mann-Whitney P-test was performed (significance  $< 0.05$ ), p value indicates degree of difference between the data sets.

### 3.3 The *Ct delta Ycg1* condensin displays DNA-stimulated ATPase activity

Given that the *Ct delta Ycg1* condensin complex compacts DNA, I next checked whether the complex also hydrolyzes ATP. Like for the holocomplex, I incubated the delta Ycg1 condensin complex with ATP for 10 min at 25, 30 and 37°C in the presence or absence of relaxed DNA.

To my surprise, the *Ct delta Ycg1* condensin complex hydrolyzed ATP and this activity was increased 2-4-fold in the presence of DNA (**Figure 26A, B**). Surprisingly, the delta Ycg1 complex displayed more ATPase activities at all temperatures tested. The difference is most prominent at 25°C, where the delta Ycg1 complex hydrolyzed twice as much ATP than the holocomplex in the presence of DNA (mean  $\pm$  SD,  $1.39 \pm 0.26$  and  $3 \pm 1.3$  molecules of ATP/s for the holocomplex and the delta Ycg1 complex, respectively). Similarly, the basal ATPase activity was almost 5 times higher (mean  $\pm$  SD,  $0.2 \pm 0.08$  and  $1.14 \pm 0.27$  for the holocomplex and the delta Ycg1 complex,

respectively). At 30 and 37°C, the DNA-stimulated ATPase rates were both similar for both condensin complexes, although the delta Ycg1 complex always had a higher basal ATPase rate.

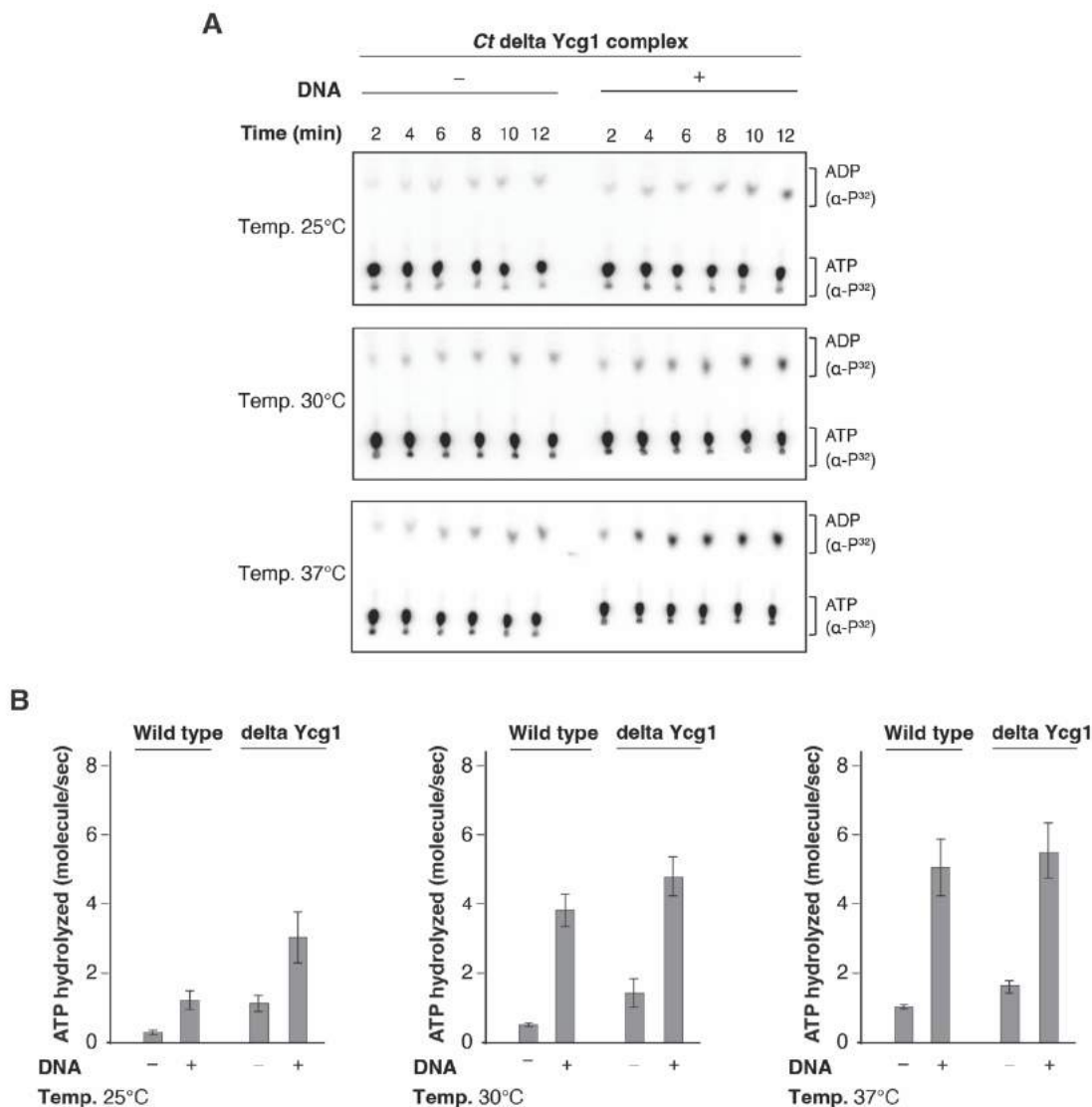


**Figure 26: The *Ct delta Ycg1* condensin displays DNA-stimulated ATPase activity.** **A.** Representative images of TLC plates with two distinct fractions of ATP and ADP after ATP hydrolysis by 0.5 μM *Ct delta Ycg1* condensin complex under various temperature as indicated; **B.** ATPase rates of *Ct* wild type and delta Ycg1 condensin complex (0.5 μM) with or without DNA (25 nM, 6.4 kb) at different temperatures as indicated. The error bars indicate standard deviation (SD) and are calculated from at least 3 independent experiments.

### 3.4 The *Ct* delta *Ycg1* complex binds DNA

Since I observed DNA compaction and DNA-stimulated ATPase activity for the *Ct* condensin complex lacking the *Ycg1* subunit (Figure 25, 26), I directly tested whether the *Ct* delta *Ycg1* complex still retained its DNA binding activity, in contrast to the tetrameric *Sc* delta *Ycg1* complex (Kschonsak et al., 2017). I therefore performed gel shift assay as described before.

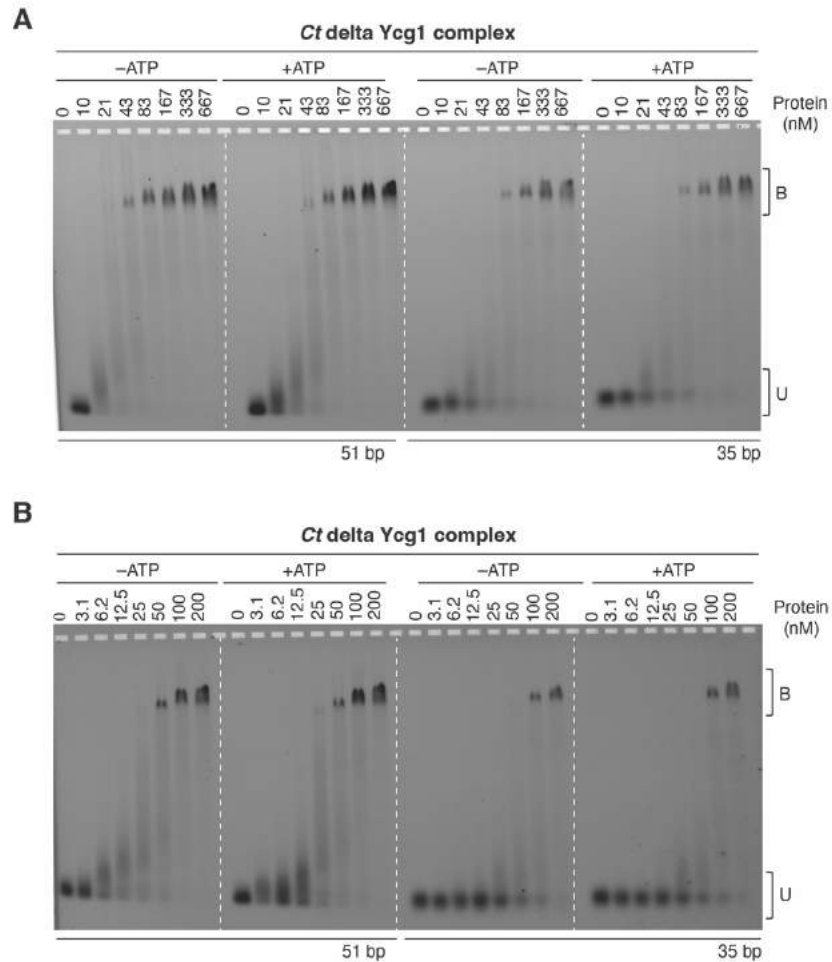


**Figure 27: The *Ct* delta *Ycg1* complex binds DNA. A-B.** Gel shift assay as in figure 14 of fluorescently labeled 35 bp and 51 bp dsDNA in presence of increasing amount of condensin complex with or without ATP. The unbound fraction of DNA is indicated as ‘U’ and the protein-bound DNA fraction is indicated as ‘B’ in the figure.

These assays revealed DNA binding of *Ct* delta *Ycg1* condensin complex to both 51 bp and 35 bp 6-carboxyfluorescein (6-FAM) labeled dsDNA substrates (5 nM) in the presence of 1 mM ATP

(**Figure 27A**). When compared to the *Ct* condensin holocomplex (**Figure 14**), the delta Ycg1 complex retained much of its DNA binding affinity. The 51 bp dsDNA started to shift up at a protein concentration as low as 10 nM, similar to what I observed for the holocomplex (**Figure 14**). In case of the 35 bp DNA substrate, DNA started to shift up at a protein concentration of around 40 nM (**Figure 27A**). When I incubated DNA with even lower protein concentrations, the delta Ycg1 complex still showed a DNA upshift (**Figure 27B**). DNA could be seen to upshift at a protein concentration as low as 6.2 nM (for 51 bp DNA), whereas 50-100 nM protein was needed to shift the 35 bp DNA.

Rotary shadowing, ATPase assay and gel shift experiments provided proof that the *Ct* delta Ycg1 complex is an active ATPase that is stimulated by DNA and that binds and compacts DNA. This is in stark contrast to what has been observed for the *Sc* delta Ycg1 condensin complex (Kschonsak et al., 2017).

## 4 The *Ct* delta *Ycg1* complex changes direction while extruding loops

### 4.1 Visualization of DNA loop extrusion by the *Ct* delta *Ycg1* condensin complex

I have purified the *Ct* delta *Ycg1* condensin complex and showed that the tetrameric complex displays ATPase activity, which can be stimulated by DNA, and binds DNA with similar affinity as the holocomplex. These findings suggested that the *Ct* delta *Ycg1* complex might also be able to extrude DNA loops.

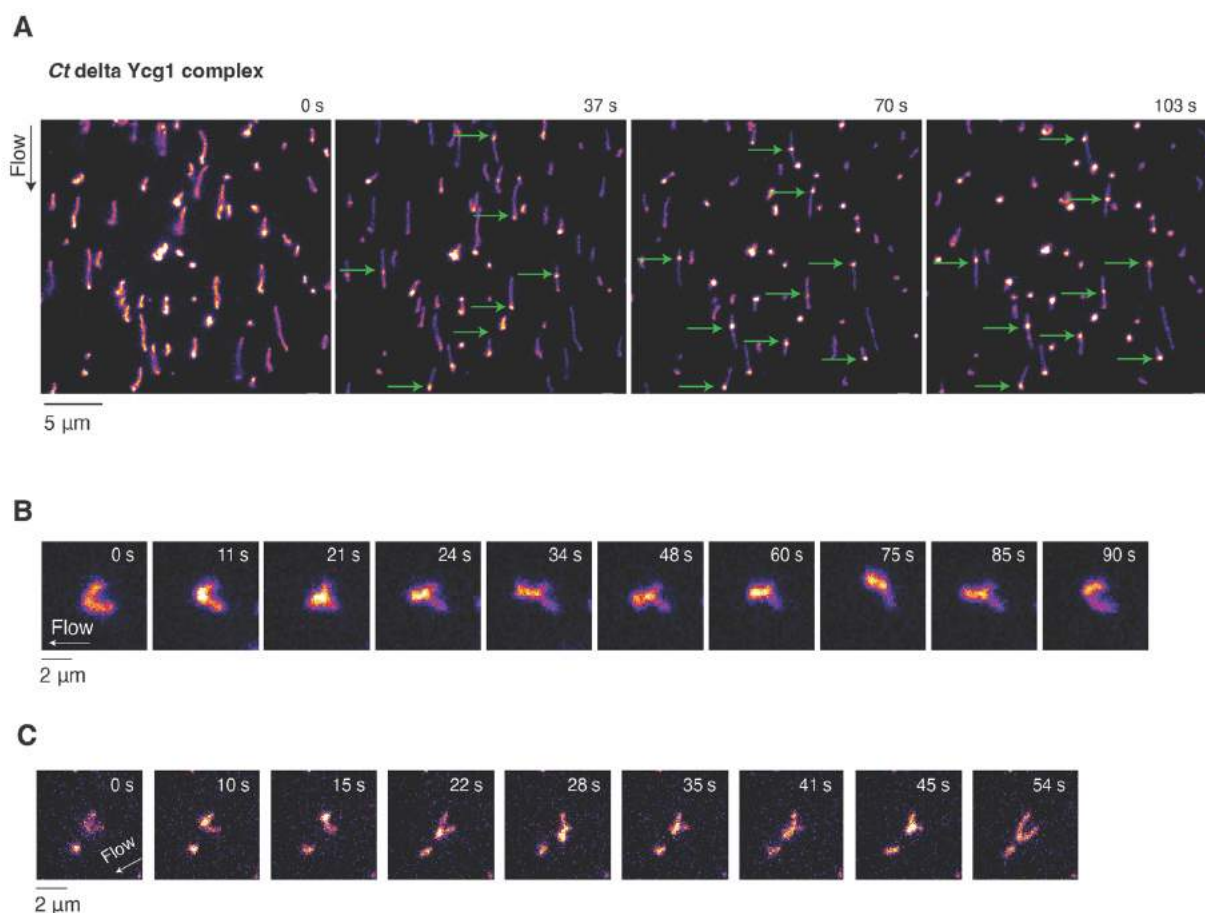


**Figure 28: Visualization of DNA loop extrusion by the *Ct* delta *Ycg1* condensin complex.** **A.** Image sequence of an entire field of view where intense dots were observed on DNA molecules after flushing in 1 mM *Ct* delta *Ycg1* condensin protein complex. The green arrows indicate the DNAs with such dots; **B-C.** Image sequence of two separate events of loop extrusion by *Ct* delta *Ycg1* condensin complex on double-tethered DNAs in the side

flow view. The arrows indicate the direction of the flow which was used to introduce protein into the imaging chamber.

To test this possibility, I flowed in 1 nM *Ct delta Ycg1* condensin complex into the imaging chambers same as the *Ct* condensin holocomplex. To my surprise, I observed intense fluorescent dots forming on double-tethered DNAs within the field of view, just like it observed for the condensin holocomplex (**Figure 28A**). I also performed imaging with side flow to extend the compacted DNA part and confirmed that the bright fluorescence intensities created by *Ct delta Ycg1* condensin correspond to DNA loops (**Figure 28B, C**). This experiment proves that the intense fluorescent dots formed on the DNA are not due to protein aggregation or the creation of a DNA plectoneme, but due to the DNA loop extrusion activity of the tetrameric condensin complex without the ‘anchor’ Ycg1 subunit.

## 4.2 *Ct delta Ycg1* condensin switches direction while extruding DNA loops

My experiments showed that the *Ct delta Ycg1* condensin complex also loop extrudes (**Figure 28**), as previously also seen in real time for the holocomplex. When I analyzed the extrusion events carefully, I made an interesting discovery.

Soon after addition of protein to the imaging chamber, I frequently observed an intense fluorescent dot that moved back and forth along the DNA length as the fluorescence intensified (for an example, see **Figure 29A**, DNA is marked with a green dotted circle). This movement of the DNA loop is different from that depicted in **Figure 21** of the holocomplex, where anchor slippage causes loops to migrate in one direction, since in the cases observed for the delta Ycg1 complex, the loop abruptly changed its direction (from 52 s to 81.2 sec, **Figure 29A**). The difference was clearly visible in the kymograph (**Figure 29B**), since the bright yellow/orange line (DNA loop) changed its position back and forth as it continued to grow in size. The quantification plot of this event revealed a two-sided extrusion pattern (**Figure 29C**), unlike the strictly one-sided extrusion observed for the holocomplex: in the blue shaded region, the red line (the loop) increases at the expense of the blue line, whereas the yellow line remained unchanged in the beginning but then started to increase due to anchor slippage. Shortly after the initial extrusion event, in the yellow

shaded region (at around 30 s), DNA is reeled into the loop (red line increases) from the yellow line, while the blue line now first stays unchanged before it increases again due to anchor slippage.

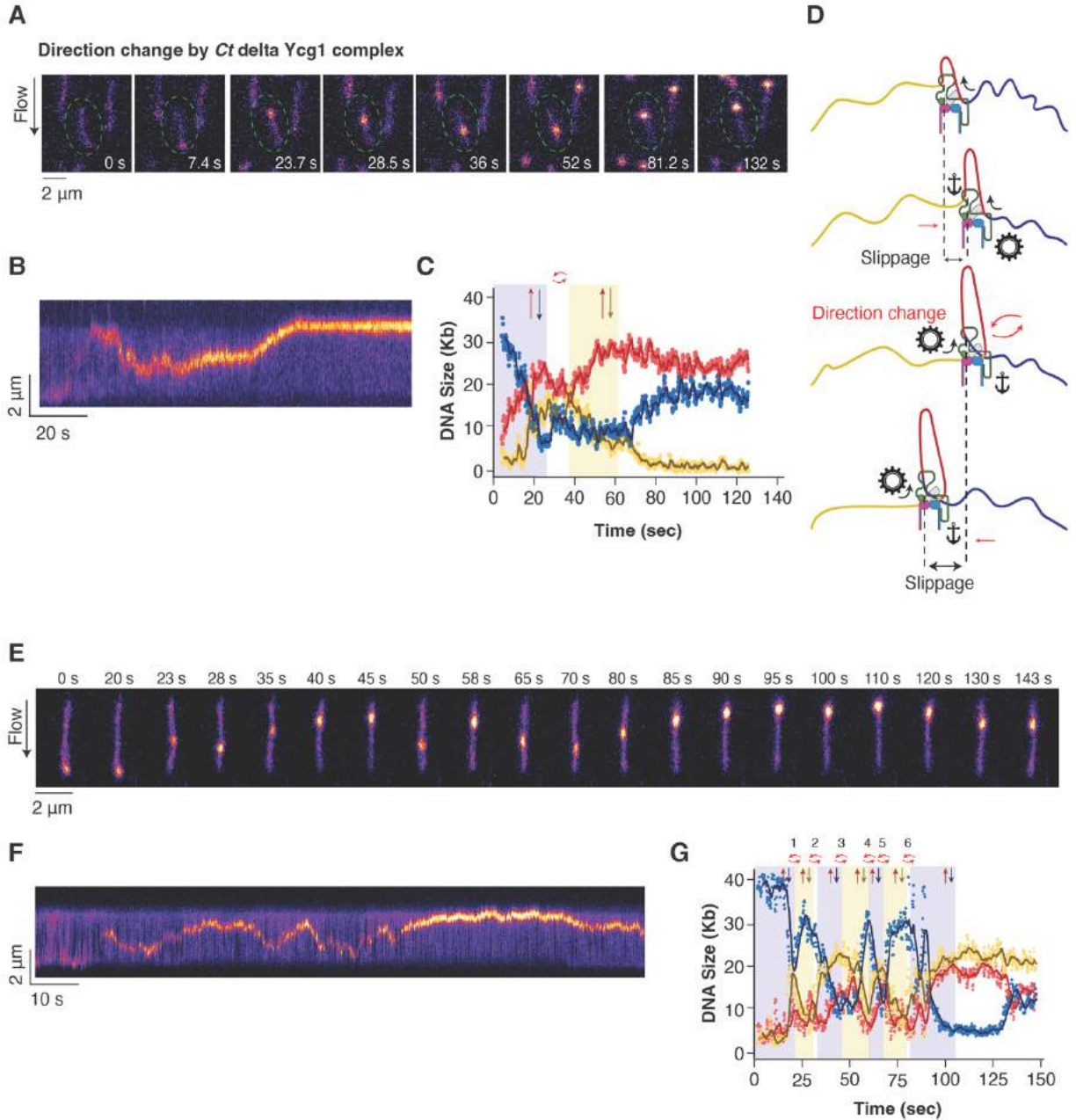


**Figure 29: *Ct delta Ycg1* condensin switches direction while extruding DNA loops.** **A.** Image sequence of a DNA loop extrusion event by *Ct delta Ycg1* condensin complex with direction change, DNA is stained with SxO and is visualized using pseudo color in FIJI. The arrow indicates the direction of flow used to add protein, the green circle marks the DNA in question; **B.** The kymograph here represents the extrusion event, the loop moves along the length of the DNA as extrusion takes place; **C.** The quantification plot shows change in the DNA size during the loop extrusion event, the red line indicates the DNA within the loop whereas the blue and yellow lines

indicate DNA on either side of the loop (it is difficult to correspond blue or yellow mark to either of the sides of the loop due to its dynamic nature). The red, blue and the yellow arrows indicates changes in the DNA. The red curved arrows represent the change in direction; **D.** Schematic representation of the sequence of events happening in A, the red arrows indicate the direction of the slippage by condensin complex and the curved arrows represent the switch in direction of the extrusion event; **E.** Image sequence of a second loop extrusion event with 6 times direction changes where the loop travels the entire length of the DNA. The arrow indicates the direction of the flow used to add the protein; **F.** A representative kymograph of event depicted in E; **G.** Quantification of the loop extrusion event shown in E as in C. The first blue shaded region shows the main extrusion event whereas the subsequent yellow or blue regions represents change in direction of the extrusion event. The red curved arrows and number indicated above them represents direction change as in C.

Although the combination between direction change and anchor slippage generates a complicated pattern, it is clear that the tetrameric complex changed the direction from where it reeled DNA into the loop once. The schematic representation of the event discussed above shows possible steps of the extrusion event, where a tetrameric complex binds DNA and starts extruding a loop while slipping, then changes its direction and extrudes DNA from the other side, again with anchor slippage (**Figure 29D**).

The change in DNA-loop-extrusion directions with the delta Ycg1 condensin complex can be as many as six times during an imaging window of 140 sec (**Figure 29E**). The intense fluorescent dot traveled along the length of the DNA in alternating directions as it intensified with time as it can be seen from the kymograph as well (**Figure 29F**). Upon quantification of the DNA sizes over time, the direction change became very clear. The initial extrusion phase (first blue shaded region), where the blue line decreases with small increase of the red line along with increase of the yellow line (due to anchor slippage), was followed by frequent changes in the reduction of either the blue or the yellow arm of the DNA with the corresponding changes in the red line. As each blue and yellow region indicates a reduction of the blue or yellow arm (condensin reels DNA from the blue or yellow line into the DNA loop), respectively, every transition from blue to yellow and vice versa represents a switch in the direction of extrusion by the *Ct* delta Ycg1 condensin complex (**Figure 29G**). This is clearly an independent and active event, as the change in direction also moves against the buffer flow (**Figure 29E, F**).

### 4.3 Properties of DNA loop extrusion by the *Ct* delta Ycg1 condensin complex

I first tested the effect of tension in the DNA molecule on DNA loop extrusion by the delta Ycg1 complex. As for the holocomplex, I observed an inverse correlation when I plotted the rate of loop extrusion by the delta Ycg1 complex against the relative extension of the double-tethered DNA molecules (**Figure 30A**). As the end-to-end tether length of the DNA determines the internal tension realized by the DNA molecule, short end-to-end tethered DNA allows faster loop extrusion whereas long end-to-end tethered DNA slows down extrusion by the condensin complex. Similar like the holocomplex, delta Ycg1 exhibited the same inverse correlation behavior when I plotted the loop extrusion rates against relative DNA extension. I observed a similar trend when I plotted the extrusion rate against the stall force (**Figure 30B**). Loop extrusion by the *Ct* delta Ycg1 complex stalled when the internal force on the DNA reached close to 0.2 pN.

Whereas the basic biophysical properties of the loop extrusion process are quite similar between the holocomplexes and the delta Ycg1 complexes, the latter frequently changed its direction. I therefore quantified the rate of DNA reeling from either side of the loop before and after switching direction (**Figure 30C**). I calculated these reeling rates to be similar (-693 bp/s and -652 bp/s before and after direction change, respectively) from the decrease in the blue and the yellow line in blue and yellow shaded region, respectively (for an example see quantification plot in **Figure 30D**). This suggests that the change in direction is most presumably by one delta Ycg1 condensin complex, as two different complexes would have generated twice as high or twice as low reeling rates if they were either reeling in the same or opposite direction, respectively.

Since anchor slippage events were more frequent for the delta Ycg1 complex, oftentimes the direction change occurred simultaneously with slippage. In these cases, even though condensin reeled in DNA from the other side of the loop, the overall size of the loop did not always increase (**Figure 30E**). When I plotted the rate of extrusion (increase in the red line, as shown in **Figure 30F**; by red arrows) before (solid red arrow) and after (dotted red arrow) the direction switch, I observed three categories. In a few instances the loops decreased in size after direction switch (4/57 DNAs, rate below -140 bp/s), few retained their loops to a similar size (6/57 DNAs, rate between -140 and +140 bp/s), whereas in the majority of cases the loops increased in size after the

direction change (47/57 DNAs, rate above +140 bp/s; **Figure 30E**). The quantification plot of an extrusion event shown here reflects a typical example of a direction change combined with a slippage event and represents the dynamic nature of DNA loop extrusion by the delta Ycg1 complex (**Figure 30D, F**).

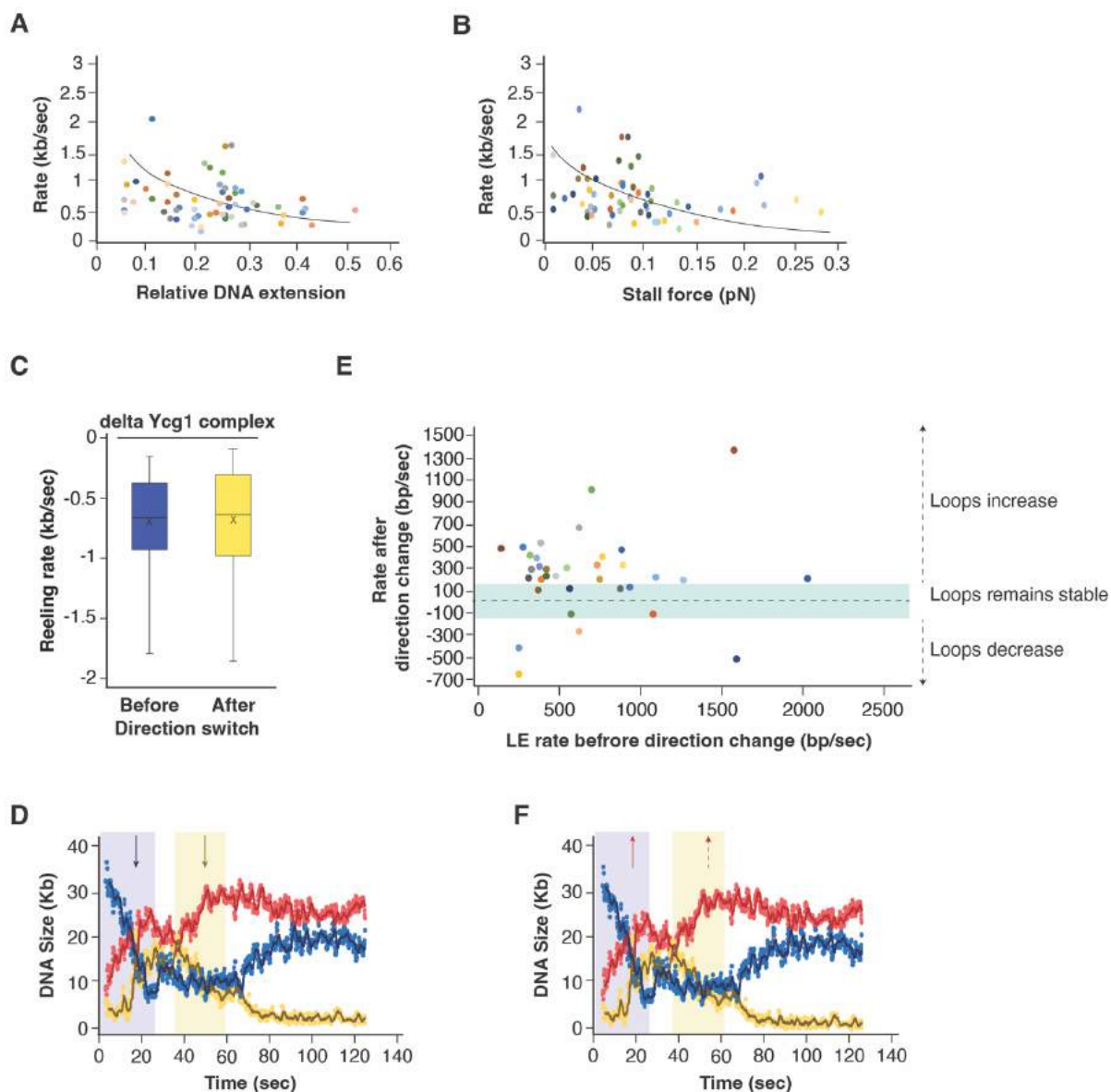


**Figure 30: Properties of DNA loop extrusion by the *Ct* delta Ycg1 condensin complex.** **A.** Rate of loop extrusion is plotted against the relative DNA extension in relation to its 16.5  $\mu\text{m}$  contour length. The solid line serves as a visual guide; **B.** Rate of loop extrusion is plotted against the force exerted within the DNA due to increased DNA stretching upon loop size increase. The solid line serves as a visual guide; **C.** Rate of reeling measured in negative values from different DNA arms before (blue) and after (yellow) direction change; **D.**

Quantification plot of the example shown in figure 29A, the blue and the yellow arrows represents the reduction of the DNA arms respectively before and after direction switch and shown here a guide for C; E. Rate of DNA within the loop before and after direction change shown as a scatter plot to see the effects of direction change on the overall loop size.; F. Quantification plot of the example shown in figure 29A, the solid and the dotted red arrows represents the rate of the DNA within the loop before and after direction switch respectively and shown here a guide for E.

#### 4.4 Fluorescence labeling of *Ct* condensin to track condensin during loop extrusion

To directly visualize condensin at the bases of the DNA loops, I attempted to fluorescently label the condensin complex and co-image both, DNA and protein, using dual color excitation. In an attempt to fluorescently label the *Ct* condensin complex, I attached a short 11-amino-acids peptide tag (ybbr tag – GTDSSLEFIASKLA, the underlined serine residue is fused to a fluorescence probe by an enzymatic reaction, Yin et al., 2006) to either Smc2, Smc4, or Brn1. The table in **Figure 31A** lists the positions on different subunits where I added the ybbr tag for labeling. However, in all cases, the labeled constructs had drastically reduced loop extrusion activity. Furthermore, the labeled protein frequently stuck to the imaging surface and covered the entire field of view soon after it was added to the imaging chamber.

*Ct* condensin holocomplex tagged with ybbr at Brn1 position 110 and labelled with Atto647N as a typical example: shortly after flowing 1 nM protein into the microfluidics chamber, the protein started to stick to the imaging surface, making it impossible to determine the number of condensin at each loop base. Binding of the protein to the surface of the imaging chamber did not prevent loop extrusion, as seen in the kymographs. However, due to non-specific protein binding to the imaging surface, I could not determine the number of proteins bound to the base of the DNA loop (**Figure 31B**). Although I tried various subunit positions for ybbr tagging, various fluorophore dyes and an alternative labelling strategy via a SNAP tag, all of these attempts rendered the protein less functional and resulted in the same sticking issue (**Figure 31A**).

Thus, my attempts to directly determine whether the DNA loops were created by a single *Ct* condensin molecule failed.

However, I did observe Z-loops, compound loops generated by two (or more) independent condensin complexes traversing each other and forming a loop within a pre-existing loop (Kim et al., 2020), with *Ct* delta Ycg1 complex (**Figure 31C**). The DNA with the Z-loop here has multiple delta Ycg1 complex bound and can be easily distinguished by its characteristic elongated form. The corresponding kymograph shows beginning of loop extrusion close to the bottom anchor point of the DNA but became more stretched until snapped (**Figure 31C**).

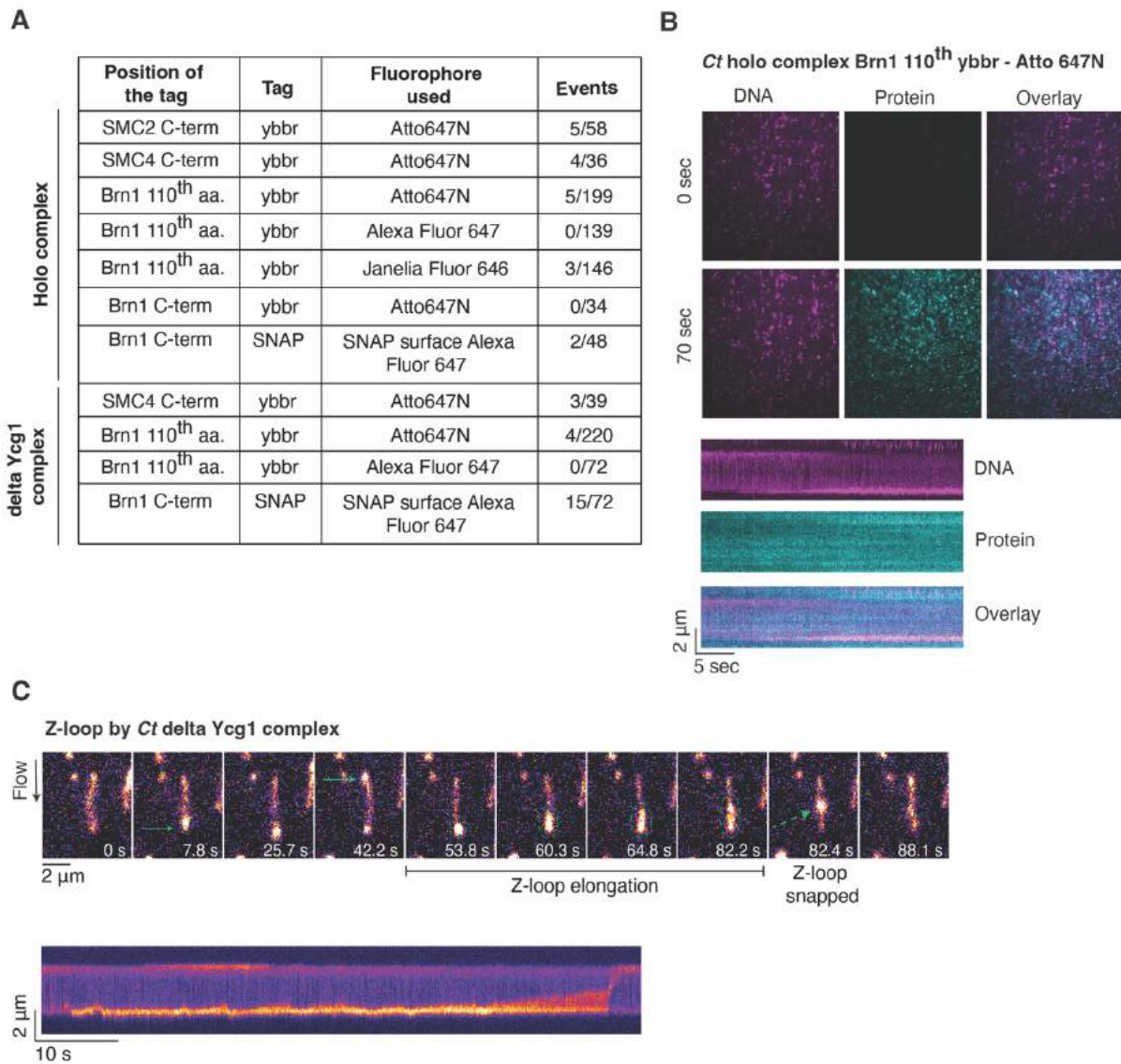


**Figure 31: Fluorescence labeling of *Ct* condensin to track condensin during loop extrusion.** **A.** List of all the fluorescently labeled condensin complex that was tested for imaging, the numbers represent DNA with loops; **B.** Example images of entire field of view and kymographs with holo complex labelled with Atto647N (tagged at Brn1 110<sup>th</sup> aa.). DNA is stained with SxO, protein is labeled with Atto6457N, the DNA and protein were illuminated with 532 and 646 nm LASER respectively; **C.** Example image sequence and kymograph of a DNA with Z-loop formed by *Ct* delta Ycg1 complex. The solid green arrows indicate multiple loops formed on the DNA; the dotted green arrow indicates the snapping of the Z-loop into a single loop.

#### 4.5 Differences between DNA loop extrusion properties of holocomplexes and delta Ycg1 complexes

To check whether their differences among the loops formed by delta Ycg1 and holocomplexes in addition to the changes in directionality of the former, I first quantified is the efficiency of loop extrusion by counting the number of DNAs with intense fluorescence dots in the entire field of view. Around 60% of double-tethered DNA molecules (316/519) displayed loops in the presence of the condensin holocomplex, compared to ~83% of double-tethered DNA molecules (256/307) in the presence of the delta Ycg1 complex (**Figure 32A**). Among the DNAs that had loops, about 13% (41/316) of loops generated by holocomplexes and only in about 2% (6/256) of loops generated by delta Ycg1 complexes snapped within the typical imaging window of 2-8 min (**Figure 32A**).

I then calculated the rate of loop extrusion for both complexes by manually selecting 50-75 consecutive data points in the region with most linear increase (such as red line in **Figures 20C, G and 29C**) and determining the slope of the line segment. The holocomplex extruded DNA loops at  $780 \pm 530$  bp/s, whereas the delta Ycg1 complex extruded loops at  $522 \pm 379$  bp/s (median  $\pm$  SD, **Figure 32B**). In addition, I calculated the lifetime of the loops by calculating the time from the emergence of a visible intense fluorescence dot on the DNA till its disappearance or the end of the imaging experiment. This revealed almost 3 times longer lifetimes for the loops formed by the delta Ycg1 complex than for the loops formed by the holocomplex (48 and 124 sec, median, respectively; **Figure 32C**). Both complexes displayed very similar force dependence in terms of loop extrusion, since they stalled when the force reached close to 0.1 pN (median  $\pm$  SD,  $0.05 \pm 0.03$  and  $0.07 \pm 0.06$ , for the holocomplex and the delta Ycg1 complex respectively; **Figure 32D**).

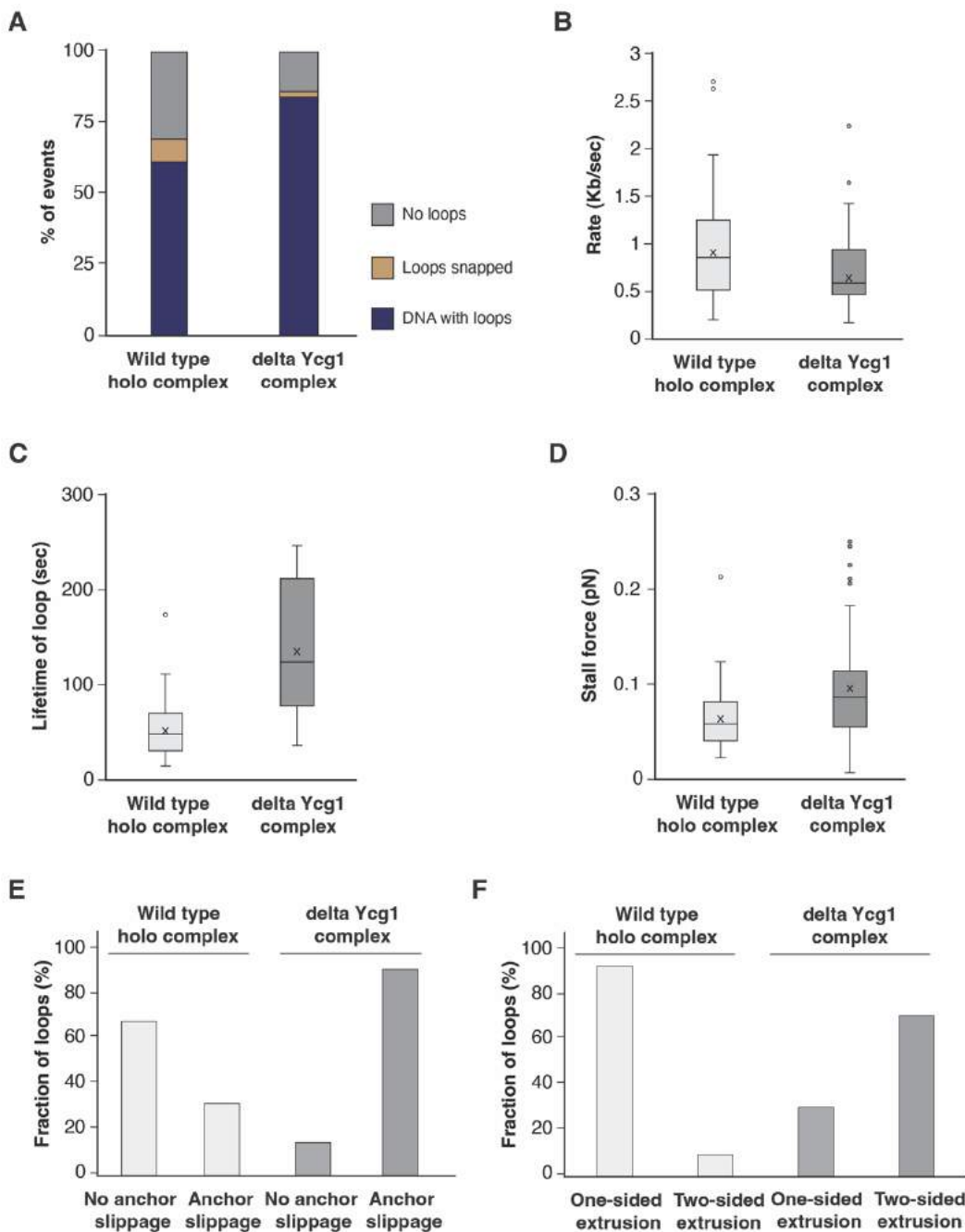


**Figure 32: Differences between DNA loop extrusion properties of holocomplexes and delta Ycg1 complexes.** **A.** Comparison of loop extrusion efficiency between the wild type and the delta Ycg1 complex; **B-D.** Box-whiskers plot comparison of the loop extrusion rate, lifetime of loop and stall force dependence are in B, C and D respectively. The lines indicate median, crosses indicate mean, box represents first and third quartile of the data and the whiskers mark the median  $\pm 1.5$  (third quartile – first quartile).  $N = 55$  for wild type and  $n = 73$  for delta Ycg1. Mann-Whitney P-test was performed to indicate the level of significant difference as depicted by the number of stars; **E, F.** Fraction of loops with slippage and direction change as seen with wild type and delta Ycg1 complex respectively.

When I calculated the number of stable loops without any sign of slippage (e.g., increase in the yellow line as shown in **Figure 21C, G**), it became evident as two thirds (36/55) of DNAs had stable loops, whereas the remaining third (17/55) of DNAs showed slippage in the presence of the holocomplex complex (**Figure 32E**). The fraction of loops that displayed slippage dramatically increased (63/73) in the presence of the delta Ycg1 complex, with only a minority of loops remaining stable (10/73; **Figure 32E**). Of those loops that displayed anchor slippage, about 81% (51/63) also changed directions, whereas more than 95% (53/55) of the DNA loops generated by the holocomplex displayed no change in direction (**Figure 32F**). Deletion of the Ycg1 subunit from the condensin complex hence has weakened but not completely abolished its anchoring function.

#### **4.6 The tendency to change direction of the delta Ycg1 complex is reversed by high salt**

I then tested DNA loop extrusion by the *Ct* delta Ycg1 complex in the presence of higher salt concentrations (125 mM). Surprisingly, in the presence of high salt, I did not observe any direction changes with delta Ycg1 complex (**Figure 33A-C**). The examples shown here are extrusion events with the delta Ycg1 condensin complex. The observed loops were stable and were extruded in a strictly one-sided manner, as the increase of the red line (DNA within the loop) is accompanied only by the decrease of one side of the DNA (blue line) in the shaded region. These loop extrusion events are similar to loops generated by the *Ct* condensin holocomplex. Almost all loops scored (12/15 DNAs) displayed stable loops with no direction change in the presence of high salt (**Figure 33D**). The loop extrusion rate was similar when compared to standard conditions with 50 mM salt (median  $\pm$  SD, 567.67  $\pm$  302.41 bp/s; **Figure 33E**), although the lifetime of loops was reduced (median  $\pm$  SD, 82.2  $\pm$  39.66 s for 125 mM salt; **Figure 33F**).

Taken together, I have shown that *Ct* delta Ycg1 complex not only extrudes DNA loops, the loops formed by this complex frequently change direction. This two-sided mode of extrusion is different than that has been observed before with the holocomplex. Moreover, the delta Ycg1 condensin complex has higher loop extrusion efficiency and the loops lasts longer on double-tethered DNA



**Figure 33: The tendency to change direction of the delta Ycg1 complex is reversed by high salt. A-C.** Representative kymographs and corresponding quantification plots of three extrusion events by the delta Ycg1 complex in presence of 125 mM salt, the red line in the plot indicates DNA within the loop, blue and yellow line indicates DNA of either sides of the loop; **D.** Comparison of one-sided and two-sided extrusion with the *Ct* delta Ycg1 complex (1 mM) either with 50 mM or 125 mM salt (79 and 15 DNAs with loops were included for 50 mM and 125 mM salt) concentration; **E,F.** Box-whiskers plot comparison of the loop extrusion rate and lifetime of loops with 50 and 125 mM salt. The lines indicate median, crosses indicate mean, box represents first and third quartile of the data and the whiskers mark the median  $\pm 1.5$  (third quartile – first quartile).

## 5 ‘Safety belt’ of *Ct* Brn1 plays crucial role for DNA loop extrusion

### 5.1 Differences between *Sc* and *Ct* Brn1 ‘safety belt’

My previous experiments showed that the *Ct* delta Ycg1 condensin complex is enzymatically active, has similar DNA binding affinities as the holocomplex, and extrudes loops albeit changes direction. This is in contrast to the *Sc* delta Ycg1 condensin complex, with no DNA-stimulated ATPase activity and a much-reduced DNA binding affinity (Kschonsak et al., 2017) and does not loop extrude (Shaltiel et al., 2022). Since the *Ct* Ycg1 subunit is dispensable for the most of the ‘anchoring’ function described for the *Sc* Ycg1-Brn1 subcomplex, it is conceivable that the Brn1 subunit, or more specifically its ‘safety belt’ region, is mainly responsible for this. This raises the question whether the *Ct* Brn1 ‘safety belt’ has any special features that ensure that it is sufficient for DNA binding and that are missing in the *Sc* Brn1 safety belt.

To address this issue, I first generated a pairwise sequence alignment of the safety belt regions of the *Sc* and *Ct* Brn1 proteins. Even with a low overall sequence similarity, the two proteins share distinguishable features: Two patches called ‘latch’ (L521, F524, W532 and W538) and ‘buckle’ (L604, P605, D606, D607, K608, H609, F610) interact with Ycg1 and close the safety belt and two positively charged patches called ‘BC1’ (R539, I540, R541, K542, I543, K544) and ‘BC2’ (R554, Q555, R556, K557, E558, K559; the amino acids are from *Ct* Brn1; **Figure 34A**).

As both Brn1 proteins presumably have similar structural features (**Figure 34B**), I hypothesized that any difference in functionality might lie within the safety belt sequence. I first compared the pI (isoelectric point) of the two proteins. The overall pI of both proteins is low (4.57 for *Sc* and 4.67 for *Ct*), whereas the safety belt regions have significantly higher pI values (9.61 for the *Sc* Brn1 ‘safety belt’, aa. 384-531; 10.12 for the *Ct* Brn1 ‘safety belt’, aa. 515-634; **Figure 34C**). When I counted the number of charged residues in the safety belt region of both proteins using a sliding window of 9 aa, I found that the *Ct* Brn1 safety belt has a lower number of negatively charged residues compared to its *Sc* counterpart (**Figure 34D**).

When I plotted the distribution of charged residues along the length of the ‘safety belt’, I noticed that the positively charged BC1/BC2 regions in *Ct* were much closer together due to an overall shorter length of the safety belt (**Figure 34E, F**). The distribution of the charged residues within the safety belt in *Ct* is also different from the one in *Sc*, most notably the number of negatively charged residues is lower (**Figure 25D**) and absent at the beginning of the safety belt region (**Figure 25G, H**). These higher density of effective positive charge in the *Ct* Brn1 safety belt might explain why it could be more efficient in DNA binding and maintain the ‘anchor site’ for condensin loop extrusion in the absence of Ycg1.

# Results

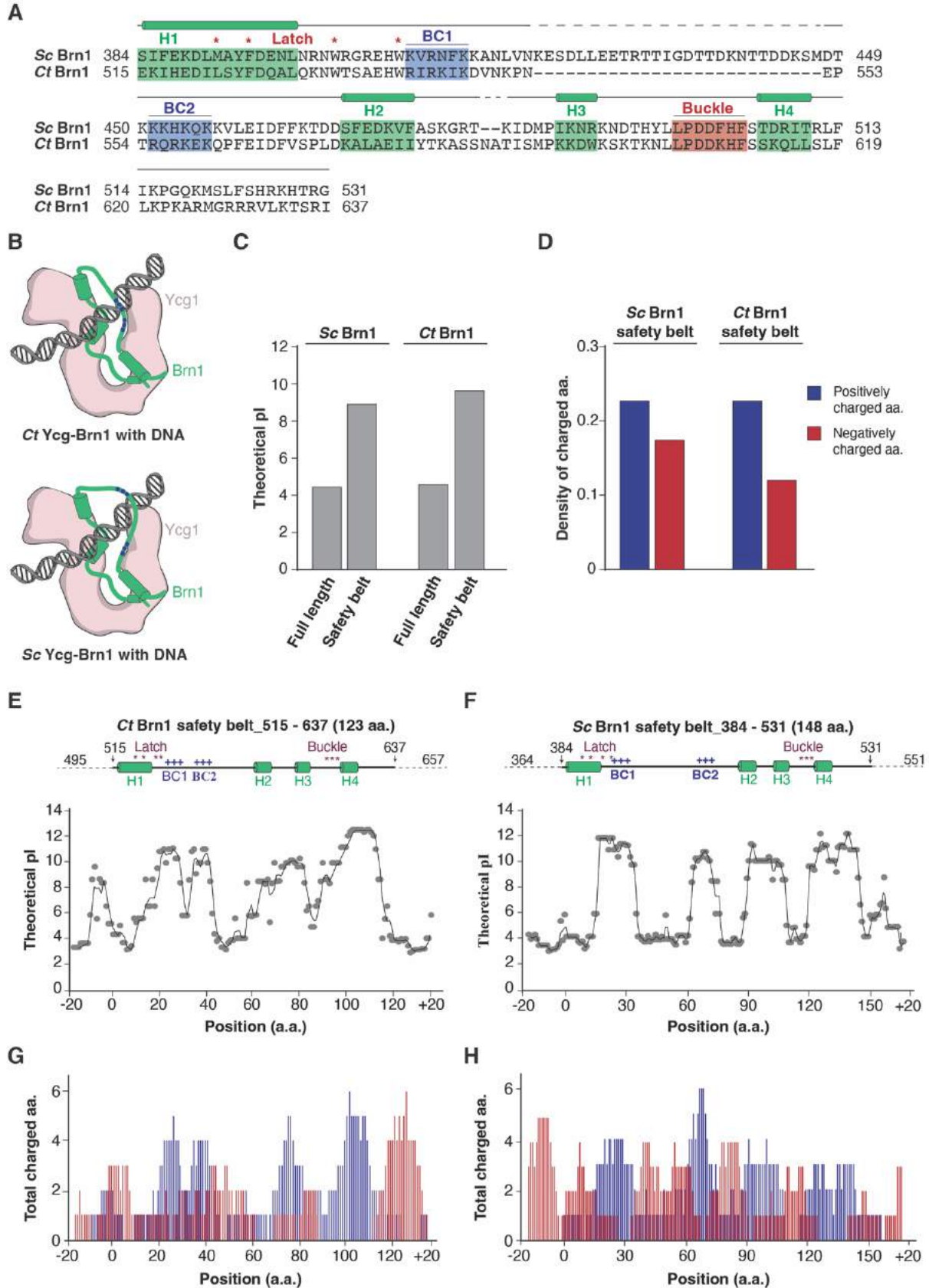


**Figure 34: Differences between *Sc* and *Ct* Brn1 ‘safety belt’.** **A.** Pairwise sequence alignment of *Sc* and *Ct* Brn1 ‘safety belt’ using Jalview. The region forming helices are marked shown with green from H1 to H4, the residues with red asterisks indicates the ‘Latch’, the BC1 and BC2 patches are shown with blue shaded boxes and the residues forming the ‘Buckle’ are in red shaded box; **B.** Model of Ycg1-Brn1 bound DNA (modified from Kschonsak et al, 2017). Ycg1 is shown in pink, Brn1 in green and DNA is in dark grey; **C.** Theoretical pI of *Sc* and *Ct* Brn1 full length protein and the ‘safety belt’; **D.** Density of positive and negative charged residues within ‘safety belt’ of *Sc* and *Ct* Brn1 protein (total number of positive or negative charged residue/length of ‘safety belt’); **E, F.** Top panel - schematics of *Sc* and *Ct* Brn1 ‘safety belt’ region with 20 amino acids flanking on either sides, the numbers with the arrows indicate beginning and end of ‘safety belt, BC1/2 shows two positively charged patches and the H1-H4 indicates the alpha helices. Bottom panel – theoretical pI distribution over the length of ‘safety belt’ measured by a 9 aa. sliding window; **G, H.** Distribution of positive and negative charged residues over the length of ‘safety belt’ measured by a 9 aa. sliding window.

## 5.2 The ‘safety belt’ of *Ct* Brn1 is essential for condensin activity

Based on my previous findings, I hypothesized that the safety belt (aa. 515-634) of *Ct* Brn1 is crucial for condensin’s activity. When I combined a safety belt deletion construct of the Brn1 with deletion of Ycg1 (*Ct* delta Ycg1 Brn1 $\Delta$ 515-634), DNA binding by the complex was greatly reduced (**Figure 35A, B**). The majority of DNA upshift (bound fraction) can only be visible with 333 nM protein which is almost 10-15-fold more compared to the holocomplex or the delta Ycg1 complex. Furthermore, this complex neither displayed a basal nor a DNA-stimulated ATPase activity (**Figure 35C**).

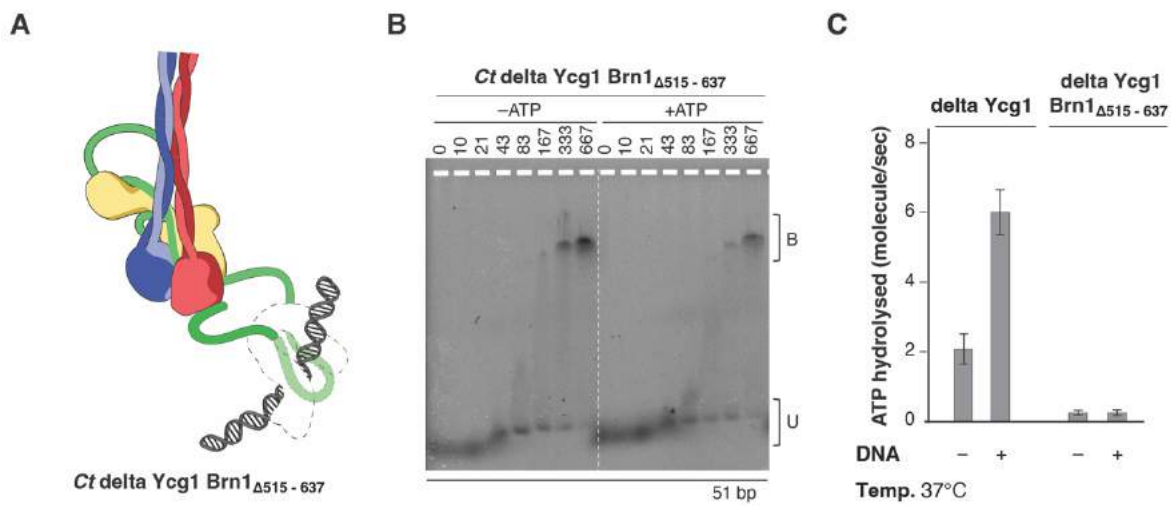


**Figure 35: The ‘safety belt’ of *Ct* Brn1 is essential for condensin activity.** **A.** Schematic representation of DNA bound within the ‘safety belt’ of Brn1 lacking the Ycg1 subunit; **B.** Gel shift assay of fluorescently labeled 51mer dsDNA in presence of increasing amount of condensin complex with or without ATP. The unbound fraction of DNA is indicated as ‘U’ and the protein-bound DNA fraction is indicated as ‘B’ in the figure; **C.** ATPase rates of *Ct* delta Ycg1 and delta Ycg1 Brn1 $_{\Delta 515-634}$  condensin complex (0.5  $\mu$ M) with or without DNA (25 nM 6.4 kbp) at 37°C. The error bars indicate standard deviation (SD) and are calculated from at least 3 independent experiments.

### 5.3 A Positively charged BC patch in Brn1 ‘safety belt’ is required for loop extrusion

Previously, the two positively charged patches in the *Sc* Brn1 ‘safety belt’ (BC1 and BC2) have been shown to be important for DNA binding (Kschonsak et al., 2017). To test whether these patches are also important in the context of the *Ct* holocomplex, I generated charge-reversal mutations (Brn1<sub>BC1</sub> – R539D, R541D, K542D, K544D and Brn1<sub>BC2</sub> – R554D, R556D, K557D, K559D) in the *Ct* condensin holocomplex.

Condensin complexes with mutations in the BC patches were active ATPase, with or without the Ycg1 subunit (*Ct* Brn1<sub>BC</sub> and *Ct* delta Ycg1 Brn1<sub>BC</sub>; mean  $\pm$  SD;  $2.95 \pm 0.06$  and  $2.60 \pm 0.10$  ATP/sec for *Ct* Brn1<sub>BC</sub> and *Ct* delta Ycg1 Brn1<sub>BC</sub> respectively; **Figure 36B**). However, only the *Ct* delta Ycg1 Brn1<sub>BC</sub> complex showed DNA stimulation ( mean  $\pm$  SD;  $3.73 \pm 0.44$  ATP/sec and  $5.22 \pm 0.39$ , *Ct* Brn1<sub>BC</sub> and *Ct* delta Ycg1 Brn1<sub>BC</sub> respectively; **Figure 36B**).

When I tested the DNA loop extrusion activity of the *Ct* delta Ycg1 Brn1 $_{\Delta 515-634}$  complex, I did not observe the formation of loops (**Figure 36C**). Similarly, the *Ct* Brn1<sub>BC</sub> complex with Ycg1 did not generate DNA loops. These data suggests that the ‘safety belt’ of *Ct* Brn1, or more specifically the positively charged residues within the BC patches, are essential for DNA loop extrusion.

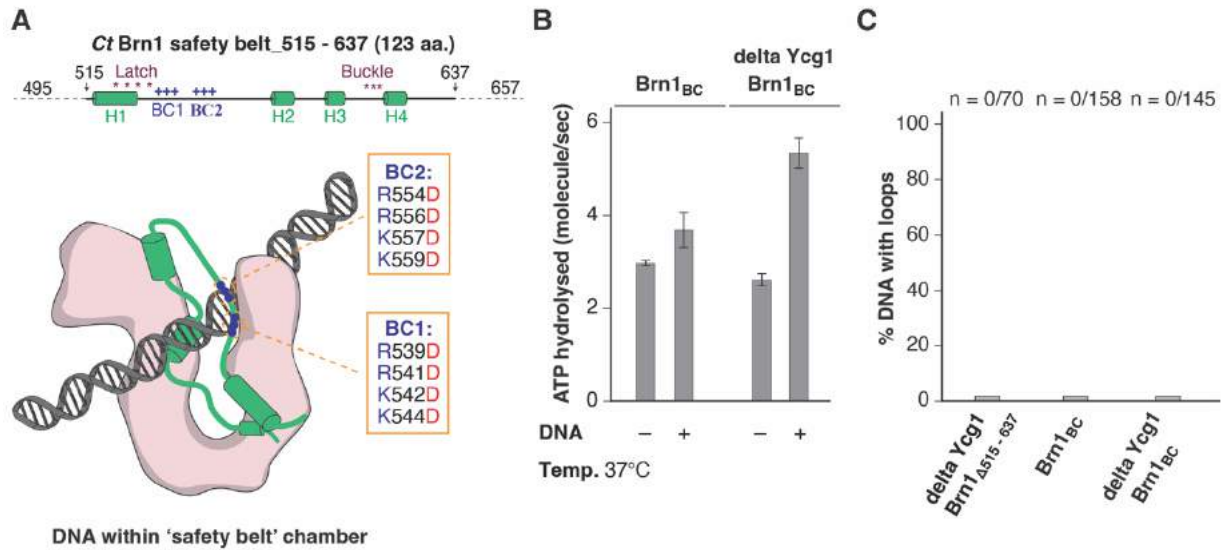


**Figure 36: A positively charged BC patch in Brn1 'safety belt' is required for DNA loop extrusion.** **A.** Schematic representation of *Ct* Brn1 'safety belt' and model of *Ct* Ycg1-Brn1 with DNA, the BC patch residues have been shown in blue dots, the residues with mutations have been indicated in boxes; **B.** ATPase rates of *Ct* Brn1<sub>BC</sub> and *Ct* delta Ycg1 Brn1<sub>BC</sub> condensin complex (0.5 μM) with or without DNA (25 nM 6.4 kbp) at 37°C. The error bars are calculated from at least 3 independent experiments; **C.** Events of loop extrusion with *Ct* delta Ycg1 Brn1<sub>Δ515-634</sub>, Brn1<sub>BC</sub> and delta Ycg1 Brn1<sub>BC</sub> complexes (1 mM). The numbers on top indicate the number of DNAs analyzed.

## 5.4 Closure of the Brn1 'safety belt' is necessary for DNA loop extrusion

The previously reported structure of Ycg1-Brn1 with DNA identified Brn1 'latch' residues (L521, F524, W532 and W538) that interact with the C terminus of the safety belt region. Substitution of these residues by aspartic acid (D) reduced DNA binding affinity when measured with the Ycg1-Brn1 subcomplex (Kschonsak et al., 2017).

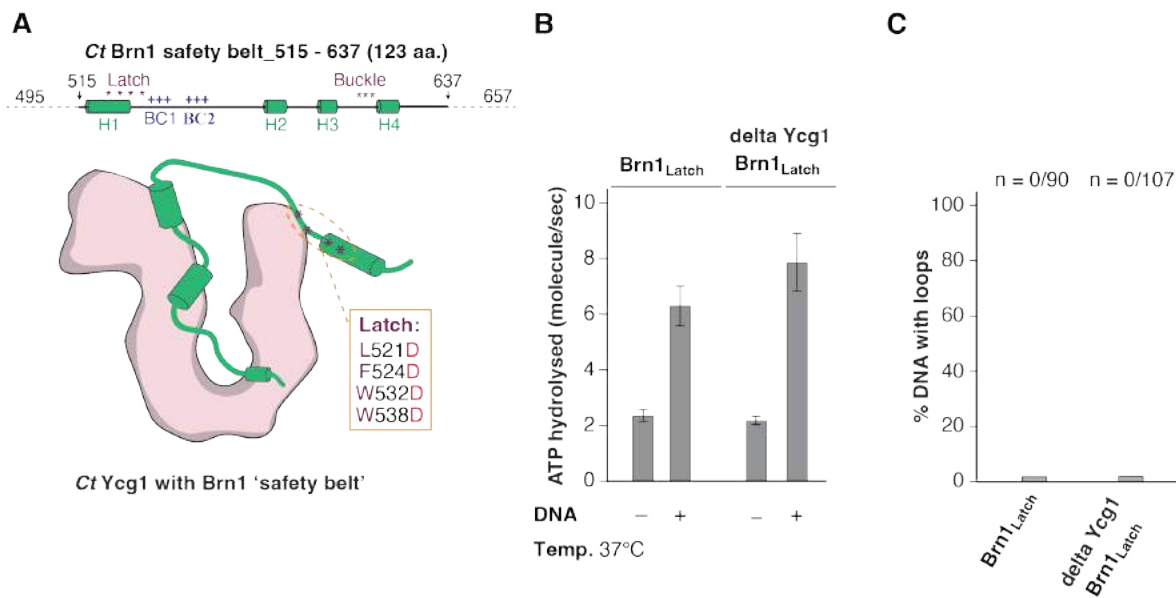


**Figure 37: Closure of Brn1 ‘safety belt’ is necessary for DNA loop extrusion.** **A.** Schematic representation of *Ct* Brn1 ‘safety belt’ and model of *Ct* Ycg1-Brn1 with DNA, the residues that form the Latch are shown with red asterisk, the residues with mutations have been indicated in boxes; **B.** ATPase rates of *Ct* Brn1<sub>Latch</sub> and *Ct* delta Ycg1 Brn1<sub>Latch</sub> condensin complex (0.5  $\mu$ M) with or without DNA (25 nM 6.4 kbp) at 37°C. The error bars are calculated from at least 3 independent experiments; **C.** Events of loop extrusion with *Ct* Brn1<sub>Latch</sub> and *Ct* delta Ycg1 Brn1<sub>Latch</sub> complexes (1 mM). The numbers on top indicate the number of DNAs analyzed.

To test the effect of mutation of the latch residues in the context of the condensin holocomplex, I performed ATPase assays. To my surprise, both the *Ct* Brn1<sub>Latch</sub> and *Ct* delta Ycg1 Brn1<sub>Latch</sub> complexes with the corresponding mutations in *Ct* Brn1 (L521D, F524D, W532D and W538D; **Figure 37A**) were active in these assays (mean  $\pm$  SD,  $3.04 \pm 0.65$  ATP/s and  $2.56 \pm 0.46$  ATP/s, for Brn1<sub>Latch</sub> and delta-Ycg1 Brn1<sub>Latch</sub> complexes, respectively) and could be stimulated by DNA (mean  $\pm$  SD,  $7.14 \pm 1.10$  ATP/s and  $7.94 \pm 1.77$  ATP/s, for Brn1<sub>Latch</sub> and delta-Ycg1 Brn1<sub>Latch</sub> complexes respectively; **Figure 37B**). However, when I tested the complexes in the single-molecule DNA loop extrusion assay, neither of the complexes extruded DNA loops (**Figure 37C**).

Taken together, my data suggests that Brn1 ‘safety belt’ needs to be closed and contain positively charged patches for DNA loop extrusion. In contrast to what has been assumed (Kschonsak et al., 2017; Ganji et al., 2018), the **Brn1 ‘safety belt’** and not the Ycg1 component of the Ycg1-Brn1 subcomplex acts as the true ‘**anchor**’ for condensin-mediated DNA loop extrusion.



## **Part III**

### **Discussion and outlook**

SMC protein complexes, such as cohesin and condensin, are the key players of chromosome organization and were hypothesized to organize genomes by generating large chromatin loops (Goloborodko et al., 2016). Although recent in vitro studies have shown that these complexes are capable of ‘loop extrusion’, the detailed molecular mechanism that underlies this activity remains enigmatic (Bauer et al., 2021; Davidson et al., 2019; Ganji et al., 2018; Golfier et al., 2020; Higashi et al., 2021; Kim et al., 2019; Kong et al., 2020). Structural and biochemical studies have provided information crucial to our understanding of how SMCs work (Kschonsak et al., 2017; Hassler et al., 2019; Lee et al., 2020; Shi et al., 2020; Bürmann et al., 2021, Lee et al., 2022). Recent studies with cohesin complex have suggested ‘swing and clamp’ and ‘Brownian ratchet’ models for loop extrusion (Bauer et al., 2021; Higashi et al., 2021). However, how condensin extrudes DNA loops, remains a mystery.

At the time of the beginning of this study, only the *Sc* condensin was shown to extrude DNA loops (Ganji et al., 2018). I set out to generalize this process using condensin from the thermophilic yeast *Chaetomium thermophilum* (*Ct*) and to gain molecular insights into this process.

## **1 The *Ct* condensin holocomplex is functionally active**

### **1.1 The *Ct* condensin is structurally intact**

The first experimental evidence for DNA loop extrusion came from the *Sc* condensin complex purified from yeast (Ganji et al., 2018), however a question remained whether a contaminant like endogenous helicase or translocase were actually responsible for this process. To rule out this possibility, I decided to work with a different condensin complex and chose condensin from a thermophilic yeast species *Chaetomium thermophilum* (*Ct*, optimum growth temperature 50-55°C) and purified it from insect cells (Sf21). The idea was to try a different condensin complex, expressed in heterologous system to rule out any possibility of co-expressing contaminant from the same host system and check if this complex also shows the similar extrusion activity.

I purified *Ct* condensin from insect cells and analyzed the purified complex by mass spectrometry. Since the complex eluted in a single peak from gel filtration and no void peak was detected, I conclude that *Ct* condensin is monomeric and does not aggregate (**Figure 10B**). Mass spectrometry analysis did not detect major contaminants like endogenous helicase or translocase that could potentially have accounted for any DNA loop extrusion activity. Moreover, traces of endogenous insect cell condensin subunits were very low (**supplementary table 1**). Further analysis of the complex revealed that the different subunits of condensin were present at ratios of Brn1:Smc2:Smc4:Ycg1:Ycs4 1.3:1.0:1.0:0.7:0.7 (**Figure 11B**). The kleisin subunit Brn1 was presumably predominant because I used the His tag fused to its C terminus for the first round of affinity purification. The SMC subunits, Smc2 and Smc4, were slightly less abundant, presumably because the tripartite ring (Smc2-Smc4-Brn1) forms a stable subcomplex with higher affinity protein-protein interactions than the remaining two subunits. These two subunits, Ycs4 and Ycg1, which are characterized by extensive HEAT-repeat motifs, were present at sub stoichiometric ratios. This suggests that the two subunits might be bound to the rest of the complex with a relatively lower binding affinity. It is possible that these HEAT repeats are required to present in a low amount to facilitate the flip-flop behavior where it was shown that the ATP binding triggers exchange of Ycg1 with Ycs4 with the core complex (Lee et al., 2020).

My rotary shadowing experiment showed electron density that I could clearly assign to the globular SMC hinge domain, the coiled-coil arms, the SMC ATPase head domains and the HEAT-repeat subunits (**Figure 12A**). This suggests that the majority of condensin complexes purified this way are holocomplexes. Previous rotary shadowing images of condensin complexes isolated from bacteria, budding yeast, *Xenopus laevis* and human cultured cells already revealed the flexible nature of the coiled-coil arms (Anderson et al., 2002; Melby et al., 1998; Terakawa et al., 2017). High-speed liquid atomic force microscopy (AFM) studies also showed similar results, including folding of the hinge domain, and highly dynamic coiled coils (Bauer et al., 2021; Eeftens et al., 2017; Ryu et al., 2020). Taken together, it is evident that the SMC coiled-coil arms can adopt either open or closed conformations. The coiled-coil arms of the *Ct* condensin holocomplex looked similar to the previously imaged condensin complexes (**Figure 12B**), suggesting that *Ct* condensin is also flexible in nature and assumes the ‘V’ and ‘O’ shaped structures reminiscent of the classical ring-like configurations of SMC complexes. *Ct* condensin holocomplex also displayed additional

conformations, with the arms partially aligned or fully aligned with each other, resembling like either ‘Y’ or ‘I’ shapes. The *Sc* condensin complex was also shown to adopt a ‘B’ shaped conformation under similar conditions, suggesting the coiled-coil arms can also bend over along their lengths (Ryu et al., 2020). Cryo-EM studies with condensin and cohesin also reported folded conformations (Kong et al., 2020; Lee et al., 2020; Petela et al., 2021). However, I did not observe bending of the coiled coils for *Ct* condensin to the same degree as seen for the other complexes. Clearly, the *Ct* condensin complex requires further structural characterization. I conclude that rotary shadowing offers an easy way to test for the integrity of the condensin holocomplex, but note that protein conformations might be subject to experimental artifacts due to the drying of the proteins on a mica surface.

## 1.2 Enzymatic activities of the *Ct* condensin holocomplex

Rotary shadowing electron microscopy however offers an additional opportunity to test for DNA compaction by the *Ct* condensin complex. Previously, single mitochondrial DNA (mtDNA) has been used to study genome compaction (Kukat et al., 2015). When I imaged only relaxed circular plasmid DNAs, the DNAs dispersed on the mica surface, allowing me to calculate the area within. Upon addition of *Ct* condensin without ATP, the area decreased, and this decrease was significantly higher upon simultaneous addition of ATP (**Figure 15F**). This suggests that this assay measures an active mode of DNA compaction by the *Ct* condensin complex. The finding that the DNA area was already reduced when DNA was incubated only with protein might reflect an indirect (non-catalytic) mode of compaction, possibly due to protein-DNA interactions. This result is the first indication of DNA compaction by a condensin complex from a thermophilic fungus.

The common features that SMC proteins share with ABC transporters are their ATP-binding motifs located at their head domains (Anderson et al., 2002; Stray & Lindsley, 2003). Purified *Sc* condensin, as well as human condensin and cohesin complexes, have been shown to have ATPase activity that can be stimulated by DNA (Davidson et al., 2019; Kim et al., 2019; Kong et al., 2020; Terakawa et al., 2017). I have measured the ATPase activity of *Ct* condensin and found that, at room temperature (25°C), the complex is moderately active. At higher temperatures, such as 30°C

and 37°C, the complex showed an increased DNA-stimulated ATPase activity (**Figure 13B**) however, under these conditions, the basal ATPase activity remained at ~1 molecule/sec per condensin. The increase in ATPase rates in the presence of DNA might mediate structural rearrangements which would in turn trigger increased ATP hydrolysis and this stimulation is proportional to increase in temperature. At 50°C, the basal ATPase rate also increased, which might, however, partially be a result of spontaneous ATP hydrolysis at this temperature. The DNA stimulation observed at this temperature was the highest among all. Human cohesin complexes in presence of NIPBL-MAU2 and DNA were reported to hydrolyze 2 molecules ATP/sec, whereas human condensin I and II were reported to hydrolyze 2-3 molecules ATP/sec (Davidson et al., 2019; Kong et al., 2020). In contrast, the *Ct* condensin complex hydrolyzed ~5 molecule ATP/sec at 37°C. Overall, this result indicates that *Ct* condensin is an active ATPase with activity that exceeds other SMC complexes tested to date.

Previously, the *Sc* condensin complex and human condensin I and II complexes have been shown to bind DNA in gel shift assay (Kschonsak et al., 2017; Kong et al., 2020). I have used the same method to visualize the DNA-binding activity of the *Ct* condensin complex. Condensin binds to 51-bp dsDNA at a relatively low concentration (10-20 nM), which is 10-20 times lower than the concentration required to observe DNA binding by the *Sc* condensin complex. Human condensin II has been shown to upshift DNA at a protein concentration of ~50 nM. The addition of ATP does not increase DNA binding by condensin. I obtained similar results when I used a shorter DNA substrate (35 bp), where the complex upshifted DNA from around 40 nM (**Figure 14**).

Taken together, the purified *Ct* condensin complex displays ATP-dependent DNA compaction, DNA-stimulated ATPase activity, and binds DNA.

## 2 Loop extrusion by the *Ct* condensin holocomplex

### 2.1 Strictly asymmetric loop extrusion by the *Ct* condensin holocomplex

The purified *Sc* condensin complex, the fission yeast cohesin complex, and human cohesin and condensin complexes have been previously shown to extrude DNA loops. I have used single-molecule imaging to test whether the *Ct* condensin complex has same activity. I observed the formation of intense fluorescence dots on double-tethered DNAs and confirmed that these are DNA loops using side flow to extend the compacted DNA region. (**Figure 18, 19**). Hence, for the first time, a condensin complex from a thermophilic yeast has been shown to extrude DNA loops. The fact that loop extrusion has now been observed for different SMC complexes from different species makes it very unlikely that this activity stems from any contaminants in the protein preparations. The *Ct* condensin holocomplex extrudes loops in an asymmetric manner, similar to the activity of the *Sc* condensin complex. However, this is different from the observation made for human condensin, where both symmetric and asymmetric DNA loop extrusion has been reported (Davidson et al., 2019; Kim et al., 2019; Y. Kong et al., 2020). This result suggests that condensin from yeast species might require to only extrude DNA loops in an asymmetric manner, probably because they need to compact a relatively small genome. The ability of human condensin complexes to extrude symmetric loops might facilitate compaction of a large genome, as asymmetric extrusion alone was shown to be inefficient for the complete folding of mammalian genomes (Banigan et al., 2020; Banigan & Mirny, 2020a, 2020b). It is also possible that two condensin complexes might be involved in the case of symmetric loop extrusion, each one only extruding loops in an asymmetric manner. In the case of cohesin, which extrudes DNA loop in a symmetric manner, Davidson and colleagues showed the presence of only one cohesin complex at the base of the extruded DNA loop (Davidson et al., 2019).

## 2.2 Anchor slippage by the *Ct* condensin complex

I made an intriguing observation with the *Ct* condensin holocomplex. In around 30 percent of the visualized loops, the anchor seemed to slip during loop extrusion (‘anchor slippage’; **Figure 21**). This can be explained if the complex is loosely bound to the double-tethered DNA at its anchor site and then slips due to the tension in the DNA that is being built up it is being extruded into a loop from one side. In these cases, the distance between the anchor point of condensin-bound DNA and one of the surface-tethered ends of the DNA increases over time as the anchor slips, instead of remaining constant as in the case of ‘normal’ asymmetric loop extrusion events (**Figure 38**). This anchor slippage is not caused by the drag of the buffer flow in the microfluidics chamber, since slipping frequently occurred against the direction of the flow. Despite the anchor moving, the condensin holocomplex reeled DNA only from one side into the loop.

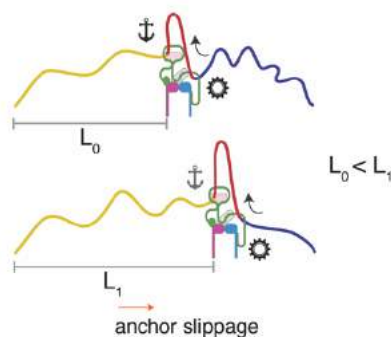


**Figure 38: Anchor slippage by *Ct* condensin holocomplex.** *Ct* condensin binds to DNA using the anchor site and starts reeling DNA into the loop only from one side via the motor site. However, during the anchor slippage the complex slips in one direction and the length between the tethered anchor and the protein bound DNA increase. Here  $L_0$  and  $L_1$  indicates initial and final distance between the surface tethered anchor point and the protein bound DNA before and after anchor slippage respectively.

Previously when a ‘safety belt’ mutant of *Sc* condensin holocomplex was tested in imaging assay, the complex seem skip on DNA (Ganji et al., 2018). However, it is the first time that a wild-type condensin holocomplex also showed anchor slippage behavior. It is speculative to think that as *Ct* is a thermophilic species, the condensin complex is not tightly bound to the DNA at the working imaging temperatures ( $\sim 22^\circ\text{C}$ ). Whereas, such is not the case for *Sc* condensin or human SMC complexes where the imaging temperature is within optimum range ( $25\text{-}37^\circ\text{C}$ ).

### 3 An active *Ct* delta *Ycg1* condensin complex

#### 3.1 The *Ct* delta *Ycg1* condensin complex is enzymatically active

I purified the *Ct* delta *Ycg1* condensin complex analogous to the holocomplex. The tetrameric complex eluted as a single peak from gel filtration, indicating that the complex is monomeric. Mass spectrometric analysis confirmed the absence of the *Ycg1* subunit and failed to detect an endogenous *Ycg1* homolog from the expression host, which suggests that the tetrameric complex indeed lacks the *Ycg1* subunit.

When the *Sc* delta *Ycg1* condensin complex had previously been tested in ATPase or in gel shift assays, the tetrameric complex was inactive and displayed highly reduced DNA-binding activity, respectively (Kschonsak et al., 2017). In contrast, when I imaged a circular plasmid DNA in the presence of the *Ct* delta *Ycg1* complex using rotary shadowing, I observed DNA compaction to a similar extent to the compaction I observed with the condensin holocomplex with ATP (**Figure 25**). This suggests that the *Ct* delta *Ycg1* complex has maintained some activity.

Surprisingly, the basal ATPase activity of the *Ct* delta *Ycg1* complex was higher than the activity of the holocomplex at elevated temperatures (30°C and 37°C). Furthermore, the DNA-stimulated ATPase rate was 20-50% higher than that of the holocomplex (**Figure 26**). This was unexpected, since the *Ycg1* subunit of the *Sc* condensin complex was previously reported to be important for DNA binding (Kschonsak et al., 2017). This result furthermore indicates that the *Ycg1* might play a negative regulatory role for the ATPase activity of the condensin complex. *Ycg1* might, for example, interact with the ATPase heads and block access of ATP. However, this notion is not supported by a previously solved condensin structure, where the *Ycg1* subunit bound to the *Smc2* head in the presence of ATP (Lee et al., 2020). The higher DNA stimulation indicates that *Ycg1* might either limit DNA binding to condensin, or that its presence restricts any structural changes that follow DNA binding. No structural evidence that would support this theory has yet been obtained.

Contrary to the *Sc* counterpart, the *Ct* delta Ycg1 condensin complex binds to DNA with a similar binding affinity as the *Ct* condensin holocomplex. This is surprising, since Ycg1 in budding yeast contributes to the formation of a major DNA binding site (Kschonsak et al., 2017). It is possible that in case of the *Ct* condensin complex, another DNA binding site, probably the kleisin subunit, Brn1 contributes to majority of the DNA binding than that of the Ycg1 subunit.

### 3.2 Direction changes by the *Ct* delta Ycg1 complex

My previous results from the DNA compaction, ATPase, and DNA binding assays indicate that the *Ct* delta-Ycg1 complex might have retained DNA loop extrusion activity. I indeed saw loop formation by the tetrameric complex, unlike for its *Sc* counterpart (Shaltiel et al., 2022). However, the loops formed differed from the loops formed by the condensin holocomplex in one key aspect: they frequently changed directions (**Figure 39**). A change in direction can be observed when an asymmetric loop-extruding factors (LEF) changes the orientation of its motor and anchor sites (**Figure 39**). The possibility of DNA strand switching has been postulated before (Hassler et al., 2018; Marko et al., 2019; Banigan et al., 2020), but has never been observed experimentally so far.

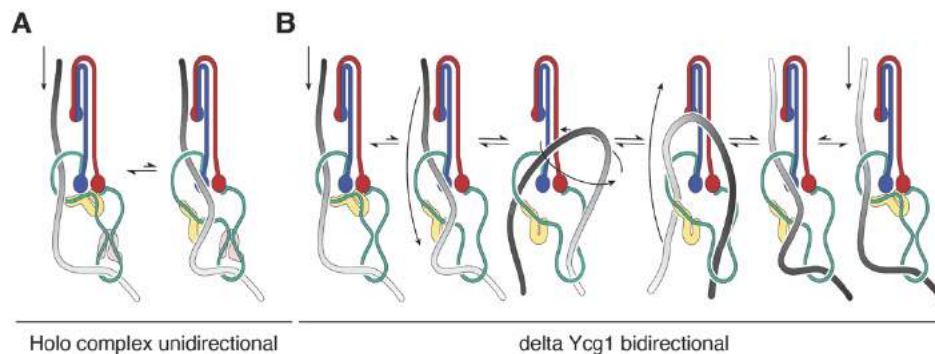


**Figure 39: Bidirectional loop extrusion by delta Ycg1 complex.** Schematic representation of the events during unidirectional and bidirectional loop extrusion by wild type and delta Ycg1 condensin complex respectively. Image adopted and modified from Shaltiel et al., 2022.

I hypothesize that, in the absence of the Ycg1 subunit, the ‘safety belt’ compartment is not properly closed and the DNA strands enclosed by the Ycs4-Brn1 ‘motor’ chamber and Ycg1-Brn1 ‘anchor’ chamber can randomly exchange. As a result, the tetramer sometimes reels DNA in from one side and sometimes from the other side. This behavior is visible in the quantification plots (**Figure 29**), where the increase in the red line (DNA loop) sometimes takes place at the expense of the blue and sometimes at the expense of the yellow line (DNA at either side of the loop). A direction change was visible in around two thirds of the DNAs with loops extruded by the delta Ycg1 complex, thus marking a striking difference to the holocomplex. However, this direction change was abolished in the presence of higher salt conditions (125 mM) It is speculative to think that perhaps the ‘safety belt’ chamber remains closed at higher salt concentration. Additional DNA binding experiments and DNA entrapment within this ‘safety belt’ in various salt concentrations can shed more light on this aspect.

### **3.3 Ycg1 acts as a negative regulator for condensin function**

In line with the higher ATPase rate, deleting the Ycg1 subunit increased the DNA loop extrusion efficiency and loop lifetimes (**Figure 32**). Higher extrusion efficiency and longer lifetime of loops are an indication that protein complex is more efficient in DNA binding and can accommodate the DNA for longer time; although an increased DNA binding was not observed in gel shift assay with the *Ct* delta Ycg1 complex. However, the extrusion rate and the stall force dependence were similar between delta Ycg1 complexes and holocomplexes.

My findings are consistent with the observation that human condensin I complex depleted of the Ycg1 homolog CAPG were able to support the formation of mitotic chromosomes in *Xenopus* egg extracts (Kinoshita et al., 2015). In a recent study, Yoshida and colleagues showed that the Ycg1 homolog CAPG2 plays a negative role in the activity of the human condensin II complex (Yoshida et al., 2022). It is hence possible that Ycg1 or its corresponding vertebrate homologs have a negative role in regulating their ATPase and DNA compaction activities to prevent the over-compaction of mitotic chromosomes.

## 4 The kleisin ‘safety belt’ is the anchor for condensin-mediated DNA loop extrusion

From sequence homology, both *Sc* and *Ct* Brn1 kleisin subunits contain a ‘safety belt’ region, although they differ in certain aspects. The *Sc* Brn1 safety belt harbors more negatively charged residues compared to the *Ct* Brn1 safety belt. In addition, the spacing between the two positively charged patches within the safety belt is lower for *Ct* than for *Sc* Brn1, which might allow the *Ct* Brn1 to bind DNA with higher efficiency. Efficient DNA binding by the kleisin safety belt could be one of the reasons why *Ct* delta Ycg1 complex is active, whereas the *Sc* delta Ycg1 complex is inactive.

Consistent with this hypothesis, deletion of the Brn1 safety belt region in addition to Ycg1 deletion resulted in *Ct* condensin complexes that could no longer hydrolyze ATP and had a reduced DNA binding affinity. These complexes did not extrude DNA loops either. Charge reversal mutations of the positively charged patches within the safety belt (BC<sub>1/2</sub>) had the same phenotype as deletion of the entire safety belt, as they did not show DNA loop extrusion activity. However, these complexes were still active ATPases with a similar activity as that of the delta Ycg1 complex with an unmodified Brn1 kleisin. It is not clear why these complexes can still hydrolyze ATP but no longer extrude DNA loops.

Mutation of the hydrophobic residues that constitute the ‘latch’ region, which closes the kleisin safety belt, also still displayed DNA-stimulated ATPase activity, but were no longer able to extrude DNA loops. Together, these results prove that the kleisin safety belt plays a pivotal role in DNA loop extrusion and acts as the true anchor; a function that had previously been assigned to the Ycg1 subunit.

Based on my results, I propose a model where the Brn1 safety belt is open during the search for a DNA substrate. When in close vicinity, DNA is docked into the safety belt chamber by electrostatic interactions between the negatively charged DNA backbone and the positively charged BC patches. This process is independent of the presence of the Ycg1 subunit. Once the DNA has been

placed into the safety belt chamber, the latch residues close the safety belt and entrapment of DNA within the kleisin loop functions as anchor for the condensin complex (**Figure 40**). Any change within the positive charge patch or latch residues interferes with this process and prevents DNA loop extrusion.

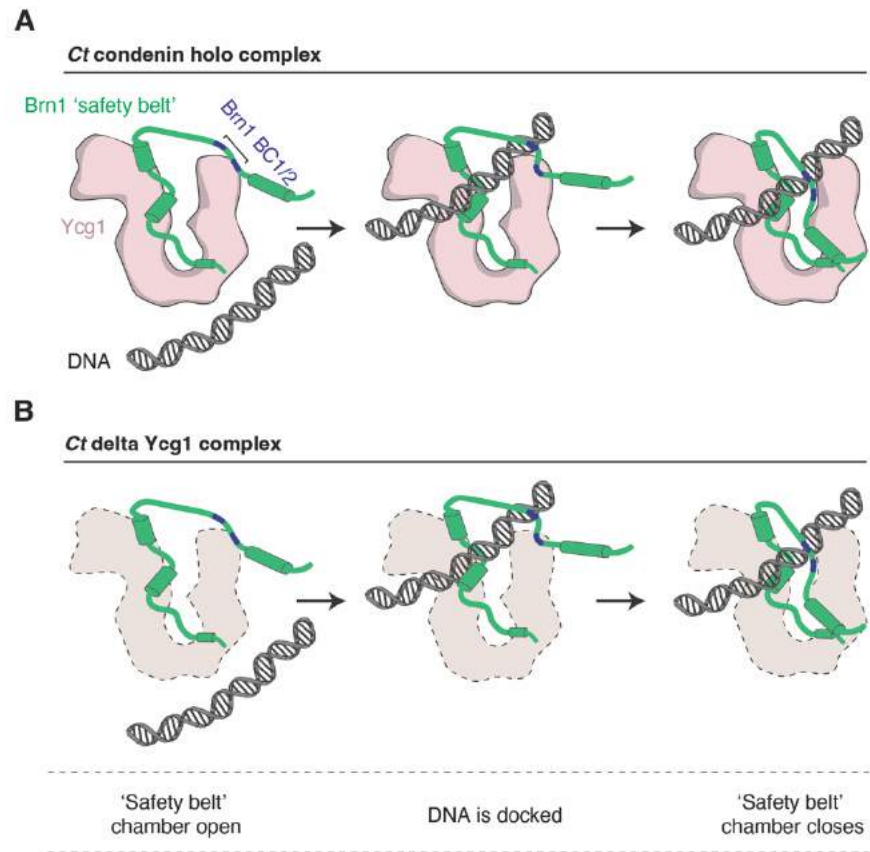


**Figure 40: DNA within the 'safety belt' chamber. A, B.** Schematic representation of the 'safety belt' chamber of *Ct* condensin holo complex and delta Ycg1 complex respectively with Brn1 subunit. DNA is docked into an open 'safety belt' chamber via the Brn1<sub>BC1/2</sub> interaction and 'safety belt' closes when the latch residues interact with C-terminal of Brn1.

## 5 Physiological relevance of DNA loop direction changes

Asymmetric extrusion has been shown to be inefficient to fully compact large genomes in mathematical simulations. In these experiments, symmetric loop extrusion was required to explain available Hi-C data. One possibility to achieve symmetric loop extrusion can be an intrinsically asymmetric mode of extrusion that frequently changes its direction (Banigan et al., 2020; Banigan & Mirny, 2020b).

Consider an array of one-sided LEFs placed on a linear chromatin fiber with different orientations of motor and anchor domains. In the case where two such extruders face each other with their anchor (25% or random orientations), the chromatin in between them will not be reeled into a loop and will be left uncompact (Figure 41). With two-sided extruders, this problem can be easily overcome. But a similar result can be obtained with a fraction of one-sided LEFs that can change direction at random. So far, such a direction switch has only been observed for the *Ct* delta Ycg1 complex. It is tempting to speculate that a fraction of condensin that lacks the Ycg1 subunit is actually beneficial and important for the complete compaction of genomes.

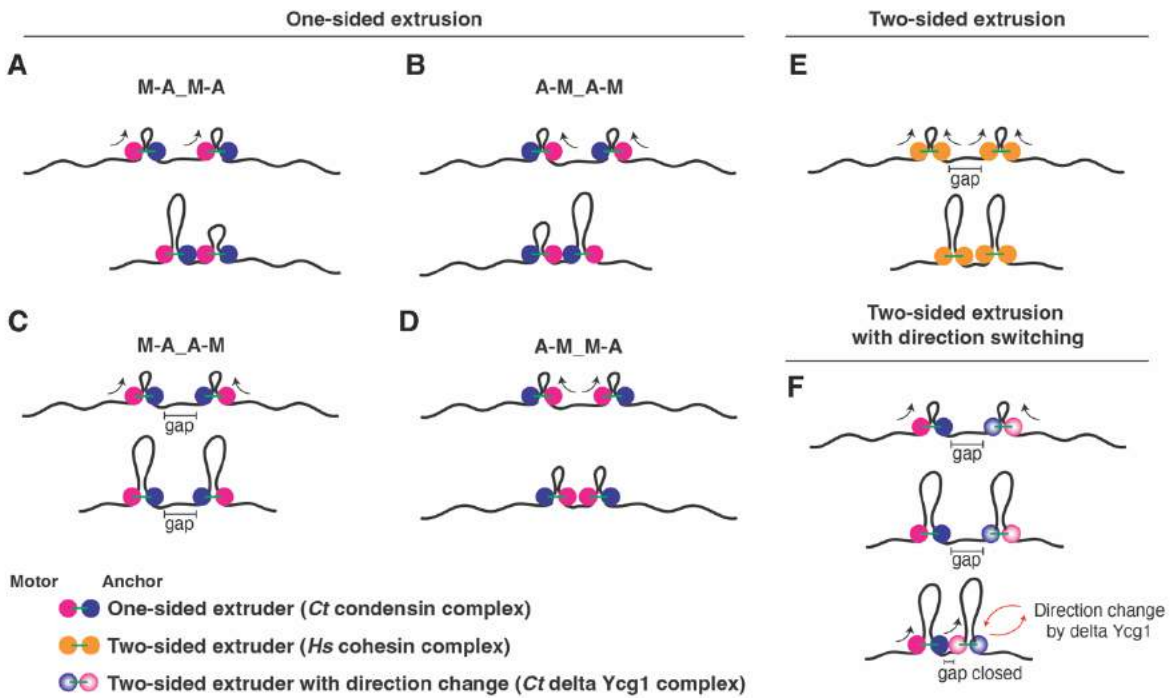


**Figure 41: Complete genome compaction by loop extrusion with direction switch. A – D.** Exemplary cases of one-sided loop extrusion by LEF such as *Ct* wild type complex, two LEFs are positioned on genome with different orientations of their motor (M) and anchor (A). Every one case out of four will leave gap in the genome like in C, where the two LEF have their anchor faced to each other. **E.** Two-sided extruder such as human cohesin and condensin complex will close the gap in genome and achieve full compaction; **F.** One-sided extruder can also achieve full genome compaction with few extruders than can switch direction such as *Ct* delta Ycg1 complex.

## 6 Outlook

The condensin complex has been attributed to compaction of interphase chromatin that plays crucial role in cell division. Biochemical, biophysical and structural studies have shed lights into how condensin might function and it has been unanimously accepted that condensin complex extrudes DNA loops to accomplish chromosome condensation. It is still quite a mystery how all five subunits of condensin complex come together to achieve such a feat. A recent study by Shaltiel and colleague has given more insights to the underlying mechanism of condensin's loop extrusion activity (Shaltiel et al., 2022). Although, the dynamics of each subunit during their active cycle is not fully understood. Different forms of condensin have been shown by structural studies (Lee et al., 2020) and using biochemistry and single-molecule imaging, functionality of different subunits have been characterized (Ganji et al., 2018; Hassler et al., 2019; Kschonsak et al., 2017). However, more detailed mode of action that governs the catalytic cycle of condensin is not fully understood. Methods such as single-molecule FRET can be useful to unravel the complete dynamics of condensin's function.



**Part IV**  
**Materials and Methods**

# 1 Materials

## 1.1 Laboratory equipment

Table 1: Standard laboratory equipment used in this study

Standard laboratory equipment	Source
Analytical FPLC-system ÄKTA Ettan	GE Healthcare
Cell lysis sonicator SFX 550	Branson
Centrifuge 1.5 - 2 ml tubes 4°C Heraeus Fresco 21	Thermo Fisher Scientific
Centrifuge 1.5 - 2 ml tubes Centrifuge 8424	Eppendorf
Centrifuge 15 ml and 50 ml tubes Heraeus Multifuge 3SR+	Thermo Fisher Scientific
Centrifuge 50 ml and 1000 ml tubes Avanti J-20 XP	Beckmann
Fluorescence gel imager Typhoon FLA 9,500 scanner	Cytiva
Nanodrop ND-1000	Thermo Fisher Scientific
PCR Machine DNAEngine	Bio-Rad
Preparative FPLC-systems ÄKTA purifier 100, ÄKTA purifier 10, ÄKTA pure 25	GE Healthcare
Ultrasonic cleaner USC-T	VWR
Leica GSDIM TIRF Microscope	Leica
Epoxy	Wiko
Drill	Dremel
Rotary shadowing machine	EMBL EM core facility
Carbon coater Leica ACE 600 coater	Leica
Morgagni TEM	FEI

## 1.2 Protein purification columns

Table 2: Protein purification columns used in this study

Column	Purification
Ni-Sepharose 6FF beads (GE Healthcare)	Affinity purification of His-tagged proteins
RESOURCE Q, 6 ml (GE Healthcare)	Anion exchange purification
Superose6 10/300 GL column, 24 ml (GE Healthcare)	Preparative size exclusion chromatography
Superdex 200 Increase 3.2/300, 2.4 ml (GE Healthcare)	Analytical size exclusion chromatography

## 1.3 Software

Table 3: Software used in this study

Name	Source
<i>Protein sequence analysis</i>	
ProtParam tool (ExpASy server)	Gasteiger et al., 2005
Jalview (v.2.10.4b1)	Waterhouse et al., 2009

<i>DNA sequence analysis</i>	
SnapGene (v.6.0)	SnapGene® software
<i>Image analysis</i>	
FIJI-Image J (v.2.3.0/1.53f)	Schindelin et al., 2012
<i>Additional software</i>	
Office 2019	Microsoft

## 1.4 Consumables and kits

Table 4: Consumables and kits used in this study

<b>Name</b>	<b>Source</b>
DNA Gel extraction kit	Qiagen
DNA Miniprep kit	Qiagen
DNA PCR-purification kit	Qiagen
Electroporation cuvettes 0.2 cm Gene Pulser	Bio-Rad
Filter membrane Express Plus (pore size 0.22 µm, diameter 47 mm)	Merck Millipore
Filter paper Whatman (pore size 4-7 µm, grade 595 ., diameter 150 mm)	GE Healthcare
Gravity flow chromatography column, Econo-Pac (length 14 cm)	Bio-Rad
Precast SDS-Gels 3-8% Bis-Tris NuPAGE	Thermo Fisher Scientific
Protein A dynabeads	Thermo Fisher Scientific
SDS gel cassettes (1.0 mm)	Thermo Fisher Scientific
SYBR green PCR Master mix	Applied Biosystems
Syringe filter Millex GP (0.22 µm)	Merck Millipore
TLC PEI Cellulose	Merck Millipore
Ultrafiltration columns Viva spin (MWCO: 3,000; 10,000; 30,000)	Sartorius

## 1.5 Chemical reagents

All common chemicals including antibiotics, salts, buffers, precipitants and amino acids were ordered from Sigma-Aldrich, Merck, Roth or Fluka. Media components and sugars were ordered from Becton Dickinson or Biosynth. Specific chemical reagents are listed below (Table 5).

Table 5: Specific chemical and reagents used in this study

<b>Reagent</b>	<b>Abbreviation</b>	<b>Source</b>	<b>Application</b>
[ $\alpha$ - <sup>32</sup> P]-adenosin triphosphate	[ $\alpha$ - <sup>32</sup> P]-ATP	Hartmann Analytic	ATP hydrolysis assay
2-mercaptoethanol	BME	Roth	Protein purification
Agarose Ultrapure		Thermo Fisher	EMSA experiments
cOmplete protease inhibitor cocktail tablets	cOm-EDTA	Roche	Protein purification
Coomassie brilliant blue R250	CBB R250	Roth	Protein in-gel staining

## Materials and Methods

Deoxynucleotide solution mix	dNTPs	Thermo Fisher Scientific	Cloning
Dibromobimane	bBBr	Sigma	Crosslinking exp.
Dimethyl sulfoxide	DMSO	Fluka	Crosslinking exp.
Dithiothreitol	DTT	biomol	protein purification
Ethidium bromide solution 1% (w/v)	EtBr	Roth	Agarose gel electrophoresis
Imidazole		Sigma	Protein purification
Isopropyl $\beta$ -D-thiogalactopyranoside	IPTG	Peqlab	Protein expression
FuGENE.		Promega	Transfection reagent
Phenylmethylsulfonyl fluoride	PMSF	Appllichem	Protease inhibitor

### 1.6 Biological reagents

All restriction enzymes were ordered from New England Biolabs (NEB)

Table 6: Biological reagents used in this study

Reagent	Source
<i>Cloning</i>	
2x Gibson Assembly Master Mix	NEB
Alkaline phosphatase, calf intestinal	NEB
In-fusion cloning enzyme	Clontech
Phusion DNA polymerase	Thermo Fisher Scientific
T4-ligase	Thermo Fisher Scientific
<i>Marker</i>	
1-kb DNA ladder	NEB
Page Ruler Prestained protein ladder	Thermo Fisher Scientific

### 1.7 Bacterial strains

Table 7: *E. coli* strains used in this study

Name	Genotype	Source
<i>E. coli</i> DH5 $\alpha$	F- $\phi$ 80lacZ $\Delta$ M15 $\Delta$ (lacZYA-argF) U169 recA1 endA1 hsdR17 (rk-, mk+) phoA supE44 $\lambda$ - thi <sup>-</sup> 1 gyrA96 relA1	Invitrogen, Hanahan, 1983
<i>E. coli</i> MegaX DH10B T1R	F-mcrA $\Delta$ (mrr-hsdRMS-mcrBC), $\Phi$ 80lacZ $\Delta$ M15 $\Delta$ lacX74 recA1 endA1 araD139 $\Delta$ (ara, leu)7697 galU galK $\lambda$ - rpsL nupG tonA	
<i>E. coli</i> DH10Multibac YFP	F- mcrA $\Delta$ (mrr-hsdRMS-mcrBC) $\Phi$ 80(lacZ) $\Delta$ M15 $\Delta$ lacX74 recA1 endA1 araD139 $\Delta$ (ara, leu)7697 galU galK l- rpsL nupG/BacloxP/ pBADZ-His6Cre/ pMON7124	EMBL (Berger)

## 1.8 Plasmids

Table 8: Plasmids used in this study

<b>ID</b>	<b>Genotype</b>	<b>Source</b>
3517	pACEBac1- <i>Ct</i> Ycs4	Robin Stipp
3518	pACEBac1- <i>Ct</i> Ycg1	Robin Stipp
3520	pACEBac1- <i>Ct</i> Brn1-His8	Robin Stipp
3521	pIDC- <i>Ct</i> SMC2	Robin Stipp
3541	pACEBac1- <i>Ct</i> SMC4-StrepII	Robin Stipp
3548	pACEBac1- <i>Ct</i> Ycs4- <i>Ct</i> Ycg1- <i>Ct</i> Brn1- <i>Ct</i> SMC4-StrepII	Robin Stipp
3549	cre pACEBac1- <i>Ct</i> Ycg1- <i>Ct</i> Brn1-His8- <i>Ct</i> SMC4-StrepII-pIDC- <i>Ct</i> SMC2	Robin Stipp
3550	cre pACEBac1- <i>Ct</i> Ycs4- <i>Ct</i> Brn1-His8- <i>Ct</i> SMC4-StrepII-pIDC- <i>Ct</i> SMC2	Robin Stipp
3551	cre pACEBac1- <i>Ct</i> Ycg1- <i>Ct</i> Brn1-His8- <i>Ct</i> Ycs4- <i>Ct</i> SMC4-StrepII-pIDC- <i>Ct</i> SMC2	Robin Stipp
3563	cre pACEBac1- <i>Ct</i> Brn1 ( $\Delta$ 515-634)-His8- <i>Ct</i> Ycs4- <i>Ct</i> SMC4-StrepII-pIDC- <i>Ct</i> SMC2	Robin Stipp
3584	pACEBac1- <i>Ct</i> Ycg1- <i>Ct</i> Ycs4- <i>Ct</i> Brn1-His8- <i>Ct</i> SMC4 (E1475Q)-StrepII	Marc Kschonsak
3604	pACEBac1- <i>Ct</i> Ycs4- <i>Ct</i> Ycg1- <i>Ct</i> Brn1- <i>Ct</i> SMC4-StrepII (Q421L)	Marc Kschonsak
3608	pIDC- <i>Ct</i> SMC2 (E1116Q)	Marc Kschonsak
3609	pIDC- <i>Ct</i> SMC2 (Q147L)	Marc Kschonsak
3723	pIDC- <i>Ct</i> SMC2 C-term ybbr	This work
3724	pACEBac1- <i>Ct</i> SMC4 C-term ybbr-StrepII	This work
3726	pACEBac1- <i>Ct</i> Brn1 110 <sup>th</sup> aa. ybbr-His8	This work
3730	pACEBac1- <i>Ct</i> Ycs4- <i>Ct</i> Ycg1- <i>Ct</i> Brn1-His8- <i>Ct</i> SMC4 C-term ybbr-StrepII	This work
3731	pACEBac1- <i>Ct</i> Ycs4- <i>Ct</i> Ycg1- <i>Ct</i> Brn1-110 <sup>th</sup> aa. ybbr-His8- <i>Ct</i> SMC4 -StrepII	This work
3734	cre pIDC- <i>Ct</i> SMC2 C-term ybbr-pACEBac1- <i>Ct</i> Ycg1- <i>Ct</i> Ycs4- <i>Ct</i> Brn1-His8- <i>Ct</i> SMC4-StrepII	This work
3934	cre pIDC- <i>Ct</i> SMC2-pACEBac1- <i>Ct</i> Ycg1- <i>Ct</i> Ycs4- <i>Ct</i> Brn1-His8- <i>Ct</i> SMC4 C-term ybbr-StrepII	This work
3947	pACEBac1- <i>Ct</i> SMC2	This work
3955	pACEBac1- <i>Ct</i> SMC2 BstX1 site KO at 780 <sup>th</sup> bp	This work
3956	pACEBac1- <i>Ct</i> SMC2 BstX1 site KO at 780 <sup>th</sup> bp and 117 <sup>th</sup> bp	This work
3957	pACEBac1- <i>Ct</i> Brn1 L521D F524D	This work
3958	pACEBac1- <i>Ct</i> Brn1 L521D F524D W532D W538D	This work
3964	pACEBac1- <i>Ct</i> Brn1-His8- <i>Ct</i> Ycs4- <i>Ct</i> SMC4 C-term ybbr-StrepII	This work
3966	pACEBac1- <i>Ct</i> Ycs4- <i>Ct</i> SMC4 C-term ybbr-StrepII	This work
3967	pACEBac1- <i>Ct</i> Ycs4- <i>Ct</i> SMC4 C-term ybbr-StrepII- <i>Ct</i> SMC2	This work
3973	pACEBac1- <i>Ct</i> Brn1 BC2 patch mut.	This work
3974	pACEBac1- <i>Ct</i> Brn1 BC1 patch mut.	This work
3975	pACEBac1- <i>Ct</i> Ycs4- <i>Ct</i> Brn1-His8- <i>Ct</i> SMC4 C-term ybbr-StrepII- <i>Ct</i> SMC2	This work
3976	pACEBac1- <i>Ct</i> Ycs4- <i>Ct</i> Ycg1- <i>Ct</i> SMC4 C-term ybbr-StrepII- <i>Ct</i> SMC2	This work
3993	pACEBac1- <i>Ct</i> Ycs4- <i>Ct</i> SMC4-StrepII- <i>Ct</i> SMC2	This work
3994	pACEBac1- <i>Ct</i> Ycs4- <i>Ct</i> Ycg1- <i>Ct</i> Brn1-His8- <i>Ct</i> SMC4-StrepII- <i>Ct</i> SMC2	This work
4000	pACEBac1- <i>Ct</i> Brn1 C-term ybbr-His8	This work
4016	pACEBac1- <i>Ct</i> Brn1 E514C R629C with C-term HA tag-His8	This work
4021	pACEBac1- <i>Ct</i> Brn1 E514C R629C with C-term HA tag-His8 internal BstX1 KO	This work
4025	pACEBac1- <i>Ct</i> Ycg1- <i>Ct</i> Ycs4- <i>Ct</i> SMC4-StrepII- <i>Ct</i> SMC2	This work
4028	pACEBac1- <i>Ct</i> Ycs4- <i>Ct</i> SMC4-StrepII- <i>Ct</i> SMC2- <i>Ct</i> Brn1 C-term ybbr	This work
4029	pACEBac1- <i>Ct</i> Ycs4- <i>Ct</i> SMC4-StrepII- <i>Ct</i> SMC2- <i>Ct</i> Brn1 BC1/2 patch mut.	This work

4031	pACEBac1- <i>Ct</i> Ycs4- <i>Ct</i> SMC4-StrepII- <i>Ct</i> SMC2- <i>Ct</i> Brn1 L521D F524D W532D W538D-His8	This work
4035	pACEBac1- <i>Ct</i> Ycs4- <i>Ct</i> SMC4-StrepII- <i>Ct</i> Ycg1- <i>Ct</i> SMC2- <i>Ct</i> Brn1 L521D F524D W532D W538D-His8	This work
4039	pACEBac1- <i>Ct</i> Ycg1- <i>Ct</i> Ycs4- <i>Ct</i> SMC4-StrepII- <i>Ct</i> SMC2- <i>Ct</i> Brn1 C-term ybbr	This work
4040	pACEBac1- <i>Ct</i> Ycs4- <i>Ct</i> SMC4-StrepII- <i>Ct</i> SMC2- <i>Ct</i> Ycg1- <i>Ct</i> Brn1 BC1/2 patch mut.	This work
4066	pACEBac1- <i>Ct</i> Brn1 C-term SNAP	This work
4067	pACEBac1- <i>Ct</i> Ycs4- <i>Ct</i> SMC4-StrepII- <i>Ct</i> SMC2- <i>Ct</i> Brn1 C-term SNAP	This work
4068	pACEBac1- <i>Ct</i> Ycs4- <i>Ct</i> Ycg1- <i>Ct</i> SMC4-StrepII- <i>Ct</i> SMC2- <i>Ct</i> Brn1 C-term SNAP	This work

## 1.9 Primers

Table 9: Primers used for this study

Primers	Description	Sequence
SD6	<i>Ct</i> SMC2 C-term ybbr FP	5'-GACTCTCTGGAATTCATCGCTTCTAAACTGGCTAATCTAGAGCCTGCAGTCTCG -3'
SD7	<i>Ct</i> SMC2 C-term ybbr RP	5'-GCGATGAATTCCAGAGAGTCCTTCAGATCAGCCGGCGTC -3'
SD8	<i>Ct</i> SMC4 C-term ybbr FP	5'-GACTCTCTGGAATTCATCGCTTCTAAACTGAGCTTCGGATCCCCGGG -3'
SD9	<i>Ct</i> SMC4 C-term ybbr RP	5'-GCGATGAATTCCAGAGAGTCGGGCGCCCCGCCAATGAC -3'
SD12	<i>Ct</i> Brn1 110 <sup>th</sup> aa. ybbr FP	5'-GACTCTCTGGAATTCATCGCTTCTAAACTGGCTGGCGGTAGGGCTGTTACCC -3'
SD13	<i>Ct</i> Brn1 110 <sup>th</sup> aa. ybbr RP	5'-GCGATGAATTCCAGAGAGTCAACCACGACTTCCTCATCGTC -3'
SD30	<i>Ct</i> Brn1 W532D W538D FP	5'-GACCAGGCCCTTCAGAAGAACGATACCAGTGC CGAACACGATAGGATACGAAAGATCAAGGACG -3'
SD31	<i>Ct</i> Brn1 W532D W538D RP	5'-CGTCCTTGATCTTTCGTATCCTATCGTGTTCGGC ACTGGTATCGTTCTTCTGAAGGGCCTGGTC -3'
SD47	<i>Ct</i> SMC2 261 <sup>th</sup> aa. BstXI KO FP	5'- CAGCGCGCAAAGAATTGGAGGAGTCTGCGCA TCGG -3'
SD48	<i>Ct</i> SMC2 261 <sup>th</sup> aa. BstXI KO FP	5'- GACTCTCTGGAATTCATCGCTTCTAAACTGGCT GAGGATCTCGAGGGCGGTAGCAGC -3'
SD51	<i>Ct</i> Brn1 W538D FP redesigned	5'- CGAACACGACAGGATACGAAAGATCAAGGAC G -3'
SD53	<i>Ct</i> Brn1 W538 RP redesigned	5'- GTATCCTGTCGTGTTCCGGCACTGGTATCG -3'
SD54	<i>Ct</i> Brn1 Gibson assembly FP	5'- ATAACCCCTAGGGTATACCCATCTAAGGTAGC GAGTTTAAACACTAG -3'
SD55	<i>Ct</i> Brn1 Gibson assembly RP	5'- GATTTCACTTATCTGGTTCCAATTAGTTAGATG GGTATACCCTAGG -3'
SD 56	<i>Ct</i> Brn1 510 <sup>th</sup> aa. FP	5'- CCGAGGTCAGCGGAGAAGATCC -3'
SD57	<i>Ct</i> Brn1 510 <sup>th</sup> aa. RP	5'- GCTTGTTTTAAGGACGCGCCGC -3'
SD58	<i>Sc-Ct</i> Brn1 fusion FP	5'- GGC GCGCGTCCTTAAAACAAGCAGAGGCGAC GTTAGTTCGGGG -3'
SD59	<i>Sc-Ct</i> Brn1 fusion RP	5'- GGATCTTCTCCGCTGACCTCGGGTTGACATTAT CATCATCTTGTTTCATCATGTGATG -3'

## Materials and Methods

---

SD62	<i>Ct</i> Brn1 Tn7L RP	5'- AGGGAAGAGTGACAAAATAGATGGG -3'
SD63	Gibson assembly HA tag from 2648 FP	5'- CCATCACCATCACCATCACCATGGTGGCCGCAT CTTTTACC -3'
SD64	Gibson assembly HIS tag from 4001 RP	5'- GGTAAAAGATGCGGCCACCATGGTGTGATGGTGA TGGTGATGG -3'
SD65	Gibson assembly HA tag from 2648 RP	5'- CTGCAATAAACAAGTTAACAACAACAATTGTT AATGACCAGCAGCGTAATCTGG -3'
SD66	stop codon remove Tn7L from 4001 FP	5'- CCAGATTACGCTGCTGGTCATTAACAATTGTTG TTGTAACTTGTATTGTCAGC -3'
SD68	internal BstXI site remove from 4016 RP	5'- GGGGATGAGCACCATCACCATCATCATCACCAT GGTGGCCGCATCTTTTACC -3'
MK43	<i>Ct</i> Brn1 R554D R556D K557D K559D FP	5'- CAACAAGCCCAACGAGCCCACGGATCAAGACG ATGAGGATCAGCCTTTTGAGATCGATTTTCGTC -3'
MK44	<i>Ct</i> Brn1 R554D R556D K557D K559D RP	5'- GAAATCGATCTCAAAGGCTGATCCTCATCGTC TTGATCCGTGGGCTCGTTGGGCTTGTGACG -3'
MK47	<i>Ct</i> Brn1 R539D R541D K542D K544D FP	5'- AACTGGACCAGTGCCGAACACTGGGATATAGA TGATATCGACGACGTCAACAAGCCCAACGAGCCC AC -3'
MK48	<i>Ct</i> Brn1 R539D R541D K542D K544D RP	5'- GCTCGTTGGGCTTGTGACGTCGTCGATATCAT CTATATCCCAGTGTTCCGGCACTGGTCCAGTTCT TC -3'
MK342	<i>Ct</i> Brn1 L521D F524D FP	5'- GATCCACGAAGATATCGATAGCTACGATGACC AGGCCCTTCAGAAGAAGACTGGACCAGTGCC -3'
MK343	<i>Ct</i> Brn1 L521D F524D RP	5'- GGTCCAGTTCTTCTGAAGGGCCTGGTCATCGTA GCTATCGATATCTTCGTGGATCTTC -3'
<i>Primers for EMSA</i>		
	EMSA 35mer annealed dsDNA	5'-6-FAM-CCTATAGTGAGTCGTTTCGATATTACAATT CACTGG-6-FAM-3' 5'-CCAGTGAATTGTAATATCGAACGACTCACTATA GG -3'
	EMSA 51mer annealed dsDNA	5'-6-FAM-ATTAGTTACTAAGATCCTTCCTCTGTAGA AGAATGAGATTATCGGAGACAG-6-FAM-3' 5'-6-FAM-CTGTCTCCGATAATCTCATTCTTCTACAG AGGAAGGATCTTAGTAACTAAT-6-FAM-3'

FP – Forward primer

RP – Reverse primer

## 1.10 General buffers and media

Table 10: General buffers and media in this study

Name	Composition
<i>General buffers</i>	
6x DNA-loading buffer	15% (v/v) ficoll, 0.25% (w/v) orange G
1x TAE agarose gel running buffer	40 mM Tris-Cl, 0.115% (v/v) acetic acid (glacial), 10 mM EDTA pH 8.0
Coomassie destaining solution	30% (v/v) methanol, 7% (v/v) acetic acid
Coomassie staining solution	0.2% (w/v) Coomassie brilliant blue R250, 45% (v/v) ethanol, 10% (v/v) acetic acid
SDS-PAGE TRIS-Tricine-SDS running buffer	25 mM Tris base, 50 mM Tricine, 0.1% (w/v) SDS
Phosphate Buffer Saline (PBS)	137 mM NaCl, 2.7 mM KCl, 10 mM Na <sub>2</sub> HPO <sub>4</sub> ·2H <sub>2</sub> O, 1.76 mM KH <sub>2</sub> PO <sub>4</sub> pH 7.2
5x SDS protein loading buffer	250 mM Tris-Cl pH 6.8, 10% (w/v) SDS, 50% glycerol (v/v), 0.5% (w/v) bromophenol blue, 0.5 M DTT
<i>Bacterial culture media</i>	
LB	1% (w/v) tryptone, 0.5% (w/v) yeast extract, 0.5% (w/v) NaCl
2xTY	1% (w/v) tryptone, 1% (w/v) yeast extract, 0.5% (w/v) NaCl
SOC	2% (w/v) tryptone, 0.5% (w/v) yeast extract, 8.55 mM NaCl, 2.5 mM KCl, 10 mM MgCl <sub>2</sub>
<i>Insect cell culture media</i>	
SF 900 III serum-free medium	Thermo Fisher Scientific

The EMBL media kitchen prepared standard LB plates and bacterial media with or without antibiotics: Ampicillin (100 µg/ml), Kanamycin (40 µg/ml), Gentamycin (7 µg/ml).

## 2 Methods

### 2.1 General molecular biology techniques

#### *Plasmid amplification and purification*

Plasmids were amplified by transformation in chemical competent *E. coli* DH5 $\alpha$  cells. Cells were incubated with DNA (100-200 ng) for 30 min on ice, followed by a heat shock for 45 s at 42°C and cooled down on ice for 60 sec. Cells were then recovered in SOC medium for 60 min at 37°C and plated on selective plates containing the respective antibiotics. Plates were incubated for 14 to 16 hours at 37°C. Single colonies were inoculated into 6 ml LB medium containing the respective antibiotic and incubated for 16 hours at 37°C. Plasmids were purified using a Miniprep kit (Qiagen) according to manufacturer's instructions.

#### *Polymerase chain reaction (PCR)*

Polymerase chain reactions (PCRs) were performed with Phusion polymerase (Thermo Fisher Scientific) or X7 polymerase (EMBL Pepcore team) to amplify gene fragments. Template DNA (5-20 ng) was used with final concentrations of 0.5  $\mu$ M primer, 1x Phusion-buffer (Thermo Fisher Scientific), 200  $\mu$ M dNTPs (Thermo Fisher Scientific) and 2 U DNA polymerase. DNA fragments were amplified in 35 cycles of 10 sec denaturation at 98°C, 30-45 sec primer annealing at a primer-specific temperature and elongation at 72°C for 60 sec per 1 kb PCR product.

#### *Agarose gel electrophoresis*

DNA fragments derived from PCR reactions or restriction enzyme digests were run on 0.8-1.5% (w/v) agarose gels in 1x TAE buffer at 10-15 V/cm for 30-60 min. DNA samples were supplemented with the DNA loading dye SYBR safe (Thermo Fischer Scientific). DNA samples in the agarose gel were visualized on a blue light LED transilluminator.

#### *Restriction enzyme-T4-ligase based cloning*

Vector and insert DNA were digested for 3 hours with restriction enzymes (NEB) that create complementary overhangs based on the manufacturer's instructions, followed by heat inactivation

of the enzyme. The vector was then dephosphorylated with 10 U alkaline phosphatase (rSAP, NEB) at 37°C for 60 min. Both vector and insert DNA were purified by agarose gel electrophoresis extracted from the gel using a gel-extraction kit (Qiagen) following the manufacturer's instructions. Purified vector and insert DNA were mixed at a molar ratio of 3:1 to 6:1 insert to vector in 1x ligation buffer (Thermo Fisher Scientific) with 1 U T4-ligase (Thermo Fisher Scientific) in a reaction volume of 20 µl and incubated at 25°C for 60 min. The ligation products were then transformed into chemical competent *E. coli* cells for clonal selection and amplification on LB plates containing antibiotics. Expression constructs based on the pACEBac1 vector backbone were created by this strategy.

### ***Site-directed mutagenesis***

Introduction of point mutations, insertion of short DNA sequences or deletion of DNA regions of various lengths was performed using a PCR-based site-directed mutagenesis protocol. Long oligonucleotide primers were synthesized with at least 20 bp complementary overhangs on each side of the desired mutation, insertion or deletion and with a few base-pair offset on the forward and reverse primer at the 3' end of each oligo. A mixture containing 50 ng template DNA, 1 U Phusion polymerase enzyme (Thermo Fisher Scientific), 0.1 µM forward and 0.1 µM reverse primer, 1x Phusion buffer (Thermo Fisher Scientific) and 200 µM dNTP (Thermo Fisher Scientific) in a 50 µl reaction was prepared. The plasmid was amplified in 35 cycles with 15 s denaturation at 98°C, 30-45 sec primer annealing at primer-specific temperatures and elongation at 72°C for 60 sec per 1 kb product length. After completion of the PCR reaction, 20 U DpnI (NEB) was added and the reaction was incubated at 37°C for 3 hours to digest the template DNA. The undigested product plasmid DNA was purified with a PCR-purification kit (Qiagen) according to the manufacturer's protocol and eluted in a final volume of 15-30 µl ddH<sub>2</sub>O. A volume of 5 µl of the purified plasmid was transformed into chemically competent *E. coli* DH5α cells and amplified as described above.

### ***Restriction-enzyme-free cloning***

Mutations in the different *Ct* condensin subunits for *Ct* condensin holocomplex expression were cloned by Gibson Assembly (NEB) according to the manufacturer's instructions.. Multiple PCR

fragments and/or restriction-enzyme-digested vectors were cloned with the in-fusion cloning kit (Clontech) or the 2x Gibson Assembly Master Mix (NEB).

### ***DNA concentration determination***

DNA concentrations were determined by UV spectroscopy at a wavelength of 260 nm using a NanoDrop spectrophotometer (Thermo Fisher Scientific).

## **2.2 General biochemical methods**

### ***Sample preparation for SDS-PAGE***

Recombinant protein samples or fractions from affinity chromatography runs were mixed with 4x protein loading buffer, heated at 99°C for 5 min, spun down centrifugation at 13,000 rpm for 1 min. Samples (10-15  $\mu$ l ) were loaded onto pre-cast 3-8% Bis-tris gradient gels (NuPAGE, Thermo Fischer Scientific) and separated in Tris-Tricine-SDS buffer. PageRuler Prestained protein ladder (Thermo Fischer Scientific) was used as molecular marker.

### ***Coomassie staining***

SDS-PAGE gels were stained in Coomassie staining solution for 15-45 min shaking at room temperature. Gels were afterwards de-stained and finally stored in ddH<sub>2</sub>O until scanning.

### ***Protein concentration determination***

Protein concentrations were determined by measuring the absorbance at 280 nm using the NanoDrop spectrophotometer (Thermo Fisher Scientific). The theoretical extinction coefficient at 280 nm was calculated based on the amino acid sequence of the protein using the ProtParam tool on the ExPASy server (Gasteiger et al., 2005). The concentration was calculated according to the Beer-Lambert law.

## 2.3 *Ct* condensin protein expression

### *Cloning of Ct condensin genes*

Individual genes of the subunits of the *Ct* condensin protein complex were initially cloned into the pACEBac1 vector, except the SMC2 gene, which was initially cloned into the pIDC vector. For the ease of cloning, the *BstXI* sites were removed from the SMC2 gene later on and cloned in pACEBac1 vector as well. From here on, SMC2 gene is in a pACEBac1 vector unless indicated otherwise. Deletion or insertion of small DNA sequences and site-directed mutagenesis were performed using the individual pACEBac1 plasmids. Each gene was then assembled into the final expression vector by restriction enzyme cloning using *BstXI* and *I-CeuI* or by restriction-free cloning via Gibson Assembly in case the pre-assembled vector was too big. Once the final plasmids had been created, they were confirmed by test digestion and sequencing with the appropriate primer sets.

### *Bacmid assembly and preparation*

The final plasmids with all five *Ct* condensin genes were transformed into *E. coli* DH10MultibacYFP cells by electroporation. For this, 1  $\mu$ l plasmid DNA (100 ng) was mixed with 50  $\mu$ l electrocompetent cells and electroporated using the following settings: 200  $\Omega$ , 25  $\mu$ F and 1.8 V. Pre-warmed SOC media was immediately added to the cells and the mix was incubated at 37°C for 4-5 hours. Cells were then spun down and plated onto LB plates containing kanamycin, tetracycline, gentamycin, IPTG and X-Gal. The plates were incubated at 37°C for 16 hours to overnight. Individual white colonies were then selected and streaked onto a fresh plate for confirmation. White colonies were inoculated into liquid LB media with appropriate antibiotics at 37°C for 16 hours for bacmid amplification. Cultures were then spun down and cell pellets were resuspended, lysed and neutralized using buffers from plasmid isolation kits (Qiagen) mentioned above. Plasmid DNA were then precipitated with isopropanol and pellets were washed with first with 100% and then with 70% ethanol. Bacmids were then dissolved in 30  $\mu$ l water for immediate transfection or dissolved in 70% ethanol for long-term storage at -20 °C.

### ***Insect Cell culture***

Sf21 cells (IPLB-Sf21-AE) isolated from *Spodoptera frugiperda* (Fall armyworm) were maintained in SF 900 III serum-free medium (Thermo Fisher Scientific) at 27°C. Insect cells were grown in Erlenmeyer glass flasks (DWK Life Sciences) with a culture volume of 1/5 of the total volume of the flask. Media was exchanged every 48-72 h. Cells were stained with Trypan Blue (Thermo Fischer Scientific) and the living cell concentration was determined using a Countess 3 (Invitrogen) spectrophotometer.

### ***Virus production and amplification***

For bacmid transfection, 3 ml of cells at a concentration of  $0.6 \times 10^6$  were added into a 6-well plate and allowed to settle completely for 15-20 min. In the meantime, 30  $\mu$ l bacmid DNA was incubated with 10  $\mu$ l FuGENE Transfection reagent (Promega) for 30 min. Next, 2 ml of media were aspirated from each well and the bacmid-FuGENE mixture was added to the cells drop-by-drop. The mixture was incubated at 27°C. After 24 hours, 2 ml media was added and the GFP signals were monitored every day post 48 hours of transfection. Transfected cells were then observed under a fluorescence microscope with GFP and brightfield channel to determine the transfection efficiency. Upon successful transfection, cells would emit strong green fluorescence signal and virus was harvested once at least 1/5-1/4<sup>th</sup> cells showed such signals. The medium from each well was filter-sterilized with 0.45  $\mu$ m filter to remove cells and stored at 4°C wrapped with aluminum foil as V<sub>0</sub> (Virus generation 0). For virus amplification, 3 ml of V<sub>0</sub> was added to 50 ml insect cells at a concentration of  $0.5 \times 10^6$ . Infected cells were checked every day to determine the percentage of live cells. Proliferation arrest was calculated using the following equation:

$$t = \log x/y / \log 2.3$$

where 't' is time factor for proliferation arrest, 'y' is live cell density on the (n+1)<sup>th</sup> day and 'x' is live cell density on n<sup>th</sup> day. Cells were diluted to half if the density reached  $2 \times 10^6$  to maintain cell-to-virus ratio. Virus was harvested 48 hours after proliferation arrest by spinning down the infected culture at 500xg at 4°C for 10 min, filter sterilized and stored at 4°C wrapped in aluminum foil for further use (V<sub>1</sub>, Virus generation 1). The harvested cell pellet was briefly sonicated, and the lysate was cleared by centrifugation and run on SDS-PAGE to check protein expression levels.

### *Protein expression and purification*

Sf21 cells were grown to a density of  $0.9 \times 10^6$  for large-scale protein expression and 10 ml of V<sub>1</sub> were added to 1,000 ml of cells. Live cell density was checked every day and proliferation arrest was calculated using the aforementioned formula. Cells were harvested 48 hours after proliferation arrest by centrifugation at 600xg at 4°C for 10 min, followed by washing with Phosphate Buffer Saline (PBS). The cell pellet was flash frozen in liq. N<sub>2</sub> and stored at -80°C. For protein purification, the thawed cell pellets were resuspended in 25-30 ml of buffer A (50 mM Tris-Cl pH 7.5, 200 mM NaCl, 5% (v/v) glycerol, 5 mM 2-mercaptoethanol, 20 mM imidazole) containing cOmplete EDTA-free protease inhibitors (Merck) and sonicated at 4°C for 5 cycles of 45 sec each in pulse mode, 1 sec on, 1 sec off, at 50% energy (SFX-550, Branson). The lysate was then cleared by centrifugation at 20,000 rpm at 4°C for 60 min. The cleared supernatant was incubated with pre-washed Ni-Sepharose (Cytiva) beads at 4°C on a rotating wheel for 3-4 hours. Beads were thoroughly washed in 40-50 column volumes buffer A while loaded into a gravity-flow column. Proteins were eluted in 2 ml fractions with buffer A supplemented with 300 mM imidazole. Protein concentration was checked using a Bradford assay (Bio-Rad). Peak elution fractions were pooled and subjected to buffer exchange to low salt buffer (25 mM Tris-HCl pH 7.5, 100 mM NaCl, 5% (v/v) glycerol, 1 mM DTT) on a pre-equilibrated desalting column (HiPrep 26/10 desalting column, Cytiva). The eluate was loaded onto a RESOURCE Q (Cytiva) anion exchange column pre-equilibrated with low salt buffer. The column was washed with 3 column volumes low salt buffer and proteins were eluted by increasing NaCl concentration to 1 M in a linear gradient of 60 ml in 60 min. The correct peak fractions were identified by running the fractions on an SDS-PAGE and pooled. Pooled fractions were concentrated by ultrafiltration (Vivaspin 30,000 MWCO, Sartorius). The concentrated protein fractions were subjected to size exclusion chromatography using a Superose 6 increase 10/300 column (Cytiva) pre-equilibrated with buffer B (50 mM Tris-Cl pH 7.5, 200 mM NaCl, 5% (v/v) glycerol and 1 mM DTT). The desired proteins often eluted in a single peak from size exclusion chromatography. Peak fractions were pooled, concentrated as described above, flash frozen in liq. N<sub>2</sub> and stored at -80°C in small aliquots. Purified proteins were analyzed by SDS-PAGE.

### ***Mass spectrometry analysis of Ct condensin complexes***

Mass spectrometry analysis of the samples were performed by the EMBL Proteomics Core Facility (PCF). Purified protein samples (*Ct* condensin holo complex and delta Ycg1 complex; 5-10 µg) were trypsin digested in-solution and analyzed by mass spectrometry. Peptide sequences of each subunit of the *Ct* condensin protein complex were mapped to the expected *Ct* protein sequences and an EMBL in-house Sf21 proteome database. No dominant contaminants from Sf21 insect cells were identified. In particular, no peptides corresponding to the Sf Ycg1 homolog CapG1 were identified in the delta Ycg1 sample. To obtain the stoichiometry of each subunit of the condensin complex, quantification using the iBAQ (intensity based absolute quantification) values was performed (Schwanhäusser et al., 2011), calculated as the sum of the intensities of the identified peptides and divided by the number of observable peptides of a protein. Relative protein concentrations were calculated for each subunit by dividing the iBAQ value of each subunit by the average iBAQ value of the five (four in case of the delta Ycg1 complex) subunits. Data were generated from duplicates of the *Ct* condensin holo complex and a single run of the delta Ycg1 complex.

### ***Fluorescent labeling of purified Ct condensin protein complexes***

For fluorescent labeling of the condensin protein complexes, a 13 amino acid long peptide chain, ‘ybbr tag’ (GTDSLEFIASKLA) was added at the indicated positions (Yin et al., 2006). All ybbr-tagged protein constructs were processed and purified as their non-labeled counterparts. *Ct* condensin protein complexes (2-12 µM) were used for enzymatic site-specific fluorescent labeling of the serine hydroxyl group of the ybbr tag with Sfp phosphopantetheinyl transferase (NEB; 1.2 µM) and a 5-fold molar excess CoA-dye conjugate reaction mix in buffer B (supplemented with 10 mM MgCl<sub>2</sub>). The reaction was incubated at 6 °C for 16 h. The labelled protein was separated from free dye by size-exclusion chromatography on a Superose 6 increase 3.2/300 column (Cytiva) pre-equilibrated in buffer B containing 1 mM MgCl<sub>2</sub>. Peak elution fractions were concentrated by ultrafiltration, flash-frozen and stored at -80°C until use. Fractions were analyzed by SDS-PAGE and fluorescence was detected on a Typhoon FLA9500 scanner (Cytiva) with a 635-nm laser and 665-nm long pass filter. Labelling efficiency was estimated to be around 55-85%, as calculated using the following equations –

Protein concentration (M) =  $[A_{280} - (A_{\max} \times CF)]/\epsilon$

Moles dye per mole protein =  $A_{\max}$  of the labeled protein/ $(\epsilon' \times M)$

where  $\epsilon$  = protein molar extinction coefficient;  $A_{\max}$  = Absorbance of a dye solution measured at the wavelength maximum ( $\lambda_{\max}$ ) for the dye molecule; CF = Correction factor, adjusts the amount of absorbance at 280 nm caused by the dye (at 280 nm,  $\epsilon_{280\text{nm}}/\epsilon_{650\text{nm}}=0.05$ ) and  $\epsilon'$  = molar extinction coefficient of the fluorescent dye.

## 2.4 *Ct* condensin protein characterization

### *Rotary shadowing and electron microscopy*

To visualize the integrity of purified *Ct* condensin protein complexes, Platinum (Pt)/Carbon (C) shadowing was performed according to the glycerol spraying method (Tyler & Branton, 1980). Purified condensin protein complexes (holo complex, Walker B mutant complex and delta Ycg1 complex) were diluted to 0.06  $\mu\text{M}$  in freshly prepared EM buffer (200 mM  $\text{NH}_4\text{HCO}_3$  pH 7.5, 30% (v/v) glycerol, 1 mM DTT), immediately sprayed onto freshly cleaved mica and dried under high vacuum. Pt/C shadowing was performed at an angle of  $7^\circ$  for 35-40 s, followed by a stabilizing 10-15 nm layer of carbon coating using the Leica ACE 600 coater (Leica). The Pt/C layers were then floated off and placed onto 100 and 200 mesh copper grids, which were imaged on a Morgagni TEM (FEI). The obtained images were visualized in FIJI (Schindelin et al., 2012).

### *DNA compaction assay*

DNA compaction by condensin was assayed by incubating 5.66 ng/ $\mu\text{l}$  6.4-kb plasmid DNA relaxed by *Nb. BbvCI* (NEB) cleavage with or without 0.06  $\mu\text{M}$  protein complexes in the presence or absence of 1 mM ATP in the above-mentioned EM buffer at room temperature for 5-10 min. Samples were then processed for rotary shadowing as described above and imaged on a Morgagni TEM. Image analysis was performed in FIJI (Schindelin et al., 2012). The 'Freehand line' tool from FIJI was used to mark the outer most periphery of the DNA observed in the images and the area within the boundary was measured. The median area of all data sets was calculated from ~450 individual DNA molecules for each conditions and were replicated at least 3 times. A Mann-Whitney U test was performed to calculate the significance values.

***ATP hydrolysis assay***

ATPase activity of the *Ct* condensin complexes were performed as described (Shaltiel et al., 2022). Briefly, a 6.4-kb plasmid was relaxed with *E. coli* topoisomerase I (NEB) and purified by phenol:chloroform extraction followed by ethanol precipitation. A total of 10  $\mu$ l ATP hydrolysis reactions were set up with 0.3-0.5  $\mu$ M *Ct* condensin complexes in the presence or absence of 25 nM relaxed 6.4-kb plasmid DNA in ATPase buffer (40 mM Tris-HCl pH 7.5, 125 mM NaCl, 10 % (v/v) glycerol, 5 mM MgCl<sub>2</sub>, 5 mM ATP, 1 mM DTT and 50 nM [ $\alpha$ -<sup>32</sup>P]-ATP; Hartmann Analytic). ATP hydrolysis reactions were incubated at 25°C for 10 min and were initiated by addition of [ $\alpha$ -<sup>32</sup>P]-ATP. Upon addition of radioactivated ATP, the reactions were then incubated at different temperatures (25 - 50°C). At an interval of 2 or 3 min, 1  $\mu$ l of the reaction mix was spotted onto PEI cellulose F TLC plates (Merck) for a total duration of 12 or 18 min, respectively. To separate the reaction products, TLC plates were developed in 1:1 1 M LiCl and 2 M formic acid solution and the signals were detected via a phosphor-imager screen, scanned on a Typhoon FLA 9500 scanner (Cytiva). The ATP hydrolysis rate was calculated by a linear fit of the ADP/ATP ratio during in the linear range of the reaction. All experiments were performed at least in three replicates. The calculation of the ADP fraction was performed as follows: First, an average background signal value was deducted from each value of ATP and ADP signals. The ADP fraction signals were then normalized by dividing with the total value of ADP and ATP for that time point. The slope generated by these data points was then multiplied by (initial ATP concentration/protein concentration) to calculate the number of ATP molecules hydrolyzed by each molecule of condensin.

***Electrophoretic mobility shift assay (EMSA)***

EMSAs were performed with *Sc* and *Ct* condensin protein complexes as described (Shaltiel et al., 2022). A 51-bp dsDNA substrate labeled with 6-carboxyfluorescein (6-FAM) was prepared by annealing two primers purified by HPLC (Sigma; 5'-6-FAM-ATT AGT TAC TAA GAT CCT TCC TCT GTA GAA GAA TGA GAT TAT CGG AGA CAG-6-FAM-3' and its corresponding complementary 5'-FAM-labeled oligo). A 35-bp dsDNA substrate was also used for EMSA in some cases (5'-6-FAM-CCT ATA GTG AGT CGT TCG ATA TTA CAA TTC ACT GG-3' and

the corresponding complementary 5'-FAM-labeled oligo). The annealing reaction was performed at a concentration of 20  $\mu\text{M}$  of each oligo in a temperature gradient of  $0.1^\circ\text{C}\cdot\text{s}^{-1}$  from  $95^\circ\text{C}$  to  $4^\circ\text{C}$ . To measure DNA binding, 5 nM DNA substrate was incubated with the indicated concentrations of purified proteins on ice in binding buffer (50 mM Tris-Cl pH 7.5, 125 mM NaCl, 5 mM  $\text{MgCl}_2$ , 50 mM KCl, 5 % (v/v) glycerol, 1 mM DTT) in the presence or absence of 1 mM ATP. After incubation for 10-15 min, free DNA and the DNA-protein complex were resolved by electrophoresis on 0.8% (w/v) agarose gels (Agarose ultrapure grade, nzytech) in Tris-acetate buffer (1 lit of 50x stock solution – 242 g Tris base and 57.1 ml acetic acid) for 1.5–2 h at 240 V or for 16 h at 30 V ( $8\text{ V}\cdot\text{cm}^{-1}$ ) at  $4^\circ\text{C}$ . Fluorescence of the 6-FAM-labelled DNA was then detected on a Typhoon FLA9500 scanner (Cytiva) with excitation at 532 nm using a 575-nm LP emission filter. Images were analyzed with FIJI (Schindelin et al., 2012).

## 2.5 Loop extrusion assay

### *Single-molecule DNA loop extrusion assays*

Imaging and image analysis of the loop extrusion assays were performed as described (Shaltiel et al., 2022). In detail:

#### *$\lambda$ -DNA preparation*

48,502-bp lambda phage DNA ( $\lambda$ -DNA, NEB) was used as DNA substrate. DNA molecules were biotinylated for single-molecule imaging following the protocol described previously (Ganji et al., 2018) with slight modifications: 200  $\mu\text{l}$  of  $\lambda$ -DNA (stock concentration of 100  $\mu\text{g}$ ) was incubated with an oligo pair (10  $\mu\text{l}$  of 100  $\mu\text{M}$  IAS 279, 5'-[phos]-AGGTCCGCCGCC-3'[biotin]; IAS 280, 5'-[phos]-GGGCGGCGACCT-3'[biotin]) in T4 DNA ligase buffer (NEB) at  $65^\circ\text{C}$  for 10 min. The mixture was then allowed to cool off gradually to room temperature. Upon adding 2.5  $\mu\text{l}$  T4 DNA ligase (NEB, 2000000 U/ml) to the mixture, the reaction was incubated at  $42^\circ\text{C}$  for 16 hours. Ligation reaction was subsequently heat inactivated at  $65^\circ\text{C}$  and the reaction was cooled down on ice. Small aliquots were stored at  $4^\circ\text{C}$  until use.

### *Slide preparation*

Glass slides were prepared as described (Ganji et al., 2018). Holes were drilled into cover slips as shown in **Figure 16**. Both glass slides and the cover slips were thoroughly washed with demi-water (demineralized water) twice in a water bath sonicator for 40 min total and with absolute ethanol for another 20 min. Both glass slides and cover slips were then hydroxylated with 1 M KOH for a total of 40 min. Unbound hydroxyl groups were washed off with demi-water and the glass slides and coverslips were then treated with 96% and 100% methanol respectively by sonicating at least for 10 min each. Slides and coverslips were next silanated with 1% (v/v) (3-Aminopropyl)trimethoxysilane (Sigma) in 5% (v/v) acetic acid with 100% methanol for 20 min in sonicator. Excess silane was washed off with methanol and slides were washed thoroughly with demi-water and dried completely with pressurized air. The slides were then PEGylated with a 130 g/l 1:45 mixture of biotin-PEG-SVA (MW 5,000 Da; Laysan) and methyl-PEG-SVA (MW 5,000 Da; BIO\_SVA\_M-SVA; Laysan) in 0.1 M sodium bicarbonate (NaHCO<sub>3</sub>) for 16 h. Excess PEG was washed off with demi-water and slides were dried completely and stored in vacuo at -20°C. Prior to imaging, the glass surfaces were further PEGylated with 25 mM methyl-PEG<sub>4</sub>-NHS (Thermo Fischer Scientific) dissolved in 0.1 M NaHCO<sub>3</sub> solution for at least 2 hours to overnight. They were then washed thoroughly with demi-water, dried completely and assembled for imaging (**Figure 16**).

### *Assembly of the microfluidics device*

Two-sided sticky tapes were used to attach and to create the microfluidics chamber between the glass slide and the cover slip. Small pipet tips were used as inlets for the solutions and tubing was used as outlets (**Figure 16**). The assembled chambers were washed thoroughly with T20 buffer (50 mM Tris-HCl pH 7.5, 20 mM NaCl, 0.2 mM EDTA), incubated with 10 µl streptavidin (Merck, 25 µg/ml) dissolved in 40 µl in T20 buffer for at least a minute and excess was washed off with T20 buffer. A total of 50-200 µl biotinylated λ-DNA at 1-10 pM in imaging buffer (50 mM Tris-HCl pH 7.5, 50 mM NaCl, 2.5 mM MgCl<sub>2</sub>, 5 % (w/v) D-glucose, 1 mM DTT, 500 nM Sytox Orange [SxO, Thermo Fisher Scientific], 40 µg/ml glucose oxidase [Sigma], 15 µg/ml catalase [Sigma], 2 mM Trolox [Sigma]) was loaded into the chamber with a continuous flow of 2-8 µl/min using a

PHD2000 syringe pump (Harvard Apparatus). The unbound DNA fraction was washed off with imaging buffer.

### ***Microscopy and imaging***

A Leica GSDIM TIRF microscope (Advanced Light Microscope Facility, ALMF EMBL) was used for imaging with a UPlanSApo NA 1.43 160x objective (Leica). For sample illumination, Highly Inclined and Laminated Optical sheet mode (HILO) was used with 100 ms exposure time with a 532-nm laser to visualize DNA. For fluorescently labelled proteins, a 643-nm laser was used with 100 ms exposure time in Alternative Laser Excitation (ALEX) method. All images were acquired by an EMCCD camera (iXon Ultra 897, Andor) for a duration of 2-8 min with imaging rates of 7.3 Hz for SxO-only experiments and 2.0 Hz for dual color experiments. The field of view for imaging was manually selected depending on the number of double-tethered DNA molecules. After selection of the imaging field, 0.5-1.25 nM purified *Ct* condensin protein complexes in imaging buffer with 1 mM ATP were flowed in. All buffers for imaging were pre-equilibrated at room temperature before adding protein.

### ***DNA loop extrusion analysis***

A custom-made script written in FIJI (courtesy Indra A. Shaltiel) was used for image analysis. The algorithm projects the SxO pixel intensity information from  $\lambda$ -DNA with loops in 1D. It sums up 13–25 pixels (100 nm/pixel) along the entire length of double-tethered DNA for each frame and generates a kymograph by stacking all intensity values over time. The intensity values of 5 pixels above and below the DNA were measured to determine the median background and noise from all frames. A smoothening of the kymograph was performed with a Gaussian-blurred ( $\sigma = 1.5$ ) copy. The segmentation of the general DNA-containing area was achieved by a (background + (1.5  $\times$  noise)) threshold. The median distance was noted over all time points between the outer-most pixels exceeding the median pixel intensity within the segmented area without the noise and the DNA end-to-end tether length was marked. Intensity values of 9 pixels around the maximum pixel from a smoothened copy per frame were added to attribute it to the ‘loop’ region. Regions above or below this region were referred as ‘above’ or ‘below’ the loop, respectively. Values were corrected for the non-looped DNA within the looped region by subtracting the mean intensity value

of DNA outside the ‘loop’ region from the loop region. The fluorescence intensity values were converted to the nucleotide lengths by normalizing the total intensity to the 48,502-bp length of the  $\lambda$ -DNA. Loop extrusion rates were defined by the slope of the most linear increase of the extrusion curve (red line) of at least 50 consecutive data points selected manually (usually 75-100 data points were used). The extension of the DNA outside of the loop was determined by dividing the median tether length by the expected contour length of the total calculated base pairs outside of the loop. 0.41 nm/bp was used to correct for 500 nM SxO intercalation. Tensions within the DNA were calculated from the extension values according to the worm-like chain model (Marko & Siggia, 1995), with a persistence length of 42 nm. The force within a DNA molecule with loop was calculated as follows-

$$F = \frac{k_B T}{L_p} \left[ \frac{1}{4 \left(1 - \frac{x}{L_0}\right)^2} + \frac{x}{L_0} - \frac{1}{4} \right]$$

where  $L_p$  is persistence length,  $L_0$  is contour length,  $x$  is extension,  $k_B$  is Boltzmann’s constant and  $T$  is absolute temperature (Salomo et al., 2006).

‘Slippage’ (**Figure 21**) was determined by a minimum increase within the outer DNA region, which was stable during the initial extrusion phase of 5 kb and a minimum duration of 10 sec, whereas the ‘direction change’ (**Figure 29**) events were determined by a minimum decrease of 5 kb of the other outer region of the DNA, which was stable prior to the direction switch event. Reeling or slipping rates were determined from the downward or upward slope of the relevant outer region, respectively.

## 2.6 Computational analysis

### *Sequence alignment*

*Sc* and *Ct* Brn1 ‘safety belt’ sequences were aligned with Jalview (Waterhouse et al., 2009) using the default Clustal settings.

### *Protein structure visualization*

PyMOL (Schrödinger, LLC) was used to visualize protein structures.



## Supplementary

Supplementary table 1: Mass spectrometry analysis of *Ct* condensin holocomplex

ID	Protein IDs	Fasta headers	Unique peptides	Sequence coverage [%]	Mol. weight [kDa]	Score	Intensity	MS/MS count
1	P0844_Ct_Brn1	sp P0844_Ct_Brn1 Brn1	84	87	100.05	323.31	1.81E+11	848
2	P0844_Ct_SMC2	sp P0844_Ct_SMC2 SMC2	112	74.6	133.01	323.31	2.39E+11	898
3	P0844_Ct_SMC4	sp P0844_Ct_SMC4 SMC4	123	67	178.4	323.31	2.68E+11	1278
4	P0844_Ct_Ycg1	sp P0844_Ct_Ycg1 Ycg1	88	77.9	126.25	323.31	1.42E+11	649
5	P0844_Ct_Ycs4	sp P0844_Ct_Ycs4 Ysc4	94	72.5	137.48	323.31	1.48E+11	631
6	GENE_1041_Evm.m.Sfld1164.17	Beta-tubulin	22	70.2	50.214	323.31	3.32E+09	51
7	GENE_1223_Evm.m.Sfld1201.10	Hypothetical protein	21	69.8	45.997	323.31	2.6E+09	50
8	GENE_1924_Evm.m.Sfld1299.34	70 kDa heat shock protein	18	49.8	71.392	323.31	2.27E+09	55
9	GENE_20259_Evm.m.Sfld801.50	Casein kinase II subunit alpha	13	45.1	41.317	158.61	8.44E+08	27
10	GENE_12470_Evm.m.Sfld321708.1	Hypothetical protein	11	56.9	22.985	179.19	4.65E+08	17
11	GENE_14871_Evm.m.Sfld339.41	116 kDa U5 small nuclear ribonucleoprotein component	30	40.5	108.73	323.31	2E+09	54
12	GENE_257_Evm.m.Sfld104.48	Putative U5 small nuclear ribonucleoprotein 200 kDa helicase	85	52.6	216.11	323.31	3.83E+09	134
13	GENE_15059_Evm.m.Sfld358.31	Pre-mRNA-processing-splicing factor 8	93	44.8	273.79	323.31	4.67E+09	139
14	GENE_16234_Evm.m.Sfld440.29	Small nuclear ribonucleoprotein F	4	35.6	9.5869	31.074	1.34E+08	5
15	GENE_18280_Evm.m.Sfld595.6	Small nuclear ribonucleoprotein Sm D3	2	14.7	13.976	12.631	1.8E+08	2
16	GENE_16877_Evm.m.Sfld492.15	WD-repeat protein	24	47.2	68.149	254.66	1.03E+09	40
17	GENE_17413_Evm.m.Sfld52.15	Enhancer of mRNA-decapping protein 4 isoform X3	31	32.3	122.13	323.31	1.47E+09	49
18	GENE_6198_Evm.m.Sfld2338.5	U5 small nuclear ribonucleoprotein 40 kDa protein isoform X2	14	47.7	38.506	173.14	5.12E+08	17
19	GENE_20316_Evm.m.Sfld801.117	Hypothetical protein	10	41.7	38.73	113.51	3.82E+08	15
20	GENE_4662_Evm.m.Sfld200.52	Probable small nuclear ribonucleoprotein Sm D2	3	33	12.285	26.892	1.4E+08	5
21	GENE_9422_Evm.m.Sfld321087.2	Structural maintenance of chromosomes protein 4	2	4.3	162.18	19.266	1.89E+09	5
22	GENE_18819_Evm.m.Sfld62.55	Megator	92	45.1	245.7	323.31	2.72E+09	128
23	GENE_2533_Evm.m.Sfld1491.2	E3 ubiquitin-protein ligase UBR3-like	23	30.7	162.66	323.31	1.38E+09	56

24	GENE_17009_Evm.m.Sfld504.28	Rho-associated protein kinase isoform X1	1	0.6	153.66	6.2234	1.56E+09	4
25	GENE_14223_Evm.m.Sfld321929.4	U3 small nucleolar RNA-associated protein 15-like protein	23	60.7	58.97	252.74	5.57E+08	28
26	GENE_14865_Evm.m.Sfld339.35	Heat shock cognate 70 protein	20	40.1	73.019	211.08	6.22E+08	33
27	GENE_18793_Evm.m.Sfld62.25	Cirhin	12	22.2	78.191	133.11	3.83E+08	14
28	GENE_20089_Evm.m.Sfld784.15	Pre-mRNA-processing factor 39 isoform X1	20	31.5	107.67	182.99	5.97E+08	29
29	GENE_2369_Evm.m.Sfld14400.37	Ribosomal protein S6 kinase beta-1	8	19.3	50.684	56.096	2.02E+08	13
30	GENE_16960_Evm.m.Sfld499.8	HEAT repeat-containing protein 1 isoform X1	62	37.3	237.06	323.31	1.38E+09	76
31	GENE_14202_Evm.m.Sfld321926.2	40S ribosomal protein S3	13	62.4	26.688	86.501	2.04E+08	17
32	GENE_16969_Evm.m.Sfld502.2	PAF acetylhydrolase 45 kDa subunit	10	30.9	49.963	122.99	2.08E+08	12
33	GENE_2537_Evm.m.Sfld1491.7	E3 ubiquitin-protein ligase UBR3-like	3	34.5	71.279	124.44	3.14E+08	19
34	GENE_5381_Evm.m.Sfld2184.2	Eukaryotic translation initiation factor 3 subunit I	12	51.9	36.264	97.657	1.8E+08	14
35	GENE_2724_Evm.m.Sfld153.18	Pre-mRNA-processing factor 6	30	39.9	104.26	284.63	5.67E+08	41
36	GENE_13197_Evm.m.Sfld321813.1	Nucleolar protein 11-like	1	33.9	49.65	141.37	2.58E+08	19
37	GENE_15465_Evm.m.Sfld382.18	WD repeat-containing protein 75	22	32.6	99.269	196.68	4.11E+08	30
38	GENE_20826_Evm.m.Sfld900.11	Protein AAR2 homolog	11	33.4	46.061	66.865	2.11E+08	12
39	GENE_15971_Evm.m.Sfld413.10	Probable ATP-dependent RNA helicase DDX23	27	35.5	103.55	243.27	4.02E+08	31
40	GENE_17475_Evm.m.Sfld537.6	Eukaryotic translation initiation factor 3 subunit D	14	32.4	62.652	122.35	1.76E+08	16
41	GENE_15587_Evm.m.Sfld384.137	Eukaryotic translation initiation factor 3 subunit C	26	34.5	101.69	265.88	3.15E+08	32
42	GENE_5347_Evm.m.Sfld217.21	DnaJ homolog subfamily A member 2-like	9	27	45.013	84.342	1.51E+08	9
43	GENE_11452_Evm.m.Sfld321565.2	Tubulin beta chain-like	1	9.5	44	6.9195	1.21E+08	2
44	GENE_3270_Evm.m.Sfld167.23	Hypothetical protein	12	24.6	79.889	112.43	1.69E+08	14
45	GENE_2183_Evm.m.Sfld1390.3	DnaJ	8	27.8	44.774	69.91	1.31E+08	9
46	GENE_16910_Evm.m.Sfld49787.2	LAS1-like protein	15	29.6	60.766	117.5	1.58E+08	18
47	GENE_17440_Evm.m.Sfld532.13	M7GpppN-mRNA hydrolase-like	9	33.6	48.028	64.427	98335000	8
48	GENE_16223_Evm.m.Sfld440.12	Proline-, glutamic acid- and leucine-rich protein 1-like	11	17.7	88.374	88.747	1.91E+08	10
49	GENE_13969_Evm.m.Sfld321906.16	Uncharacterized protein OBRU01_17233	7	30.9	33.71	75.906	82644000	9
50	GENE_20785_Evm.m.Sfld898.4	Hypothetical protein	6	22.6	42.076	54.882	1.18E+08	9
51	GENE_18814_Evm.m.Sfld62.50;	Protein ecdysoneless homolog	15	27.9	65.17	99.66	1.52E+08	15
52	GENE_12065_Evm.m.Sfld321651.2	Dynactin subunit 1	17	35.7	69.411	163.05	1.78E+08	18

53	GENE_13674_Evm.m.Sfld321871.5	Putative eukaryotic translation initiation factor 3, theta subunit	1	28.3	120.65	188.23	2.6E+08	30
54	GENE_13712_Evm.m.Sfld321874.3	Ubiquitin-40S ribosomal protein S27a	4	25.8	17.817	34.778	42476000	7
55	GENE_19173_Evm.m.Sfld664.21	Ribosome-binding protein 1 isoform X2	30	43.7	98.66	238.26	2.41E+08	35
56	GENE_21170_Evm.m.Sfld946.1	Dynactin subunit 1-like	15	40.4	68.804	149.34	1.65E+08	17
57	GENE_9449_Evm.m.Sfld321100.1	Hypothetical protein	1	3.1	45.437	10.666	97988000	1
58	GENE_16083_Evm.m.Sfld426.11	Eukaryotic translation initiation factor 3 subunit H	5	15.8	38.436	36.691	64613000	7
59	GENE_7754_Evm.m.Sfld318774.15	Hypothetical protein	17	37.1	74.879	171.89	1.59E+08	21
60	GENE_21244_Evm.m.Sfld959.7	E3 ubiquitin-protein ligase UBR5	34	17.7	298.48	323.31	4.66E+08	47
61	GENE_546_Evm.m.Sfld1083.1	Histone H4	2	17.5	11.381	12.59	22407000	2
62	GENE_19604_Evm.m.Sfld728.44	40S ribosomal protein S17	4	45.5	15.365	58.383	21809000	4
63	GENE_15337_Evm.m.Sfld36.28	WD repeat-containing protein 26	12	29	61.417	95.625	1.17E+08	16
64	GENE_15608_Evm.m.Sfld385.28	Ribosomal protein S11e	4	29	14.402	24.959	21250000	4
65	GENE_15833_Evm.m.Sfld402.59	Regulator of nonsense transcripts 1 homolog	34	41.2	115.97	254.01	2.39E+08	36
66	GENE_14444_Evm.m.Sfld321942.2	Eukaryotic translation initiation factor 3 subunit M	9	29.6	43.808	68.402	88220000	9
67	GENE_9217_Evm.m.Sfld321029.1	40S ribosomal protein S3a	8	33	29.481	50.266	67245000	8
68	GENE_295_Evm.m.Sfld1060.2	Neurochondrin homolog	12	14.9	83.087	79.193	1.31E+08	13
69	GENE_5447_Evm.m.Sfld2193.28	Eukaryotic translation initiation factor 3 subunit E	9	24.2	51.716	104.97	88020000	11
70	GENE_354_Evm.m.Sfld1068.4	Hypothetical protein	8	36.2	30.819	53.258	64879000	9
71	GENE_14906_Evm.m.Sfld342.19	Ribosomal protein S2	6	28	28.041	43.284	67685000	7
72	GENE_19065_Evm.m.Sfld656.17	Heat shock protein 70	1	10.6	69.76	16.182	1.11E+08	5
73	GENE_20134_Evm.m.Sfld78.15	Polynucleotide 5-hydroxyl-kinase NOL9	11	16.4	103.91	104.5	1.12E+08	12
74	GENE_14692_Evm.m.Sfld330.3	Hypothetical protein	3	15.5	54.339	22.627	42396000	6
75	GENE_17849_Evm.m.Sfld570.21	Eukaryotic translation initiation factor 3 subunit L	9	17.2	63.319	68.601	78190000	11
76	GENE_12295_Evm.m.Sfld321685.4	Actin, muscle-type A2	5	27.1	41.802	71.427	63837000	10
77	GENE_768_Evm.m.Sfld1134.4	Ribosomal protein S5	4	19.2	24.479	26.063	24430000	3
78	GENE_3253_Evm.m.Sfld167.4	Ribosomal protein L22	3	30.8	16.745	20.001	16070000	4
79	GENE_17801_Evm.m.Sfld566.4	Serine/arginine repetitive matrix protein 5-like, partial	1	3.8	23.96	6.2325	47723000	1
80	GENE_4130_Evm.m.Sfld1869.9	Cleavage and polyadenylation specificity factor	13	25.2	80.246	124.41	1.16E+08	15
81	GENE_20859_Evm.m.Sfld900.49	Trifunctional enzyme subunit alpha	14	21.2	81.273	98.743	1.11E+08	18

82	GENE_12055_Evm.m.Sfld321646.2	Serine/threonine-protein kinase minibrain isoform X5	5	28.8	26.909	30.927	27910000	4
83	GENE_4141_Evm.m.Sfld186.9	Septin-interacting protein 1	13	21.4	86.018	87.963	98779000	15
84	GENE_8300_Evm.m.Sfld320479.1	BAG domain-containing protein Samui isoform X2	13	29.4	72.621	86.347	94782000	15
85	GENE_17677_Evm.m.Sfld558.41	RNA polymerase-associated protein CTR9 homolog	15	18	134.46	127.41	1.3E+08	18
86	GENE_4293_Evm.m.Sfld1915.12	Copper-transporting ATPase 1 isoform X1	1	1.6	90.106	6.2838	83534000	2
87	GENE_17240_Evm.m.Sfld523.17	Eukaryotic translation initiation factor 3 subunit G	2	19.5	30.64	43.638	38434000	2
88	GENE_15964_Evm.m.Sfld413.3	60S acidic ribosomal protein P0	4	25.5	29.436	29.337	27444000	5
89	GENE_3680_Evm.m.Sfld1755.2	Parafibromin	12	27.1	60.762	78.665	70574000	13
90	GENE_2965_Evm.m.Sfld158.15	Hypothetical protein	3	16.4	30.718	23.487	24739000	4
91	GENE_8252_Evm.m.Sfld320431.1	Actin, partial	1	37.6	16.537	7.6095	16679000	1
92	GENE_15962_Evm.m.Sfld413.1	PAX3- and PAX7-binding protein 1	10	13.4	111.55	70.656	1.04E+08	11
93	GENE_15914_Evm.m.Sfld405.21	Unnamed protein product	3	20.5	16.217	21.342	10984000	3
94	GENE_1159_Evm.m.Sfld1181.9	Eukaryotic translation initiation factor 3 subunit F isoform X1	3	13.5	30.041	21.135	28727000	4
95	GENE_14316_Evm.m.Sfld321933.44	DDB1- and CUL4-associated factor 7	5	19.1	39.545	34.49	28048000	6
96	GENE_1143_Evm.m.Sfld117.31	RuvB-like 2	9	24.6	50.656	66.497	48005000	10
97	GENE_20854_Evm.m.Sfld900.43	40S ribosomal protein S18	4	27	17.741	29.337	21890000	4
98	GENE_6635_Evm.m.Sfld2409.4	Ribosomal protein S9	3	13.5	22.32	18.52	24958000	3
99	GENE_1834_Evm.m.Sfld1281.73	Striatin-3 isoform X1	8	19	74.352	61.81	55860000	11
100	GENE_17714_Evm.m.Sfld55.27	Metastasis-associated protein MTA3	9	17.9	69.458	63.216	67452000	10

**Supplementary table 1: Mass spectrometry analysis of *Ct* condensin holocomplex.** First 100 hits from mass spectrometry analysis based on intensity. First 5 hits marked in green are *Ct* condensin subunits with the highest intensity and iBAQ count. The other proteins are from the host Sf21 cells and the only endogenous condensin subunit from Sf21 cells, SMC4, marked in light blue is found in top 100 hits. 3 such data sets were generated, data from only one is shown here.

## Contributions

Dr. Marko Lampe (EMBL Advanced Light Microscope Facility) and Dr. Indra Alon Shaltiel helped with the microscope and imaging techniques.

Dr. Indra Alon Shaltiel wrote the script for image analysis.

Dr. Martin Schorb and Dr. Shveta Bisht helped with rotary shadowing and electron microscopy.

Sol Bravo helped with cloning, ATPase assays and purification techniques and purified *Ct* wild type holocomplex, delta Ycg1 complex, delta Ycg1 Brn1 $\Delta$ 515-637.

Mandy Rettel (EMBL Proteomics Core Facilities) performed the mass spectrometry experiments and helped with the data analysis.

EMBL kitchen staff made culture media and standard buffers for molecular biology experiments.

## References

- A D Riggs. (1990). DNA methylation and late replication probably aid cell memory, and type I DNA reeling could aid chromosome folding and enhancer function. *Philosophical Transactions of the Royal Society of London. B, Biological Sciences*, 326(1235), 285–297. <https://doi.org/10.1098/rstb.1990.0012>
- Anderson, D. E., Losada, A., Erickson, H. P., & Hirano, T. (2002). Condensin and cohesin display different arm conformations with characteristic hinge angles. *Journal of Cell Biology*, 156(3), 419–424. <https://doi.org/10.1083/jcb.200111002>
- Andrade, M. A., & Bork, P. (1995). HEAT repeats in the Huntington's disease protein. *Nature Genetics*, 11(2), 115–116. <https://doi.org/10.1038/ng1095-115>
- Aragón, L. (2018). The Smc5/6 Complex: New and Old Functions of the Enigmatic Long-Distance Relative. *Annual Review of Genetics*, 52(1), 89–107. <https://doi.org/10.1146/annurev-genet-120417-031353>
- Bak, A. L., Zeuthen, J., & Crick, F. H. (1977). Higher-order structure of human mitotic chromosomes. *Proceedings of the National Academy of Sciences*, 74(4), 1595–1599. <https://doi.org/10.1073/pnas.74.4.1595>
- Banigan, E. J., & Mirny, L. A. (2020a). Loop extrusion: theory meets single-molecule experiments. *Current Opinion in Cell Biology*, 64, 124–138. <https://doi.org/10.1016/j.ceb.2020.04.011>
- Banigan, E. J., & Mirny, L. A. (2020b). The interplay between asymmetric and symmetric DNA loop extrusion. *ELife*, 9. <https://doi.org/10.7554/eLife.63528>
- Banigan, E. J., van den Berg, A. A., Brandão, H. B., Marko, J. F., & Mirny, L. A. (2020). Chromosome organization by one-sided and two-sided loop extrusion. *ELife*, 9. <https://doi.org/10.7554/eLife.53558>
- Bauer, B. W., Davidson, I. F., Canena, D., Wutz, G., Tang, W., Litos, G., Horn, S., Hinterdorfer, P., & Peters, J.-M. (2021). Cohesin mediates DNA loop extrusion by a “swing and clamp” mechanism. *Cell*, 184(21), 5448–5464.e22. <https://doi.org/10.1016/j.cell.2021.09.016>
- Bazett-Jones, D. P., Kimura, K., & Hirano, T. (2002). Efficient Supercoiling of DNA by a Single Condensin Complex as Revealed by Electron Spectroscopic Imaging. *Molecular Cell*, 9(6), 1183–1190. [https://doi.org/10.1016/S1097-2765\(02\)00546-4](https://doi.org/10.1016/S1097-2765(02)00546-4)
- Bhat, M. A., Philp, A. V., Glover, D. M., & Bellen, H. J. (1996). Chromatid Segregation at Anaphase Requires the barren Product, a Novel Chromosome-Associated Protein That Interacts with Topoisomerase II. *Cell*, 87(6), 1103–1114. [https://doi.org/10.1016/S0092-8674\(00\)81804-8](https://doi.org/10.1016/S0092-8674(00)81804-8)
- Bolzer, A., Kreth, G., Solovei, I., Koehler, D., Saracoglu, K., Fauth, C., Müller, S., Eils, R., Cremer, C., Speicher, M. R., & Cremer, T. (2005). Three-Dimensional Maps of All Chromosomes in Human Male Fibroblast Nuclei and Prometaphase Rosettes. *PLoS Biology*, 3(5), e157. <https://doi.org/10.1371/journal.pbio.0030157>
- Bürmann, F., Funke, L. F. H., Chin, J. W., & Löwe, J. (2021). Cryo-EM structure of MukBEF reveals DNA loop entrapment at chromosomal unloading sites. *Molecular Cell*, 81(23), 4891–4906.e8. <https://doi.org/10.1016/j.molcel.2021.10.011>
- Cai, S., Chen, C., Tan, Z. Y., Huang, Y., Shi, J., & Gan, L. (2018). Cryo-ET reveals the macromolecular reorganization of *S. pombe* mitotic chromosomes in vivo. *Proceedings of the National Academy of Sciences*, 115(43), 10977–10982. <https://doi.org/10.1073/pnas.1720476115>

- Champoux, J. J. (2001). DNA Topoisomerases: Structure, Function, and Mechanism. *Annual Review of Biochemistry*, 70(1), 369–413. <https://doi.org/10.1146/annurev.biochem.70.1.369>
- Chang, L.-H., Ghosh, S., & Noordermeer, D. (2020). TADs and Their Borders: Free Movement or Building a Wall? *Journal of Molecular Biology*, 432(3), 643–652. <https://doi.org/10.1016/j.jmb.2019.11.025>
- Chen, N., Zinchenko, A. A., Yoshikawa, Y., Araki, S., Adachi, S., Yamazoe, M., Hiraga, S., & Yoshikawa, K. (2008). ATP-Induced Shrinkage of DNA with MukB Protein and the MukBEF Complex of *Escherichia coli*. *Journal of Bacteriology*, 190(10), 3731–3737. <https://doi.org/10.1128/JB.01863-07>
- Ciosk, R., Shirayama, M., Shevchenko, A., Tanaka, T., Toth, A., Shevchenko, A., & Nasmyth, K. (2000). Cohesin's Binding to Chromosomes Depends on a Separate Complex Consisting of Scc2 and Scc4 Proteins. *Molecular Cell*, 5(2), 243–254. [https://doi.org/10.1016/S1097-2765\(00\)80420-7](https://doi.org/10.1016/S1097-2765(00)80420-7)
- Cockerill, P. N., & Garrard, W. T. (1986). Chromosomal loop anchorage sites appear to be evolutionarily conserved. *FEBS Letters*, 204(1), 5–7. [https://doi.org/10.1016/0014-5793\(86\)81377-1](https://doi.org/10.1016/0014-5793(86)81377-1)
- Cuylen, S., Metz, J., & Haering, C. H. (2011). Condensin structures chromosomal DNA through topological links. *Nature Structural & Molecular Biology*, 18(8), 894–901. <https://doi.org/10.1038/nsmb.2087>
- D'Ambrosio, C., Schmidt, C. K., Katou, Y., Kelly, G., Itoh, T., Shirahige, K., & Uhlmann, F. (2008). Identification of *cis*-acting sites for condensin loading onto budding yeast chromosomes. *Genes & Development*, 22(16), 2215–2227. <https://doi.org/10.1101/gad.1675708>
- Datta, S., Lecomte, L., & Haering, C. H. (2020). Structural insights into DNA loop extrusion by SMC protein complexes. *Current Opinion in Structural Biology*, 65, 102–109. <https://doi.org/10.1016/j.sbi.2020.06.009>
- Davidson, I. F., Bauer, B., Goetz, D., Tang, W., Wutz, G., & Peters, J.-M. (2019). DNA loop extrusion by human cohesin. *Science*, 366(6471), 1338–1345. <https://doi.org/10.1126/science.aaz3418>
- Dekker, J., & Mirny, L. (2016). The 3D Genome as Moderator of Chromosomal Communication. *Cell*, 164(6), 1110–1121. <https://doi.org/10.1016/j.cell.2016.02.007>
- Dekker, J., Rippe, K., Dekker, M., & Kleckner, N. (2002). Capturing Chromosome Conformation. *Science*, 295(5558), 1306–1311. <https://doi.org/10.1126/science.1067799>
- Diebold-Durand, M.-L., Lee, H., Ruiz Avila, L. B., Noh, H., Shin, H.-C., Im, H., Bock, F. P., Bürmann, F., Durand, A., Basfeld, A., Ham, S., Basquin, J., Oh, B.-H., & Gruber, S. (2017). Structure of Full-Length SMC and Rearrangements Required for Chromosome Organization. *Molecular Cell*, 67(2), 334–347.e5. <https://doi.org/10.1016/j.molcel.2017.06.010>
- Dixon, J. R., Selvaraj, S., Yue, F., Kim, A., Li, Y., Shen, Y., Hu, M., Liu, J. S., & Ren, B. (2012). Topological domains in mammalian genomes identified by analysis of chromatin interactions. *Nature*, 485(7398), 376–380. <https://doi.org/10.1038/nature11082>
- Earnshaw, W. C., & Laemmli, U. K. (1983). Architecture of metaphase chromosomes and chromosome scaffolds. *Journal of Cell Biology*, 96(1), 84–93. <https://doi.org/10.1083/jcb.96.1.84>

- Eeftens, J. M., Bisht, S., Kerssemakers, J., Kschonsak, M., Haering, C. H., & Dekker, C. (2017). Real-time detection of condensin-driven DNA compaction reveals a multistep binding mechanism. *The EMBO Journal*, 36(23), 3448–3457. <https://doi.org/10.15252/embj.201797596>
- Eltsov, M., MacLellan, K. M., Maeshima, K., Frangakis, A. S., & Dubochet, J. (2008). Analysis of cryo-electron microscopy images does not support the existence of 30-nm chromatin fibers in mitotic chromosomes in situ. *Proceedings of the National Academy of Sciences*, 105(50), 19732–19737. <https://doi.org/10.1073/pnas.0810057105>
- Finch, J. T., & Klug, A. (1976). Solenoidal model for superstructure in chromatin. *Proceedings of the National Academy of Sciences*, 73(6), 1897–1901. <https://doi.org/10.1073/pnas.73.6.1897>
- Flemming, W., 1882. Zellsubstanz, kern und zelltheilung.. Leipzig, F. C. W. Vogel.
- Ganji, M., Shaltiel, I. A., Bisht, S., Kim, E., Kalichava, A., Haering, C. H., & Dekker, C. (2018). Real-time imaging of DNA loop extrusion by condensin. *Science*, 360(6384), 102–105. <https://doi.org/10.1126/science.aar7831>
- Gasser, S. M., & Laemmli, U. K. (1987). A glimpse at chromosomal order. *Trends in Genetics*, 3, 16–22. [https://doi.org/10.1016/0168-9525\(87\)90156-9](https://doi.org/10.1016/0168-9525(87)90156-9)
- Gasser, S. M., Laroche, T., Falquet, J., Boy de la Tour, E., & Laemmli, U. K. (1986). Metaphase chromosome structure. *Journal of Molecular Biology*, 188(4), 613–629. [https://doi.org/10.1016/S0022-2836\(86\)80010-9](https://doi.org/10.1016/S0022-2836(86)80010-9)
- Gasteiger, E., Hoogland, C., Gattiker, A., Duvaud, S., Wilkins, M. R., Appel, R. D., & Bairoch, A. (2005). Protein Identification and Analysis Tools on the ExPASy Server. In *The Proteomics Protocols Handbook* (pp. 571–607). Humana Press. <https://doi.org/10.1385/1-59259-890-0:571>
- Gerlich, D., Hirota, T., Koch, B., Peters, J.-M., & Ellenberg, J. (2006). Condensin I Stabilizes Chromosomes Mechanically through a Dynamic Interaction in Live Cells. *Current Biology*, 16(4), 333–344. <https://doi.org/10.1016/j.cub.2005.12.040>
- Gibcus, J. H., Samejima, K., Goloborodko, A., Samejima, I., Naumova, N., Nuebler, J., Kanemaki, M. T., Xie, L., Paulson, J. R., Earnshaw, W. C., Mirny, L. A., & Dekker, J. (2018). A pathway for mitotic chromosome formation. *Science*, 359(6376). <https://doi.org/10.1126/science.aao6135>
- Goldman, M. A. (1988). The chromatin domain as a unit of gene regulation. *BioEssays*, 9(2–3), 50–55. <https://doi.org/10.1002/bies.950090204>
- Golfier, S., Quail, T., Kimura, H., & Brugués, J. (2020). Cohesin and condensin extrude DNA loops in a cell cycle-dependent manner. *ELife*, 9. <https://doi.org/10.7554/eLife.53885>
- Goloborodko, A., Imakaev, M. v, Marko, J. F., & Mirny, L. (2016a). Compaction and segregation of sister chromatids via active loop extrusion. *ELife*, 5. <https://doi.org/10.7554/eLife.14864>
- Goloborodko, A., Marko, J. F., & Mirny, L. A. (2016b). Chromosome Compaction by Active Loop Extrusion. *Biophysical Journal*, 110(10), 2162–2168. <https://doi.org/10.1016/j.bpj.2016.02.041>
- Griese, J. J., Witte, G., & Hopfner, K.-P. (2010). Structure and DNA binding activity of the mouse condensin hinge domain highlight common and diverse features of SMC proteins. *Nucleic Acids Research*, 38(10), 3454–3465. <https://doi.org/10.1093/nar/gkq038>
- Gruber, S., Haering, C. H., & Nasmyth, K. (2003). Chromosomal Cohesin Forms a Ring. *Cell*, 112(6), 765–777. [https://doi.org/10.1016/S0092-8674\(03\)00162-4](https://doi.org/10.1016/S0092-8674(03)00162-4)

- Haering, C. H., Farcas, A.-M., Arumugam, P., Metson, J., & Nasmyth, K. (2008). The cohesin ring concatenates sister DNA molecules. *Nature*, *454*(7202), 297–301. <https://doi.org/10.1038/nature07098>
- Haering, C. H., Löwe, J., Hochwagen, A., & Nasmyth, K. (2002). Molecular Architecture of SMC Proteins and the Yeast Cohesin Complex. *Molecular Cell*, *9*(4), 773–788. [https://doi.org/10.1016/S1097-2765\(02\)00515-4](https://doi.org/10.1016/S1097-2765(02)00515-4)
- Haering, C. H., Schoffnegger, D., Nishino, T., Helmhart, W., Nasmyth, K., & Löwe, J. (2004). Structure and Stability of Cohesin's Smc1-Kleisin Interaction. *Molecular Cell*, *15*(6), 951–964. <https://doi.org/10.1016/j.molcel.2004.08.030>
- Hanahan, D. (1983). Studies on transformation of *Escherichia coli* with plasmids. *Journal of Molecular Biology*, *166*(4), 557–580. [https://doi.org/10.1016/S0022-2836\(83\)80284-8](https://doi.org/10.1016/S0022-2836(83)80284-8)
- Hara, K., Kinoshita, K., Migita, T., Murakami, K., Shimizu, K., Takeuchi, K., Hirano, T., & Hashimoto, H. (2019). Structural basis of HEAT-kleisin interactions in the human condensin I subcomplex. *EMBO Reports*, *20*(5). <https://doi.org/10.15252/embr.201847183>
- Hassler, M., Shaltiel, I. A., & Haering, C. H. (2018). Towards a Unified Model of SMC Complex Function. *Current Biology*, *28*(21), R1266–R1281. <https://doi.org/10.1016/j.cub.2018.08.034>
- Hassler, M., Shaltiel, I. A., Kschonsak, M., Simon, B., Merkel, F., Thärichen, L., Bailey, H. J., Macošek, J., Bravo, S., Metz, J., Hennig, J., & Haering, C. H. (2019). Structural Basis of an Asymmetric Condensin ATPase Cycle. *Molecular Cell*, *74*(6), 1175–1188.e9. <https://doi.org/10.1016/j.molcel.2019.03.037>
- Higashi, T. L., Pobegalov, G., Tang, M., Molodtsov, M. I., & Uhlmann, F. (2021). A Brownian ratchet model for DNA loop extrusion by the cohesin complex. *ELife*, *10*. <https://doi.org/10.7554/eLife.67530>
- Hirano, M. (2002). Hinge-mediated dimerization of SMC protein is essential for its dynamic interaction with DNA. *The EMBO Journal*, *21*(21), 5733–5744. <https://doi.org/10.1093/emboj/cdf575>
- Hirano, T. (2012). Condensins: universal organizers of chromosomes with diverse functions. *Genes & Development*, *26*(15), 1659–1678. <https://doi.org/10.1101/gad.194746.112>
- Hirano, T. (2016). Condensin-Based Chromosome Organization from Bacteria to Vertebrates. *Cell*, *164*(5), 847–857. <https://doi.org/10.1016/j.cell.2016.01.033>
- Hirano, T., Kobayashi, R., & Hirano, M. (1997). Condensins, Chromosome Condensation Protein Complexes Containing XCAP-C, XCAP-E and a *Xenopus* Homolog of the *Drosophila* Barren Protein. *Cell*, *89*(4), 511–521. [https://doi.org/10.1016/S0092-8674\(00\)80233-0](https://doi.org/10.1016/S0092-8674(00)80233-0)
- Hirano, T., & Mitchison, T. J. (1994). A heterodimeric coiled-coil protein required for mitotic chromosome condensation in vitro. *Cell*, *79*(3), 449–458. [https://doi.org/10.1016/0092-8674\(94\)90254-2](https://doi.org/10.1016/0092-8674(94)90254-2)
- Hirota, T., Gerlich, D., Koch, B., Ellenberg, J., & Peters, J.-M. (2004). Distinct functions of condensin I and II in mitotic chromosome assembly. *Journal of Cell Science*, *117*(26), 6435–6445. <https://doi.org/10.1242/jcs.01604>
- Holm, C. (1994). Coming undone: How to untangle a chromosome. *Cell*, *77*(7), 955–957. [https://doi.org/10.1016/0092-8674\(94\)90433-2](https://doi.org/10.1016/0092-8674(94)90433-2)
- HOLM, C., GOTO, T., WANG, J., & BOTSTEIN, D. (1985). DNA topoisomerase II is required at the time of mitosis in yeast. *Cell*, *41*(2), 553–563. [https://doi.org/10.1016/S0092-8674\(85\)80028-3](https://doi.org/10.1016/S0092-8674(85)80028-3)

- Hopfner, K. (2016). Invited review: Architectures and mechanisms of ATP binding cassette proteins. *Biopolymers*, *105*(8), 492–504. <https://doi.org/10.1002/bip.22843>
- Huynh, V. A. T., Robinson, P. J. J., & Rhodes, D. (2005). A Method for the In Vitro Reconstitution of a Defined “30nm” Chromatin Fibre Containing Stoichiometric Amounts of the Linker Histone. *Journal of Molecular Biology*, *345*(5), 957–968. <https://doi.org/10.1016/j.jmb.2004.10.075>
- Jeppsson, K., Kanno, T., Shirahige, K., & Sjögren, C. (2014). The maintenance of chromosome structure: positioning and functioning of SMC complexes. *Nature Reviews Molecular Cell Biology*, *15*(9), 601–614. <https://doi.org/10.1038/nrm3857>
- Kania, A., Salzberg, A., Bhat, M., D’Evelyn, D., He, Y., Kiss, I., & Bellen, H. J. (1995). P-element mutations affecting embryonic peripheral nervous system development in *Drosophila melanogaster*. *Genetics*, *139*(4), 1663–1678. <https://doi.org/10.1093/genetics/139.4.1663>
- Keenholtz, R. A., Dhanaraman, T., Palou, R., Yu, J., D’Amours, D., & Marko, J. F. (2017). Oligomerization and ATP stimulate condensin-mediated DNA compaction. *Scientific Reports*, *7*(1), 14279. <https://doi.org/10.1038/s41598-017-14701-5>
- Kellner, N., Schwarz, J., Sturm, M., Fernandez-Martinez, J., Griesel, S., Zhang, W., Chait, B. T., Rout, M. P., Kück, U., & Hurt, E. (2016). Developing genetic tools to exploit *Chaetomium thermophilum* for biochemical analyses of eukaryotic macromolecular assemblies. *Scientific Reports*, *6*(1), 20937. <https://doi.org/10.1038/srep20937>
- Kim, E., Gonzalez, A. M., Pradhan, B., van der Torre, J., & Dekker, C. (n.d.). *Condensin-driven loop extrusion on supercoiled DNA*. <https://doi.org/10.1101/2021.05.15.444164>
- Kim, E., Kerssemakers, J., Shaltiel, I. A., Haering, C. H., & Dekker, C. (2020). DNA-loop extruding condensin complexes can traverse one another. *Nature*, *579*(7799), 438–442. <https://doi.org/10.1038/s41586-020-2067-5>
- Kim, Y., Shi, Z., Zhang, H., Finkelstein, I. J., & Yu, H. (2019). Human cohesin compacts DNA by loop extrusion. *Science*, *366*(6471), 1345–1349. <https://doi.org/10.1126/science.aaz4475>
- Kimura, K., Cuvier, O., & Hirano, T. (2001). Chromosome Condensation by a Human Condensin Complex in *Xenopus* Egg Extracts. *Journal of Biological Chemistry*, *276*(8), 5417–5420. <https://doi.org/10.1074/jbc.C000873200>
- Kimura, K., & Hirano, T. (1997). ATP-Dependent Positive Supercoiling of DNA by 13S Condensin: A Biochemical Implication for Chromosome Condensation. *Cell*, *90*(4), 625–634. [https://doi.org/10.1016/S0092-8674\(00\)80524-3](https://doi.org/10.1016/S0092-8674(00)80524-3)
- Kinoshita, K., Kobayashi, T. J., & Hirano, T. (2015). Balancing Acts of Two HEAT Subunits of Condensin I Support Dynamic Assembly of Chromosome Axes. *Developmental Cell*, *33*(1), 94–106. <https://doi.org/10.1016/j.devcel.2015.01.034>
- Kong, M., Cutts, E. E., Pan, D., Beuron, F., Kaliyappan, T., Xue, C., Morris, E. P., Musacchio, A., Vannini, A., & Greene, E. C. (2020). Human Condensin I and II Drive Extensive ATP-Dependent Compaction of Nucleosome-Bound DNA. *Molecular Cell*, *79*(1), 99–114.e9. <https://doi.org/10.1016/j.molcel.2020.04.026>
- Kruihof, M., Chien, F.-T., Routh, A., Logie, C., Rhodes, D., & van Noort, J. (2009). Single-molecule force spectroscopy reveals a highly compliant helical folding for the 30-nm chromatin fiber. *Nature Structural & Molecular Biology*, *16*(5), 534–540. <https://doi.org/10.1038/nsmb.1590>

- Kschonsak, M., Merkel, F., Bisht, S., Metz, J., Rybin, V., Hassler, M., & Haering, C. H. (2017). Structural Basis for a Safety-Belt Mechanism That Anchors Condensin to Chromosomes. *Cell*, 171(3), 588–600.e24. <https://doi.org/10.1016/j.cell.2017.09.008>
- Kukat, C., Davies, K. M., Wurm, C. A., Spähr, H., Bonekamp, N. A., Köhl, I., Joos, F., Polosa, P. L., Park, C. B., Posse, V., Falkenberg, M., Jakobs, S., Köhlbrandt, W., & Larsson, N.-G. (2015). Cross-strand binding of TFAM to a single mtDNA molecule forms the mitochondrial nucleoid. *Proceedings of the National Academy of Sciences*, 112(36), 11288–11293. <https://doi.org/10.1073/pnas.1512131112>
- Lee, B.-G., Merkel, F., Allegretti, M., Hassler, M., Cawood, C., Lecomte, L., O'Reilly, F. J., Sinn, L. R., Gutierrez-Escribano, P., Kschonsak, M., Bravo, S., Nakane, T., Rappsilber, J., Aragon, L., Beck, M., Löwe, J., & Haering, C. H. (2020). Cryo-EM structures of holo condensin reveal a subunit flip-flop mechanism. *Nature Structural & Molecular Biology*, 27(8), 743–751. <https://doi.org/10.1038/s41594-020-0457-x>
- Lee, B.-G., Rhodes, J., & Löwe, J. (2022). Clamping of DNA shuts the condensin neck gate. *Proceedings of the National Academy of Sciences*, 119(14). <https://doi.org/10.1073/pnas.2120006119>
- Lewis, C. D., & Laemmli, U. K. (1982). Higher order metaphase chromosome structure: Evidence for metalloprotein interactions. *Cell*, 29(1), 171–181. [https://doi.org/10.1016/0092-8674\(82\)90101-5](https://doi.org/10.1016/0092-8674(82)90101-5)
- Lieberman-Aiden, E., van Berkum, N. L., Williams, L., Imakaev, M., Ragozy, T., Telling, A., Amit, I., Lajoie, B. R., Sabo, P. J., Dorschner, M. O., Sandstrom, R., Bernstein, B., Bender, M. A., Groudine, M., Gnirke, A., Stamatoyannopoulos, J., Mirny, L. A., Lander, E. S., & Dekker, J. (2009). Comprehensive Mapping of Long-Range Interactions Reveals Folding Principles of the Human Genome. *Science*, 326(5950), 289–293. <https://doi.org/10.1126/science.1181369>
- Losada, A., Hirano, M., & Hirano, T. (1998). Identification of *Xenopus* SMC protein complexes required for sister chromatid cohesion. *Genes & Development*, 12(13), 1986–1997. <https://doi.org/10.1101/gad.12.13.1986>
- Luger, K., Mäder, A. W., Richmond, R. K., Sargent, D. F., & Richmond, T. J. (1997). Crystal structure of the nucleosome core particle at 2.8 Å resolution. *Nature*, 389(6648), 251–260. <https://doi.org/10.1038/38444>
- Maeshima, K., & Laemmli, U. K. (2003). A Two-Step Scaffolding Model for Mitotic Chromosome Assembly. *Developmental Cell*, 4(4), 467–480. [https://doi.org/10.1016/S1534-5807\(03\)00092-3](https://doi.org/10.1016/S1534-5807(03)00092-3)
- Manalastas-Cantos, K., Kschonsak, M., Haering, C. H., & Svergun, D. I. (2019). Solution structure and flexibility of the condensin HEAT-repeat subunit Ycg1. *Journal of Biological Chemistry*, 294(37), 13822–13829. <https://doi.org/10.1074/jbc.RA119.008661>
- Marko, J. F. (2008). Micromechanical studies of mitotic chromosomes. *Chromosome Research*, 16(3), 469–497. <https://doi.org/10.1007/s10577-008-1233-7>
- Marko, J. F., De Los Rios, P., Barducci, A., & Gruber, S. (2019). DNA-segment-capture model for loop extrusion by structural maintenance of chromosome (SMC) protein complexes. *Nucleic Acids Research*, 47(13), 6956–6972. <https://doi.org/10.1093/nar/gkz497>
- McDowell, A. W., Smith, J. M., & Dubochet, J. (1986). Cryo-electron microscopy of vitrified chromosomes in situ. *The EMBO Journal*, 5(6), 1395–1402. <http://doi.org/10.1002/j.1460-2075.1986.tb04373.x>

- Melby, T. E., Ciampaglio, C. N., Briscoe, G., & Erickson, H. P. (1998). The Symmetrical Structure of Structural Maintenance of Chromosomes (SMC) and MukB Proteins: Long, Antiparallel Coiled Coils, Folded at a Flexible Hinge. *Journal of Cell Biology*, 142(6), 1595–1604. <https://doi.org/10.1083/jcb.142.6.1595>
- Meselson, M., & Stahl, F. W. (1958). The replication of DNA in *Escherichia coli*. *Proceedings of the National Academy of Sciences*, 44(7), 671–682. <https://doi.org/10.1073/pnas.44.7.671>
- Mirny, L. A., Imakaev, M., & Abdennur, N. (2019). Two major mechanisms of chromosome organization. *Current Opinion in Cell Biology*, 58, 142–152. <https://doi.org/10.1016/j.ceb.2019.05.001>
- Muir, K. W., Li, Y., Weis, F., & Panne, D. (2020). The structure of the cohesin ATPase elucidates the mechanism of SMC–kleisin ring opening. *Nature Structural & Molecular Biology*, 27(3), 233–239. <https://doi.org/10.1038/s41594-020-0379-7>
- Nasmyth, K. (2001). Disseminating the Genome: Joining, Resolving, and Separating Sister Chromatids During Mitosis and Meiosis. *Annual Review of Genetics*, 35(1), 673–745. <https://doi.org/10.1146/annurev.genet.35.102401.091334>
- Nasmyth, K., & Haering, C. H. (2009). Cohesin: Its Roles and Mechanisms. *Annual Review of Genetics*, 43(1), 525–558. <https://doi.org/10.1146/annurev-genet-102108-134233>
- Naumova, N., Imakaev, M., Fudenberg, G., Zhan, Y., Lajoie, B. R., Mirny, L. A., & Dekker, J. (2013). Organization of the Mitotic Chromosome. *Science*, 342(6161), 948–953. <https://doi.org/10.1126/science.1236083>
- Neuwald, A. F., & Hirano, T. (2000). HEAT Repeats Associated with Condensins, Cohesins, and Other Complexes Involved in Chromosome-Related Functions. *Genome Research*, 10(10), 1445–1452. <https://doi.org/10.1101/gr.147400>
- Nishino, Y., Eltsov, M., Joti, Y., Ito, K., Takata, H., Takahashi, Y., Hihara, S., Frangakis, A. S., Imamoto, N., Ishikawa, T., & Maeshima, K. (2012). Human mitotic chromosomes consist predominantly of irregularly folded nucleosome fibers without a 30-nm chromatin structure. *The EMBO Journal*, 31(7), 1644–1653. <https://doi.org/10.1038/emboj.2012.35>
- Nishiyama, T. (2019). Cohesion and cohesin-dependent chromatin organization. *Current Opinion in Cell Biology*, 58, 8–14. <https://doi.org/10.1016/j.ceb.2018.11.006>
- Nora, E. P., Lajoie, B. R., Schulz, E. G., Giorgetti, L., Okamoto, I., Servant, N., Piolot, T., van Berkum, N. L., Meisig, J., Sedat, J., Gribnau, J., Barillot, E., Blüthgen, N., Dekker, J., & Heard, E. (2012). Spatial partitioning of the regulatory landscape of the X-inactivation centre. *Nature*, 485(7398), 381–385. <https://doi.org/10.1038/nature11049>
- Olins, A. L., & Olins, D. E. (1974). Spheroid Chromatin Units (v Bodies). *Science*, 183(4122), 330–332. <https://doi.org/10.1126/science.183.4122.330>
- Onn, I., Aono, N., Hirano, M., & Hirano, T. (2007). Reconstitution and subunit geometry of human condensin complexes. *The EMBO Journal*, 26(4), 1024–1034. <https://doi.org/10.1038/sj.emboj.7601562>
- Ono, T., Losada, A., Hirano, M., Myers, M. P., Neuwald, A. F., & Hirano, T. (2003). Differential Contributions of Condensin I and Condensin II to Mitotic Chromosome Architecture in Vertebrate Cells. *Cell*, 115(1), 109–121. [https://doi.org/10.1016/S0092-8674\(03\)00724-4](https://doi.org/10.1016/S0092-8674(03)00724-4)
- Ou, H. D., Phan, S., Deerinck, T. J., Thor, A., Ellisman, M. H., & O’Shea, C. C. (2017). ChromEMT: Visualizing 3D chromatin structure and compaction in interphase and mitotic cells. *Science*, 357(6349). <https://doi.org/10.1126/science.aag0025>

- Paul, M. R., Hochwagen, A., & Ercan, S. (2019). Condensin action and compaction. *Current Genetics*, 65(2), 407–415. <https://doi.org/10.1007/s00294-018-0899-4>
- Paulson, J. R., & Laemmli, U. K. (1977). The structure of histone-depleted metaphase chromosomes. *Cell*, 12(3), 817–828. [https://doi.org/10.1016/0092-8674\(77\)90280-X](https://doi.org/10.1016/0092-8674(77)90280-X)
- Petela, N. J., Gonzalez Llamazares, A., Dixon, S., Hu, B., Lee, B.-G., Metson, J., Seo, H., Ferrer-Harding, A., Voulgaris, M., Gligoris, T., Collier, J., Oh, B.-H., Löwe, J., & Nasmyth, K. A. (2021). Folding of cohesin's coiled coil is important for Scc2/4-induced association with chromosomes. *ELife*, 10. <https://doi.org/10.7554/eLife.67268>
- Peter, B. J., Ullsperger, C., Hiasa, H., Marians, K. J., & Cozzarelli, N. R. (1998). The Structure of Supercoiled Intermediates in DNA Replication. *Cell*, 94(6), 819–827. [https://doi.org/10.1016/S0092-8674\(00\)81740-7](https://doi.org/10.1016/S0092-8674(00)81740-7)
- Piazza, I., Rutkowska, A., Ori, A., Walczak, M., Metz, J., Pelechano, V., Beck, M., & Haering, C. H. (2014). Association of condensin with chromosomes depends on DNA binding by its HEAT-repeat subunits. *Nature Structural & Molecular Biology*, 21(6), 560–568. <https://doi.org/10.1038/nsmb.2831>
- Poirier, M. G., & Marko, J. F. (2002). Mitotic chromosomes are chromatin networks without a mechanically contiguous protein scaffold. *Proceedings of the National Academy of Sciences*, 99(24), 15393–15397. <https://doi.org/10.1073/pnas.232442599>
- Pradhan, B., Barth, R., Kim, E., Davidson, I. F., Bauer, B., van Laar, T., Yang, W., Ryu, J.-K., van der Torre, J., Peters, J.-M., & Dekker, C. (n.d.). SMC complexes can traverse physical roadblocks bigger than their ring size. <https://doi.org/10.1101/2021.07.15.452501>
- Rattner, J. B., & Hamkalo, B. A. (1978). Higher order structure in metaphase chromosomes. *Chromosoma*, 69(3), 363–372. <https://doi.org/10.1007/BF00332139>
- Robinson, P. J. J., Fairall, L., Huynh, V. A. T., & Rhodes, D. (2006). EM measurements define the dimensions of the “30-nm” chromatin fiber: Evidence for a compact, interdigitated structure. *Proceedings of the National Academy of Sciences*, 103(17), 6506–6511. <https://doi.org/10.1073/pnas.0601212103>
- Ryu, J.-K., Katan, A. J., van der Sluis, E. O., Wisse, T., de Groot, R., Haering, C. H., & Dekker, C. (2020). The condensin holocomplex cycles dynamically between open and collapsed states. *Nature Structural & Molecular Biology*, 27(12), 1134–1141. <https://doi.org/10.1038/s41594-020-0508-3>
- Saitoh, N., Goldberg, I. G., Wood, E. R., & Earnshaw, W. C. (1994). ScII: an abundant chromosome scaffold protein is a member of a family of putative ATPases with an unusual predicted tertiary structure. *Journal of Cell Biology*, 127(2), 303–318. <https://doi.org/10.1083/jcb.127.2.303>
- Saka, Y., Sutani, T., Yamashita, Y., Saitoh, S., Takeuchi, M., Nakaseko, Y., & Yanagida, M. (1994). Fission yeast cut3 and cut14, members of a ubiquitous protein family, are required for chromosome condensation and segregation in mitosis. *The EMBO Journal*, 13(20), 4938–4952.
- Sakai, A. (2003). Condensin but not cohesin SMC heterodimer induces DNA reannealing through protein-protein assembly. *The EMBO Journal*, 22(11), 2764–2775. <https://doi.org/10.1093/emboj/cdg247>
- Salomo, M., Kegler, K., Gutsche, C., Struhalla, M., Reinmuth, J., Skokow, W., Hahn, U., & Kremer, F. (2006). The elastic properties of single double-stranded DNA chains of different lengths as measured with optical tweezers. *Colloid and Polymer Science*, 284(11), 1325–1331. <https://doi.org/10.1007/s00396-006-1517-4>

- Schalch, T., Duda, S., Sargent, D. F., & Richmond, T. J. (2005). X-ray structure of a tetranucleosome and its implications for the chromatin fibre. *Nature*, *436*(7047), 138–141. <https://doi.org/10.1038/nature03686>
- Schindelin, J., Arganda-Carreras, I., Frise, E., Kaynig, V., Longair, M., Pietzsch, T., Preibisch, S., Rueden, C., Saalfeld, S., Schmid, B., Tinevez, J.-Y., White, D. J., Hartenstein, V., Eliceiri, K., Tomancak, P., & Cardona, A. (2012). Fiji: an open-source platform for biological-image analysis. *Nature Methods*, *9*(7), 676–682. <https://doi.org/10.1038/nmeth.2019>
- Schleiffer, A., Kaitna, S., Maurer-Stroh, S., Glotzer, M., Nasmyth, K., & Eisenhaber, F. (2003). Kleisins: A Superfamily of Bacterial and Eukaryotic SMC Protein Partners. *Molecular Cell*, *11*(3), 571–575. [https://doi.org/10.1016/S1097-2765\(03\)00108-4](https://doi.org/10.1016/S1097-2765(03)00108-4)
- Schmiesing, J. A., Ball, A. R., Gregson, H. C., Alderton, J. M., Zhou, S., & Yokomori, K. (1998). Identification of two distinct human SMC protein complexes involved in mitotic chromosome dynamics. *Proceedings of the National Academy of Sciences*, *95*(22), 12906–12911. <https://doi.org/10.1073/pnas.95.22.12906>
- Schwanhäusser, B., Busse, D., Li, N., Dittmar, G., Schuchhardt, J., Wolf, J., Chen, W., & Selbach, M. (2011). Global quantification of mammalian gene expression control. *Nature*, *473*(7347), 337–342. <https://doi.org/10.1038/nature10098>
- Shaltiel, I.A., Datta, S., Lecomte, L., Hassler, M., Kschonsak, M., Bravo, S., Stober, C., Eustermann, S., & Haering, C. H. (2022). A hold-and-feed mechanism drives directional DNA loop extrusion by condensin. *Science* (in press).
- Shi, Z., Gao, H., Bai, X., & Yu, H. (2020). Cryo-EM structure of the human cohesin-NIPBL-DNA complex. *Science*, *368*(6498), 1454–1459. <https://doi.org/10.1126/science.abb0981>
- Shintomi, K., Inoue, F., Watanabe, H., Ohsumi, K., Ohsugi, M., & Hirano, T. (2017). Mitotic chromosome assembly despite nucleosome depletion in *Xenopus* egg extracts. *Science*, *356*(6344), 1284–1287. <https://doi.org/10.1126/science.aam9702>
- Shintomi, K., Takahashi, T. S., & Hirano, T. (2015). Reconstitution of mitotic chromatids with a minimum set of purified factors. *Nature Cell Biology*, *17*(8), 1014–1023. <https://doi.org/10.1038/ncb3187>
- Soh, Y.-M., Bürmann, F., Shin, H.-C., Oda, T., Jin, K. S., Toseland, C. P., Kim, C., Lee, H., Kim, S. J., Kong, M.-S., Durand-Diebold, M.-L., Kim, Y.-G., Kim, H. M., Lee, N. K., Sato, M., Oh, B.-H., & Gruber, S. (2015). Molecular Basis for SMC Rod Formation and Its Dissolution upon DNA Binding. *Molecular Cell*, *57*(2), 290–303. <https://doi.org/10.1016/j.molcel.2014.11.023>
- Song, F., Chen, P., Sun, D., Wang, M., Dong, L., Liang, D., Xu, R.-M., Zhu, P., & Li, G. (2014). Cryo-EM Study of the Chromatin Fiber Reveals a Double Helix Twisted by Tetranucleosomal Units. *Science*, *344*(6182), 376–380. <https://doi.org/10.1126/science.1251413>
- Spell, R. M., & Holm, C. (1994). Nature and distribution of chromosomal intertwinnings in *Saccharomyces cerevisiae*. *Molecular and Cellular Biology*, *14*(2), 1465–1476. <https://doi.org/10.1128/mcb.14.2.1465-1476.1994>
- Staynov, D. Z. (2000). DNase I digestion reveals alternating asymmetrical protection of the nucleosome by the higher order chromatin structure. *Nucleic Acids Research*, *28*(16), 3092–3099. <https://doi.org/10.1093/nar/28.16.3092>

- Stray, J. E., & Lindsley, J. E. (2003). Biochemical Analysis of the Yeast Condensin Smc2/4 Complex. *Journal of Biological Chemistry*, 278(28), 26238–26248. <https://doi.org/10.1074/jbc.M302699200>
- Strick, T. R., Kawaguchi, T., & Hirano, T. (2004). Real-Time Detection of Single-Molecule DNA Compaction by Condensin I. *Current Biology*, 14(10), 874–880. <https://doi.org/10.1016/j.cub.2004.04.038>
- Strunnikov, A. v, Hogan, E., & Koshland, D. (1995). SMC2, a *Saccharomyces cerevisiae* gene essential for chromosome segregation and condensation, defines a subgroup within the SMC family. *Genes & Development*, 9(5), 587–599. <https://doi.org/10.1101/gad.9.5.587>
- Sundin, O., & Varshavsky, A. (1981). Arrest of segregation leads to accumulation of highly intertwined catenated dimers: Dissection of the final stages of SV40 DNA replication. *Cell*, 25(3), 659–669. [https://doi.org/10.1016/0092-8674\(81\)90173-2](https://doi.org/10.1016/0092-8674(81)90173-2)
- Sutani, T., Sakata, T., Nakato, R., Masuda, K., Ishibashi, M., Yamashita, D., Suzuki, Y., Hirano, T., Bando, M., & Shirahige, K. (2015). Condensin targets and reduces unwound DNA structures associated with transcription in mitotic chromosome condensation. *Nature Communications*, 6(1), 7815. <https://doi.org/10.1038/ncomms8815>
- Terakawa, T., Bisht, S., Eeftens, J. M., Dekker, C., Haering, C. H., & Greene, E. C. (2017). The condensin complex is a mechanochemical motor that translocates along DNA. *Science*, 358(6363), 672–676. <https://doi.org/10.1126/science.aan6516>
- Tyler, J. M., & Branton, D. (1980). Rotary shadowing of extended molecules dried from glycerol. *Journal of Ultrastructure Research*, 71(2), 95–102. [https://doi.org/10.1016/S0022-5320\(80\)90098-2](https://doi.org/10.1016/S0022-5320(80)90098-2)
- Uemura, T., Ohkura, H., Adachi, Y., Morino, K., Shiozaki, K., & Yanagida, M. (1987). DNA topoisomerase II is required for condensation and separation of mitotic chromosomes in *S. pombe*. *Cell*, 50(6), 917–925. [https://doi.org/10.1016/0092-8674\(87\)90518-6](https://doi.org/10.1016/0092-8674(87)90518-6)
- Vazquez Nunez, R., Ruiz Avila, L. B., & Gruber, S. (2019). Transient DNA Occupancy of the SMC Interarm Space in Prokaryotic Condensin. *Molecular Cell*, 75(2), 209–223.e6. <https://doi.org/10.1016/j.molcel.2019.05.001>
- Wang, B.-D., Eyre, D., Basrai, M., Lichten, M., & Strunnikov, A. (2005). Condensin Binding at Distinct and Specific Chromosomal Sites in the *Saccharomyces cerevisiae* Genome. *Molecular and Cellular Biology*, 25(16), 7216–7225. <https://doi.org/10.1128/MCB.25.16.7216-7225.2005>
- Waterhouse, A. M., Procter, J. B., Martin, D. M. A., Clamp, M., & Barton, G. J. (2009). Jalview Version 2--a multiple sequence alignment editor and analysis workbench. *Bioinformatics*, 25(9), 1189–1191. <https://doi.org/10.1093/bioinformatics/btp033>
- Wischnitzer, S. (1973). *The Submicroscopic Morphology of the Interphase Nucleus* (pp. 1–48). [https://doi.org/10.1016/S0074-7696\(08\)61933-6](https://doi.org/10.1016/S0074-7696(08)61933-6)
- Woodcock, C.L. (1973). Ultrastructure of Inactive Chromatin. *The Journal of Cell Biology* 59, 368a
- Yatskevich, S., Rhodes, J., & Nasmyth, K. (2019). Organization of Chromosomal DNA by SMC Complexes. *Annual Review of Genetics*, 53(1), 445–482. <https://doi.org/10.1146/annurev-genet-112618-043633>
- Yeong, F. M., Hombauer, H., Wendt, K. S., Hirota, T., Mudrak, I., Mechtler, K., Loregger, T., Marchler-Bauer, A., Tanaka, K., Peters, J.-M., & Ogris, E. (2003). Identification of a Subunit of a Novel Kleisin- $\beta$ /SMC Complex as a Potential Substrate of Protein

## References

---

- Phosphatase 2A. *Current Biology*, 13(23), 2058–2064.  
<https://doi.org/10.1016/j.cub.2003.10.032>
- Yin, J., Lin, A. J., Golan, D. E., & Walsh, C. T. (2006). Site-specific protein labeling by Sfp phosphopantetheinyl transferase. *Nature Protocols*, 1(1), 280–285.  
<https://doi.org/10.1038/nprot.2006.43>
- Yoshida, M. M., Kinoshita, K., Aizawa, Y., Tane, S., Yamashita, D., Shintomi, K., & Hirano, T. (n.d.). *Molecular dissection of condensin II-mediated chromosome assembly using in vitro assays*. <https://doi.org/10.1101/2022.04.04.487030>
- Yoshimura, S. H., & Hirano, T. (2016). HEAT repeats – versatile arrays of amphiphilic helices working in crowded environments? *Journal of Cell Science*.  
<https://doi.org/10.1242/jcs.185710>
- Zhou, M. (n.d.). *DNA sliding and loop formation by E. coli SMC complex: MukBEF 1*.  
<https://doi.org/10.1101/2021.07.17.452765>

## Appendix

### 1 Abbreviations

3C	Chromosome conformation capture
ABC	ATP binding cassette
AFM	Atomic force microscopy
ATP	Adenosine triphosphate
BME	2-mercaptoethanol
bp	Base pairs
ChIP	Chromatin immunoprecipitation
Cryo-EM	Cryogenic electron microscopy
Ct	<i>Chaetomium thermophilum</i>
DNA	Deoxyribonucleic acid
dsDNA	double-stranded DNA
DTT	Dithiothreitol
<i>E. coli</i>	<i>Escherichia coli</i>
EMSA	Electrophoretic mobility shift assay
FAM	Fluorescein-amidite
FRET	Förster resonance energy transfer
HEAT	Huntingtin, elongation factor 3, protein phosphatase 2A, Tor1 kinase
Hi-C	High throughput sequencing 3C
Hs	<i>Homo sapiens</i>
HTH	Helix-turn-helix
kb	kilobase pair
PMSF	Phenylmethylsulfonyl fluoride
rRNA	Ribosomal RNA
SAXS	Small angle X-ray scattering
Sc	<i>Saccharomyces cerevisiae</i>
SDS-PAGE	Sodium dodecyl sulfate - polyacrylamide gel electrophoresis
SEC	Size exclusion chromatography
SMC	Structural Maintenance of Chromosomes
Sp	<i>Schizosaccharomyces pombe</i>
ssDNA	Single-stranded DNA
WHD	Winged-helix domain

## 2 List of figures

Figure 1: The cell cycle.....	2
Figure 2: Chromosome organization during interphase in 3D.....	4
Figure 3: Condensin complex.....	8
Figure 4: Structure of condensin complex.....	10
Figure 5: ATP binding and structural rearrangement of condensin.....	12
Figure 6: DNA loops arrangement for chromosome organization.....	16
Figure 7: DNA loop extrusion by <i>Sc</i> condensin complex.....	17
Figure 8: Symmetric vs asymmetric loop extrusion.....	19
Figure 9: Models of condensin mediated loop extrusion.....	22
Figure 10: Purification of the <i>Ct</i> condensin protein complex.....	27
Figure 11: Mass spectrometry analysis of <i>Ct</i> condensin holocomplex.....	28
Figure 12: Structural characterization of purified <i>Ct</i> condensin holocomplexes.....	29
Figure 13: <i>Ct</i> condensin holocomplex displays DNA-stimulated ATPase activity.....	31
Figure 14: <i>Ct</i> condensin holocomplex has DNA binding activity.....	32
Figure 15: DNA compaction by the <i>Ct</i> condensin holocomplex.....	33
Figure 16: Microfluidics set up .....	35
Figure 17: Imaging set up.....	37
Figure 18: Visualization of DNA loop extrusion by <i>Ct</i> condensin holocomplex.....	38
Figure 19: Resolving DNA loop extrusion by side flow.....	40
Figure 20: DNA loop extrusion by <i>Ct</i> condensin is strictly asymmetric.....	41
Figure 21: Anchor slippage by <i>Ct</i> condensin holocomplex during loop extrusion.....	44
Figure 22: Properties of loop extrusion by <i>Ct</i> condensin holocomplex.....	46
Figure 23: Effect of high salt on <i>Ct</i> condensin-mediated DNA loop extrusion.....	48
Figure 24: Purification of the <i>Ct</i> delta Ycg1 condensin complex.....	50
Figure 25: The <i>Ct</i> delta Ycg1 complex can compact DNA.....	52
Figure 26: The <i>Ct</i> delta Ycg1 condensin displays DNA-stimulated ATPase activity.....	53
Figure 27: The <i>Ct</i> delta Ycg1 complex binds DNA.....	54
Figure 28: Visualization of DNA loop extrusion by the <i>Ct</i> delta Ycg1 condensin complex....	56
Figure 29: <i>Ct</i> delta Ycg1 condensin switches direction while extruding DNA loops.....	58
Figure 30: Properties of DNA loop extrusion by the <i>Ct</i> delta Ycg1 condensin complex.....	61
Figure 31: Fluorescence labeling of <i>Ct</i> condensin to track condensin during loop extrusion.....	63
Figure 32: Differences between DNA loop extrusion properties of holocomplexes and delta Ycg1 complexes.....	65
Figure 33: The tendency to change direction of the delta Ycg1 complex is reversed by high salt.....	67
Figure 34: Differences between <i>Sc</i> and <i>Ct</i> Brn1 ‘safety belt’.....	71
Figure 35: The ‘safety belt’ of <i>Ct</i> Brn1 is essential for condensin activity.....	72

Figure 36: A positively charged BC patch in the Brn1 ‘safety belt’ is required for DNA loop extrusion.....74

Figure 37: Closure of the Brn1 ‘safety belt’ is necessary for DNA loop extrusion.....75

Figure 38: Anchor slippage by *Ct* condensin holocomplex.....83

Figure 39: Bidirectional loop extrusion by delta Ycg1 complex.....85

Figure 40: DNA within the ‘safety belt’ chamber.....88

Figure 41: Complete genome compaction by loop extrusion with direction switch.....89

### 3 List of tables

Table 1: Standard laboratory equipment used in this study.....	94
Table 2: Protein purification columns used in this study.....	94
Table 3: Software used in this study.....	94
Table 4: Consumables and kits used in this study.....	95
Table 5: Specific chemical and reagents used in this study.....	95
Table 6: Biological reagents used in this study.....	96
Table 7: <i>E. coli</i> strains used in this study.....	96
Table 8: Plasmids used in this study.....	97
Table 9: Primers used for this study.....	98
Table 10: General buffers and media in this study.....	100
Supplementary table 1: Mass spectrometry analysis of <i>Ct</i> condensin holocomplex.....	114

Research is what I am doing when I don't know what I am doing

- Wernher von Braun

